

CHAPTER I

Introduction to indoles

1.1 Introduction

Indole, C_8H_7N , is a heterocyclic organic compound occurring in some flower oils, such as jasmine and orange blossom, in human feces, and in coal tar. It has an aromatic bicyclic structure, consisting of a five-member pyrrole ring fused to a six-membered benzene ring, thus can also called Benzopyrrole (Figure 1-1).

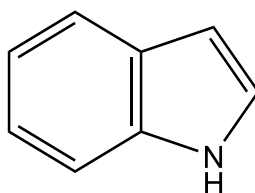
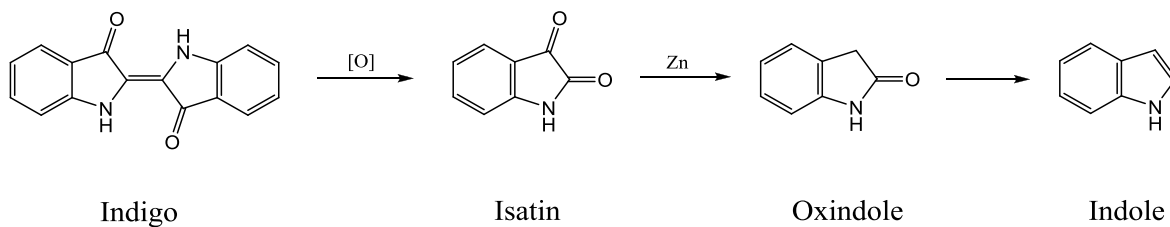


Figure 1-1 Chemical Structure of indole.

The name indole arose from the merging of the words indigo and oleum, since it was first isolated by the treatment of indigo with a sulfuric acid/sulfuric anhydride mixture. In 1866, Adolf von Baeyer synthesized indole through reduction of isatin by zinc dust (Scheme 1-1) [1] and in 1869 he proposed the formula of indole that is accepted today [2].

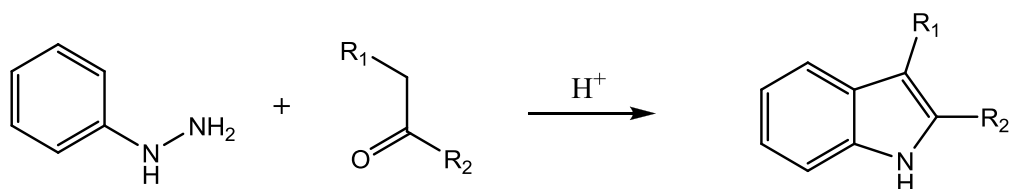


Scheme 1-1.

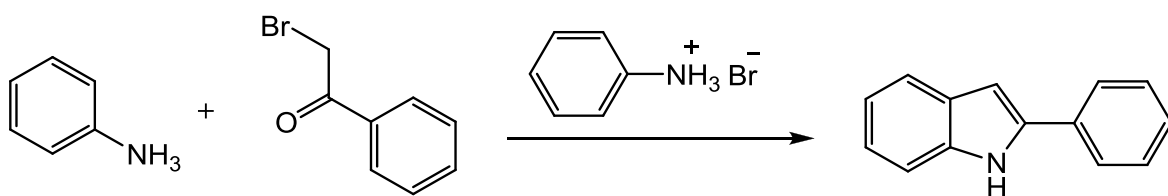
In 1883, Emil Fischer introduced a new method for the synthesis of indoles which is often used to generate indoles substituted in the 2- and/or 3-positions [3]. Since then, several other methods have been developed for the synthesis of indole and its derivatives, the most famous ones being Bischler [4], Bartoli [5], Reissert [6], Nenitzescu [7] and Madelung methods [8] (Scheme 1-2).

Scheme 1-2 Indole synthesis methods.

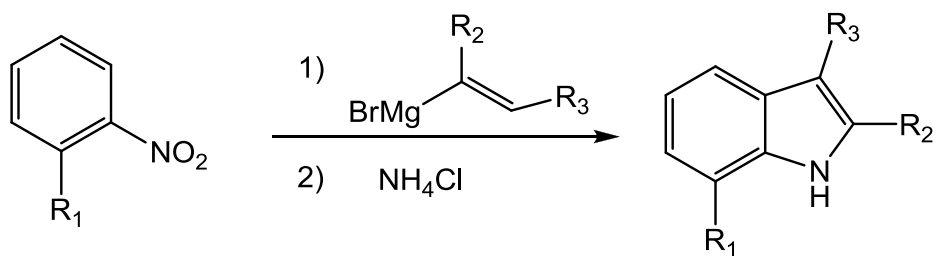
Fisher method:



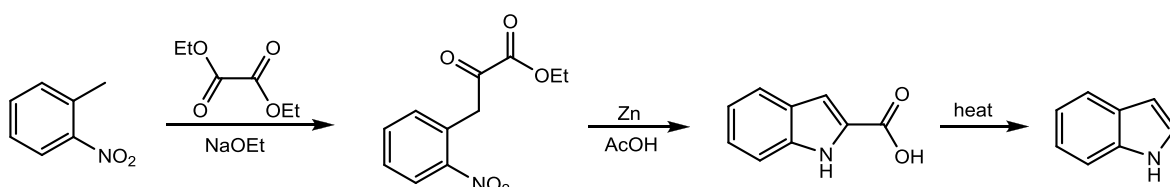
Bischler method:



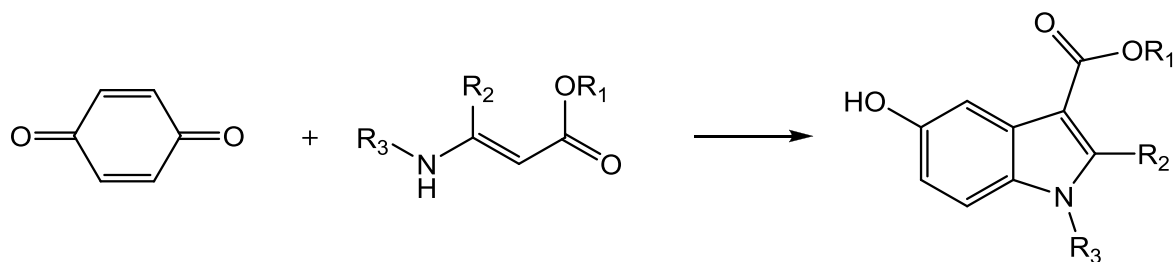
Bartoli method:



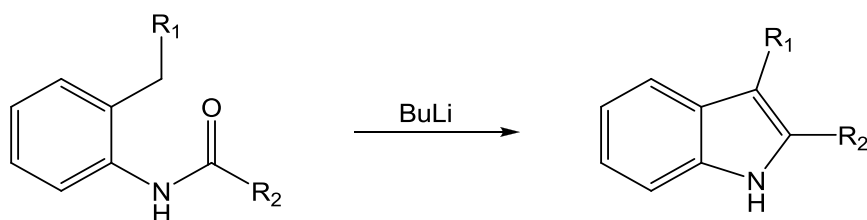
Reissert method:



Nenitzescu method:

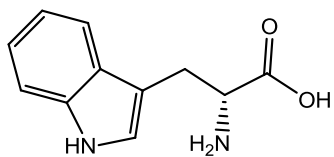


Madelung method:

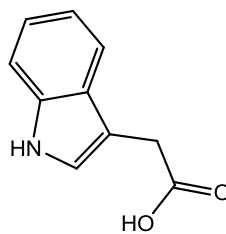


Interest in indole/indole derivatives chemistry intensified in the 1930s when it was discovered that the indole nucleus exists in the essential amino acid, tryptophan, the plant growth hormone, heteroauxin and several natural alkaloids [9] and bioactive molecules (Figure 1-2). As an example, melatonin, the main secretory product of the pineal gland, is an indole-based compound. Studies have demonstrated the role of melatonin in many physiological processes, such as the regulation of circadian rhythm [10] and immune functions [11]. In addition, different therapeutic functions have been proposed for melatonin and its derivatives [12–14].

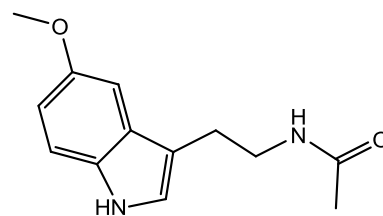
The disclosure of indolic structures of many biologically important molecules has resulted in much attention being paid to the development of bioactive synthetic compounds possessing indole ring (Figure 1-3). These compounds have been shown to possess various biological properties including antibacterial [15], antifungal [16], antiviral [17], antimalarial [18], anti-HIV [19], anticancer [20-22] and antioxidant [23, 24] activities.



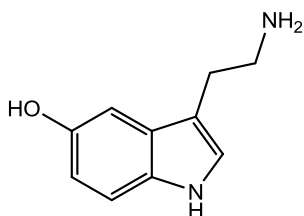
L-Tryptophan



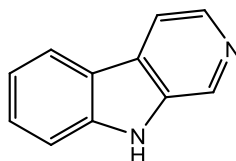
Heteroauxin (IAA)



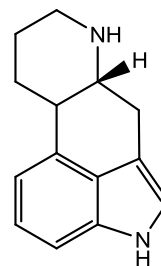
Melatonin



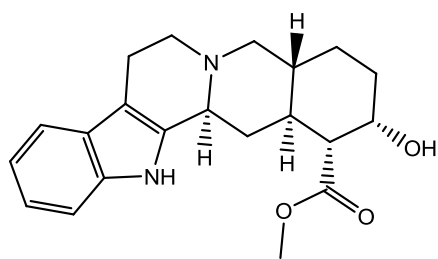
Serotonin



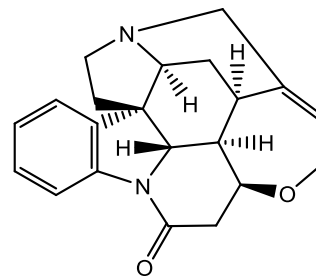
β -Carboline



Ergoline



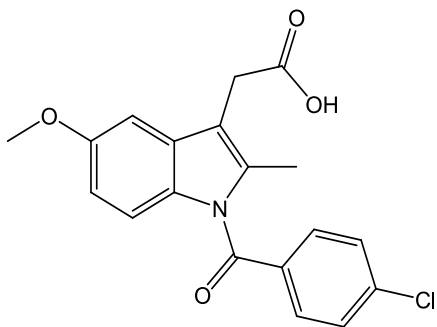
Yohimbine



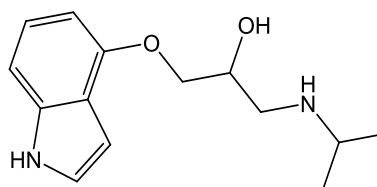
Strychnine

Figure 1-2 Examples of naturally occurring indole compounds.

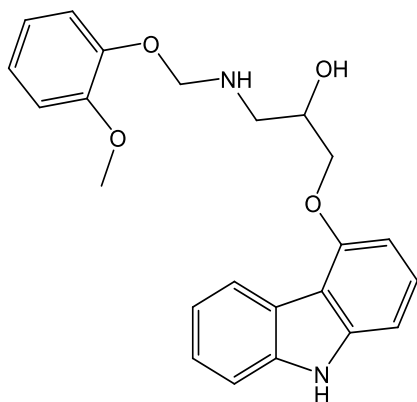
Indomethacin (commonly branded as Indocin), a non-steroidal anti-inflammatory drug, Pindolol, a Beta-blocker, Coreg, a Beta-blocker, and Imitrex Oral, a serotonin receptor agonist used to to relieve migraines, are among the commercial synthetic drugs, having the indole moiety.



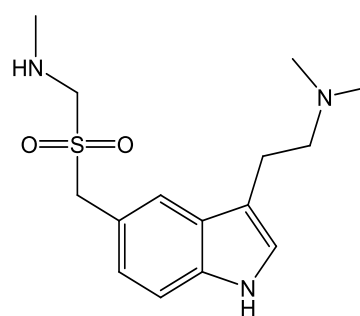
Indomethacin
Non-steroidal anti-inflammatory drug



Pindolol
Beta-blocker



Coreg
Beta-blocker



Imitrex Oral
Serotonin receptor agonist used to
relieve migraines

Figure 1-3 Examples of synthetic drugs possessing indole ring.

Indole, being a weak acid (pK_a 21.3 [25]) and a weak base (pK_b -3.5 [26]), forms ions only in strongly basic or strongly acidic media. Upon the NH deprotonation, indolyl ligands generate a very powerful anionic sp^2 -N σ -donor group and can bind strongly to positively charged metal ions.

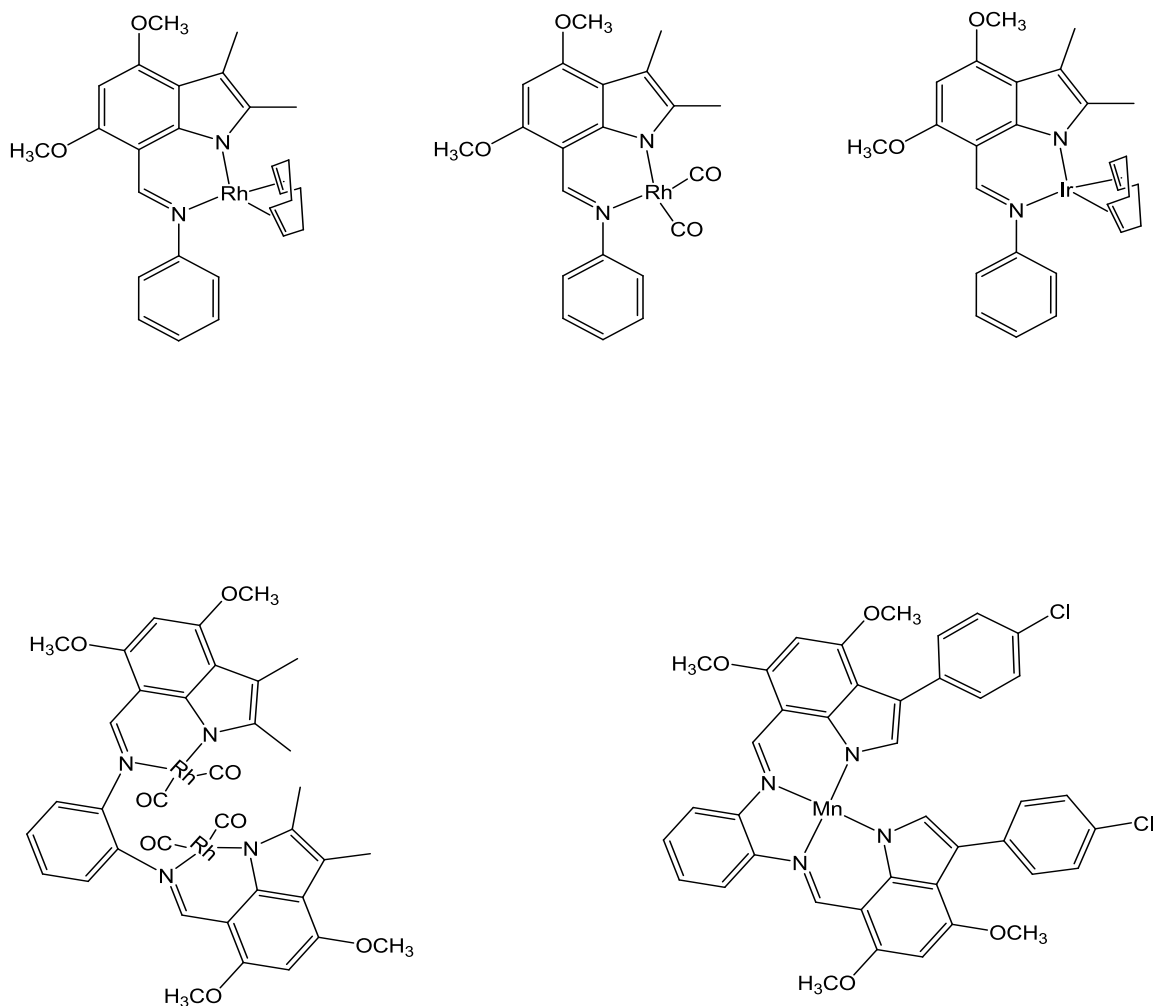


Figure 1-4 Indole derivatives having catalytic activities.

Indolyl-based ligand systems have been designed to include more labile donors such as imines as well as take advantage of the strongly binding N-donor of the indolyl system, and have been complexed with transition metals Ti [27], Ni [28], Rh and Ir [29]. Some of these complexes have been shown to possess catalytic activities. For example, the complexes with Rh(I) and Ir(I), shown in Figure 1-4 are active catalysts for intramolecular hydroalkoxylation, while the displayed Mn(II) complex shows catalytic activity for the epoxidation of alkenes [30].

1.2 Overview of the Dissertation

The present work deals with the chemistry and biological properties of some new series of indolic compounds. The work has been divided into the following sections:

- Chapter two is devoted to the study of coordination chemistry of newly synthesized indole-based S-benzylthiocarbazones towards divalent metal ions.
- Chapter three reports the synthesis of a new series of hybrid molecules combined from two pharmacophores, *i.e.*, indole and gallic acid nuclei. The compounds have been evaluated for their antioxidant and cytotoxic activities.
- Chapter four deals with the coordination behavior of an indole-based aminomethylene-malonaldehyde, towards late transition metal ions is studied. The ligand showed ambidentate behavior towards the metal ions, resulting in formation of some interesting metal-organic supramolecular architectures.
- Chapter five describes the synthesis of a new series of pyrazolyindolenine derivatives through Knorr pyrazole synthesis.

- Chapter six is about 14-membered dibenzotetraaza macrocyclic compounds containing indolic fragments.

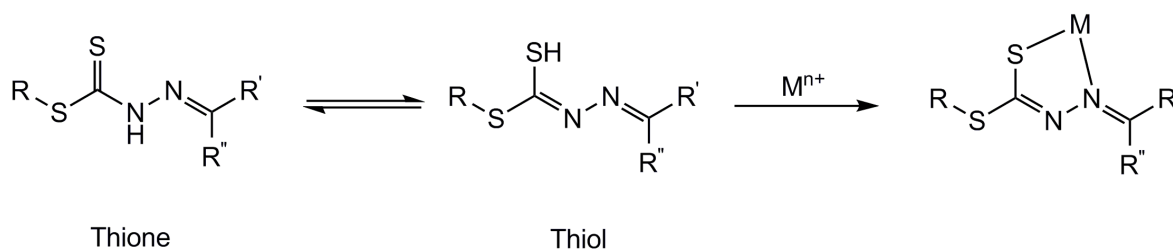
The products were characterized on the basis of spectroscopic methods and, where possible, X-ray crystallographic analysis.

CHAPTER II

*Indole-based S-benzylthiocarbazonates:
coordination behavior towards nickel, zinc
and cadmium divalent ions*

2.1 Introduction

Schiff bases derived from S-alkyl- and S-aryl esters of dithiocarbazic acid constitute an important class of chelating agents containing both soft sulfur and intermediate nitrogen donor atoms in their structural backbones. They can, in principle, show thione-thiol tautomerism which upon reaction with metal ions, accompanied by deprotonation, generate stable metal complexes (Scheme 2-1). In most of the cases, complexations involve the imine nitrogen and the thioamide sulfur atoms to form five-membered chelate rings with the metal atoms.



Scheme 2-1

If the imine moiety contains another donor atom, appropriately located for coordination to the metal ion, the Schiff base ligand can act as a tridentate chelate. Two examples are the Schiff bases derived from 2-hydroxy acetophenone [31] and pyridine-2-carbaldehyde [32] which upon deprotonation can chelate metal ions as dianionic *N,O,S*- and monoanionic *N,N,S*-tridentate ligands respectively (Figure 2-1).

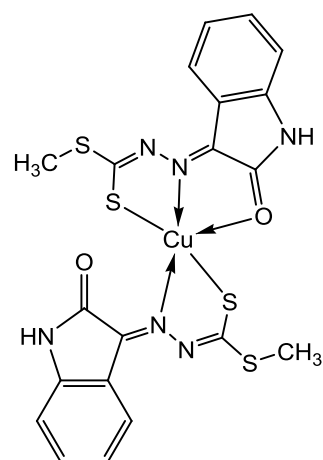
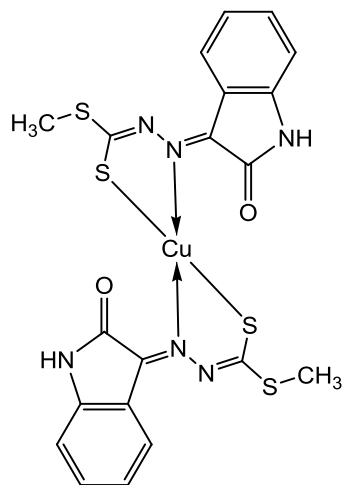
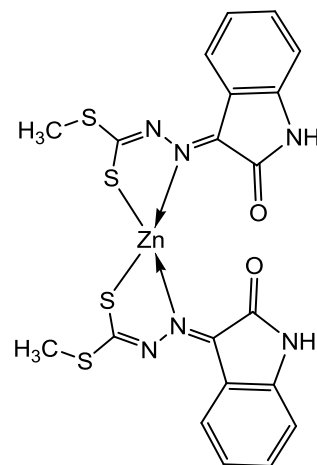
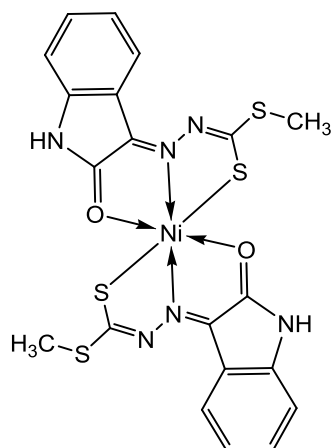
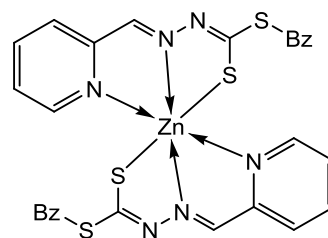
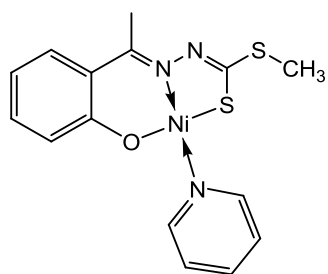
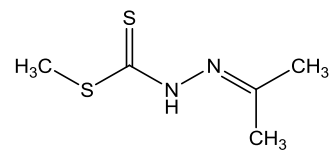
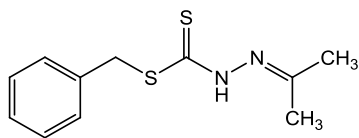


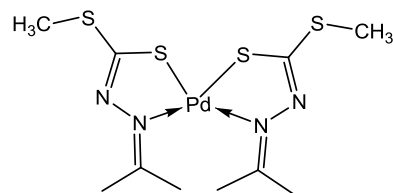
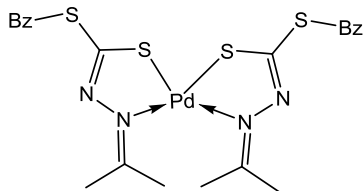
Figure 2-1 Tridentate and ambidentate S-methyl/benzylthiocarbonyl ligands.

Another example shown in Figure 2-1 is the isatin Schiff base of *S*-methyldithiocarbamate which shows ambidentate behavior towards metal ions [33]. Thus, while the ligand coordinated nickel(II) ion in an *N,O,S*-tridentate mode, towards zinc(II) ion acts as an *N,S*-bidentate chelate. With copper(II), in the solid state, the ligand behave both as an *N,S*-bidentate as well as an *N,O,S*-tridentate chelate producing a structure comprising both four- and five-coordinate copper(II) complexes within the asymmetric unit.

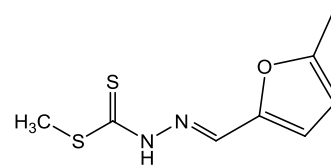
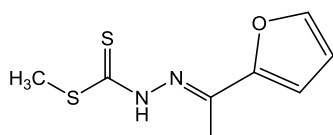
During the past decades a large number of these ligands and metal complexes have been prepared and studied for their biological properties. As some examples (Figure 2-2), the acetone Schiff bases of *S*-methyl- and *S*-benzyldithiocarbamate have been found to exhibit strong antimicrobial activities while their palladium(II) complexes show strong cytotoxicities against T-lymphoblastic leukemia cancer cells [34]. The Schiff bases derived from the condensation of 2-furyl-methylketone and 5-methyl-2-furaldehyde with *S*-methyldithiocarbamate show significant antifungal activities. The copper(II) and zinc(II) complexes of the 2-furyl-methylketone Schiff base are highly active against cervical cancer cells with CD_{50} values of 1.5 and 2.1 $\mu\text{g ml}^{-1}$ [35].



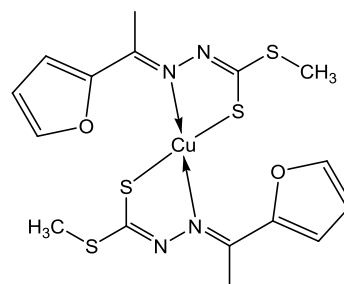
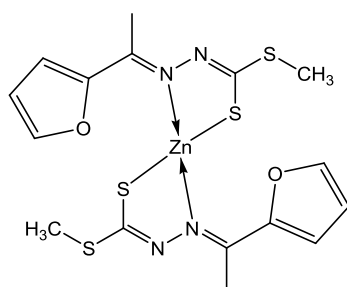
Antimicrobially active



Cytotoxicologically active



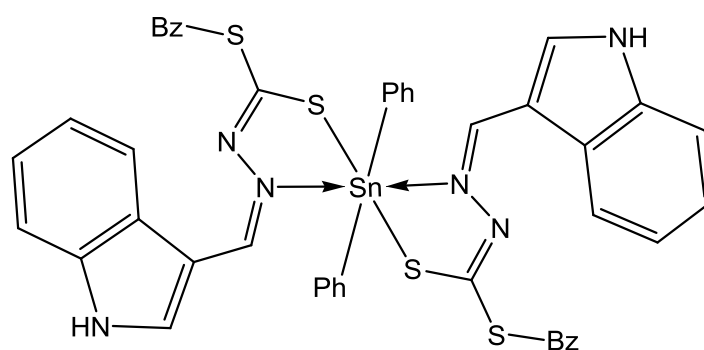
Antifungally active



Active against cervical cancer cells (HELA cells)

Figure 2-2 Examples of biologically active S-methyl/benzyl dithiocarbazonates and their metal complexes

Among the large number of the applied carbonyl compounds, indole-3-carbaldehyde has been used for synthesizing the corresponding S-benzylthiocarbamate Schiff base which upon coordination to diphenyltin(IV) gave an antibacterial and antifungal active compound (Figure 2-3) [36].



Antibacterially and antifungally active

Figure 2-3 Diphenyltin(IV) complex of an indole S-benzylthiocarbamate.

Herein, we report the crystal structure of this Schiff base (H_2L^2 , Figure 2-4) and its 2-imineindole isomer (H_2L^1 , Figure 2-4). In order to explore the coordination behavior of this type of the chelating agents, we studied the complexation of these two Schiff bases as well as the analogues 7-imineindole ligand (H_2L^3 , Figure 2-4) with nickel, zinc and cadmium divalent ions.

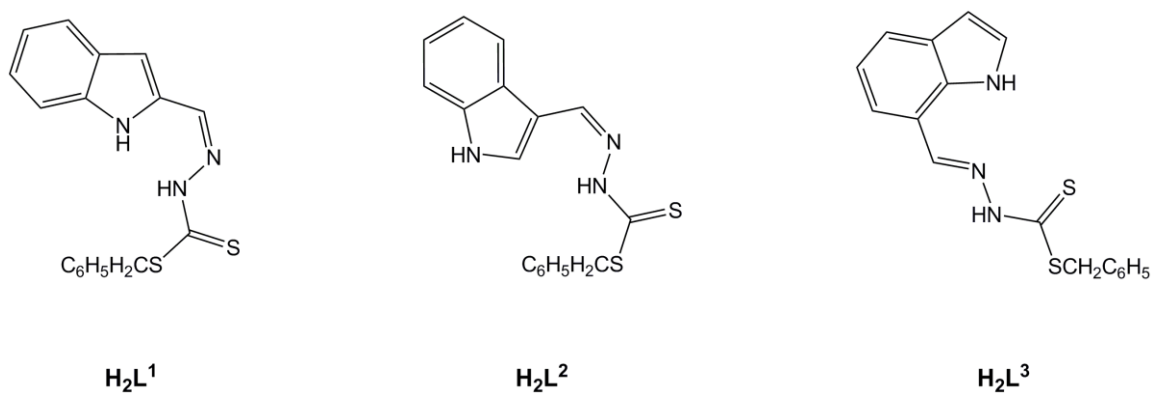


Figure 2-4 Structures of the neutral ligands.

2.2 Results and discussion

2.2.1 General characterizations

Condensation of indole-2-carbaldehyde, indole-3-carbaldehyde and indole-7-carbaldehyde with S-benzylthiocarbamate gave the expected Schiff bases, H_2L^1 , H_2L^2 and H_2L^3 , respectively. Like most thiosemicabazones and esters of dithiocabazones they can undergo thione-thiol tautomerization. However, spectroscopic data show the existence of the Schiff bases as their thione tautomers in the solid state and in solution. The solid state IR spectra show thioamide N-H bands at 3119, 3272 and 3107 cm^{-1} , but do not reveal any S-H band at *ca.* 2700 cm^{-1} . ^1H NMR spectra of the compounds exhibit the thioamide NH, but no signal attributable to a thiol proton at *ca.* δ 4.00 ppm.

Treatment of the ligands with the acetate salts of metal(II) ions in ethanol, accompanied by mono-deprotonation, led to the formation of the metal diligand complexes.

This is reflected in omission of the thioamide *NH* resonance of the ligands in the ^1H NMR and disappearance of the $\nu(\text{N-H})$ bands in the IR spectra. The splitting of the $\nu(\text{CSS})$ bands of the free ligands at $1022\text{-}1028\text{ cm}^{-1}$ in the IR of the complexes indicates the involvement of the thioamide sulfur in the complexations. This is supported by upfield shifts of the CSS ^{13}C NMR signals on chelation. The shifts are significant for the complexes of HL^1 and HL^2 (13-15 ppm), but relatively small for $[\text{Cd}(\text{HL}^3)_2]$ (~ 5 ppm). The assignment of the ^{13}C signals are based on the chemical shifts, intensity patterns and coordination induced shifts, and are in agreement with those suggested by others [36,37]. $[\text{Ni}(\text{HL}^1)_2]\cdot\text{H}_2\text{O}$ is diamagnetic, thus the nickel(II) ion is chelated in a square planar environment provided by two mono-anionic ligands. The water molecule is most likely hydrogen bonded to the ligand of the complex. The presence of the indole *NH* signal in ^1H NMR spectra of the obtained complexes and the related $\nu(\text{N-H})$ bands in their IR spectra show that the indole nitrogens are not bound to the metal atoms.

There are few reports in the literature on metal complexes of 7-imineindoles, in all of which the indole nitrogens are coordinated to the metal ions [38,39]. Since the indole nitrogen in the 7-imineindole H_2L^3 can be suitably located to participate in coordination to the metal center, we were prompted to apply more basic reaction conditions to ease deprotonation of the indole *NH* of H_2L^3 and take advantage of its nitrogen donor atom. Thus H_2L^3 was treated with the selected metal(II) ions in the presence of KOH in ethanol. Analyses of the obtained products showed the formation of metal complexes of the type $[\text{M}(\text{L}^3)(\text{H}_2\text{O})]$ ($\text{M} = \text{Cd}^{\text{II}}, \text{Zn}^{\text{II}}, \text{Ni}^{\text{II}}$). ^1H NMR investigation of the cadmium(II) and zinc(II) complexes indicates deprotonation of the thioamide *NH* and also indole *NH* on chelation, signifying the coordination through the indole nitrogen. Similar to the complexes of HL^1 and HL^2 , the ^{13}C NMR spectra of the complexes show significant upfield shifts (~ 20 ppm)

of CSS signal from that in the free ligand. The nickel(II) complex, $[\text{Ni}(\text{L}^3)(\text{H}_2\text{O})]$, is paramagnetic with magnetic susceptibility value of 1.50 B.M which is lower than the expected value for a high spin Ni(II) complex. This indicates the compound contains a mixture of high and low spin Ni(II) in different coordination geometries. A similar observation made by others was explained by the pronounced tendency of nickel thiolate complexes to form higher aggregates by Ni-S-Ni bridging [40]. The combination of fourfold square planar and six-fold pseudooctahedral geometries in the aggregates may lead to a puzzling paramagnetism observation. It is worth mentioning that use of triethylamine as the base in the reaction of H_2L^3 with nickel(II) acetate, gave the complex $[\text{Ni}(\text{L}^3)(\text{Et}_3\text{N})(\text{H}_2\text{O})]$ with magnetic susceptibility value of 1.13 B.M.

2.2.2 Crystal structure of $\text{H}_2\text{L}^1 \cdot 0.5\text{EtOH}$

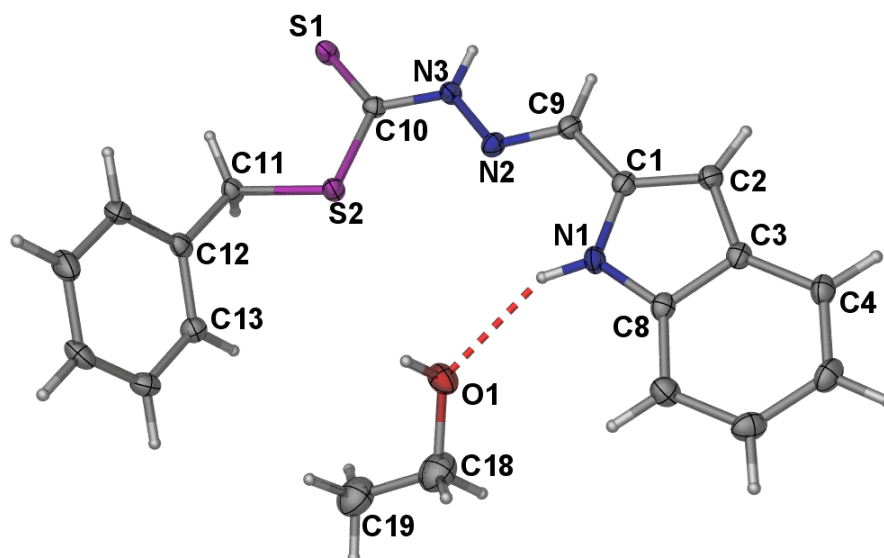


Figure 2-5 Thermal ellipsoid plot of $\text{H}_2\text{L}^1 \cdot 0.5\text{EtOH}$ at the 50% probability level.

Figure 2-5 shows the molecular structure of the ligand H_2L^1 and Table 2-1 lists the selected bond lengths and angles. The $C_{10}H_8N_3S_2$ portion of the Schiff base is nearly planar (r.m.s. deviation 0.090 Å) and makes a dihedral angle of 66.26 (4) ° with the phenyl ring. The indole nitrogen atom is hydrogen bonded to the ethanol oxygen atom.

2.2.3 Crystal structure of H_2L^2

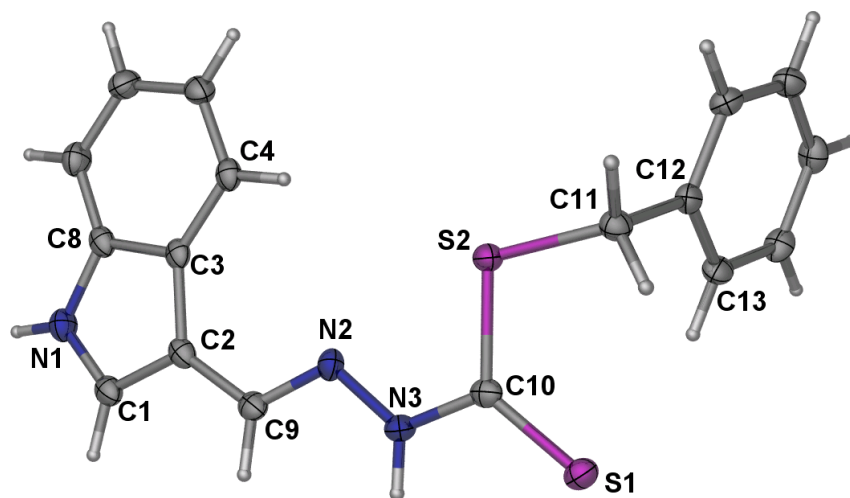


Figure 2-6 The molecular structure of H_2L^2 at the 50% probability level.

The molecular structure of the ligand, H_2L^2 , is displayed in Figure 2-6 and the selected bond lengths and angles are given in Table 2-1. The molecule is bent about the methylene-C11 atom, the dihedral angle between the $C_{10}H_8N_3S_2$ portion and the phenyl ring being 71.89 (7) °. In the crystal, the indole NH is involved in an N-H... π interaction with H...Cg distance of 2.92(2) Å.

Table 2-1 Selected bond lengths (Å) and bond angles (°) for H_2L^1 and H_2L^2 .

H_2L^1		H_2L^2	
<i>Bond lengths</i>			
S(1)-C(10)	1.6647(14)	S(1)-C(10)	1.656(3)
S(2)-C(10)	1.7505(15)	S(2)-C(10)	1.771(3)
N(2)-N(3)	1.3748(16)	N(2)-N(3)	1.380(3)
N(2)-C(9)	1.285(2)	N(2)-C(9)	1.287(3)
N(3)-C(10)	1.3394(19)	N(3)-C(10)	1.339(4)
<i>Bond angles</i>			
C(10)-S(2)-C(11)	102.42(7)	C(10)-S(2)-C(11)	102.30(13)
C(10)-N(3)-N(2)	119.65(12)	C(10)-N(3)-N(2)	121.2(2)
S(1)-C(10)-S(2)	125.40(9)	S(1)-C(10)-S(2)	126.95(17)

2.2.4 Crystal structure of $[\text{Zn}(\text{HL}^1)_2]$

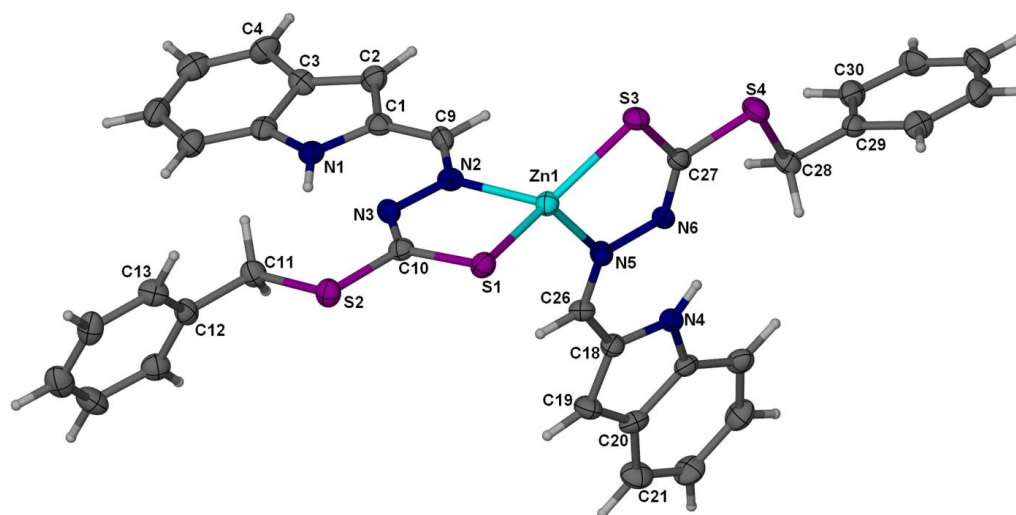


Figure 2-7 The molecular structure of $[\text{Zn}(\text{HL}^1)_2]$ showing the atom labeling scheme (50% probability ellipsoids).

The crystal structure of the zinc complex is depicted in Figure 2-7 and selected bond lengths and angles are given in Table 2-2. The crystal studied was a racemic twin with the twin parameter refined to 0.506(13). The metal ion in the complex is chelated by two monoanionic bidentate ligands via the azomethine nitrogen atoms and the thiolate sulfur atoms, forming two five-membered chelating rings. The dihedral angle between the two formed rings is 81.81(7)°, thus the geometry is best considered distorted tetrahedral. While coordinating to the zinc(II) ion, deprotonation of the ligand generates an iminothiolate ion with a negative charge delocalized over the S-C-N chain (thioamide group). This is indicated by the longer bond lengths of C10–S1 and C27–S3 [1.744(4) and 1.732(4) Å respectively] compared to the corresponding distance in the free ligand [1.6647(14) Å]. Moreover, the bond distances of N3–C10 [1.310(5) Å] and N6–C27 [1.297(5) Å] are shorter than the related one in the free ligand [1.3394(19) Å].

Table 2-2 Selected bond lengths (Å) and bond angles (°) for [Zn(HL¹)₂]

<i>Bond lengths</i>			
Zn(1)-N(2)	2.034(3)	S(1)-C(10)	1.744(4)
Zn(1)-N(5)	2.044(3)	S(3)-C(27)	1.732(4)
Zn(1)-S(1)	2.2661(13)	N(3)-C(10)	1.310(5)
Zn(1)-S(3)	2.2698(14)	N(6)-C(27)	1.297(5)
<i>Bond angles</i>			
N(2)-Zn(1)-N(5)	102.37(11)	N(2)-Zn(1)-S(3)	118.82(11)
N(2)-Zn(1)-S(1)	86.80(10)	N(5)-Zn(1)-S(3)	87.23(10)
N(5)-Zn(1)-S(1)	123.30(11)	S(1)-Zn(1)-S(3)	136.44(4)

The Zn-N distances of 2.034(3) and 2.044(3) Å and Zn-S bond lengths of 2.2667(13) and 2.2698(14) Å are comparable with the values reported in literature for the similar structures [33,35]. Intramolecular hydrogen bonding links the indole nitrogens to the thioamide nitrogens.

2.2.5 Crystal structure of [Ni(HL²)₂].2DMF

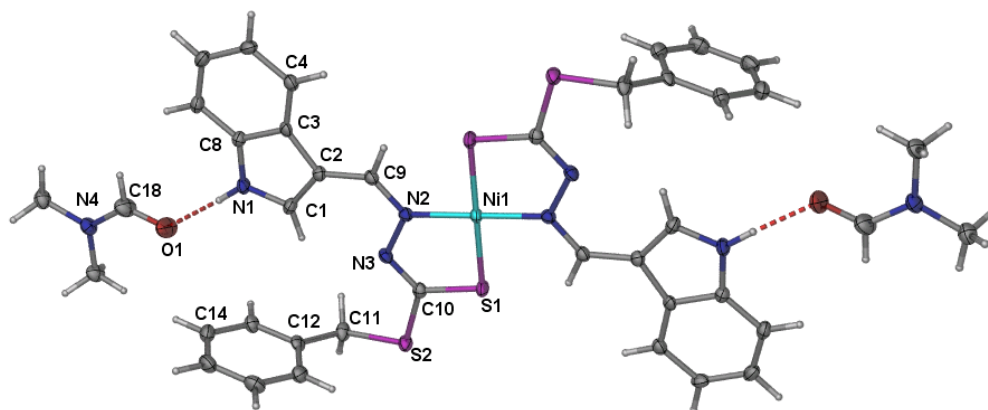


Figure 2-8 View of [Ni(HL²)₂].2DMF at the 50% probability level. The unlabelled atoms are generated by the symmetry operation (-x+1, -y+1, -z+1).

The crystal structure of the DMF disolvate Ni^{II} complex is represented in Figure 2-8 and the selected geometrical parameters are listed in Table 2-3. The mono-deprotonated Schiff base, HL², chelates the nickel(II) ion in an *N,S*-bidentate bonding mode to form a five-membered ring with the metal center. The dihedral angle between the aromatic ring planes within the ligand is 86.37 (13) °. The Ni^{II} ion, located on an inversion center, is four-coordinated by two of the Schiff base ligands in a *trans*-square-planar geometry. The *trans*

configuration of the complex is in accordance with the general observation that the square planar complexes of Schiff bases of S-alkyldithiocarbazate have a *trans* configuration when the ligand is derived from an aldehyde, whereas ketone S-alkyldithiocarbazonates yield *cis*-planar complexes [34]. In the crystal, the indolic NH groups are bonded to the dimethylformamide (DMF) solvent molecules via an N-H...O interaction.

Table 2-3 Selected bond lengths (Å) and bond angles (°) for **[Ni(HL²)₂].2DMF**

<i>Bond lengths</i>			
Ni(1)-N(2)	1.916(2)	S(1)-C(10)	1.725(3)
Ni(1)-S(1)	2.1770(7)	N(3)-C(10)	1.288(3)
<i>Bond angles</i>			
N(2)#1-Ni(1)-N(2)	180.0	N(2)-Ni(1)-S(1)	85.65(7)
N(2)#1-Ni(1)-S(1)	94.35(7)	S(1)-Ni(1)-S(1)#1	180.0

Symmetry transformations used to generate equivalent atoms: #1 -x+1,-y+1,-z+1

2.2.6 Crystal structure of [Cd(HL²)₂(py)₂].py₂

A view of the complex structure is shown in Figure 2-9 and selected bond lengths and angles are listed in Table 2-4. The structure shows a six-coordinate cadmium(II) complex in a distorted octahedral environment. The two mono-deprotonated Schiff base ligands act as *N,S*-bidentate chelating agents in an almost planar arrangement around the cadmium atom and form two five-membered rings with the metal center. The octahedral geometry is completed by the two *trans*-located pyridine ligands, the dihedral angle between them being 77.4(2) °. In the crystal structure, the indole nitrogens are hydrogen-bonded to the pyridine solvent molecules.

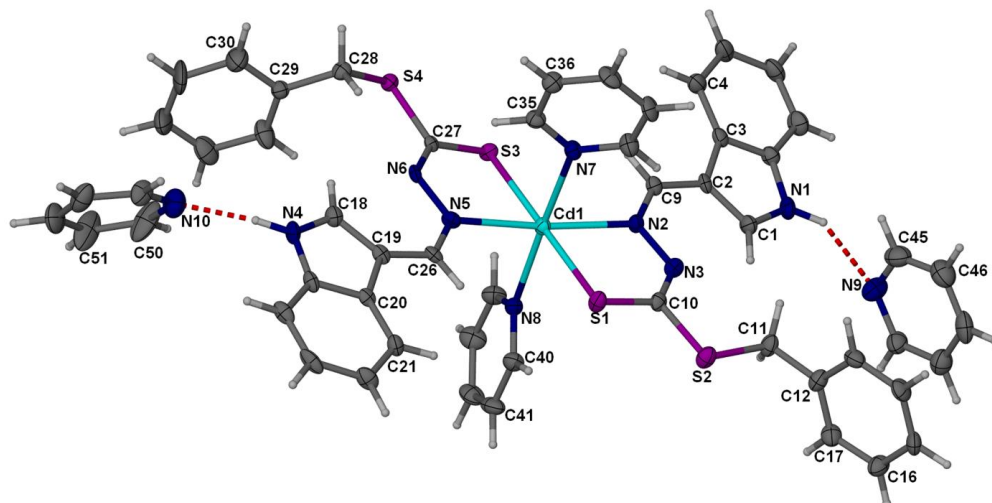


Figure 2-9 The molecular structure of $[\text{Cd}(\text{HL}^2)_2(\text{py})_2] \cdot \text{py}_2$. Ellipsoids correspond to 30% probability.

Table 2-4 Selected bond lengths (Å) and bond angles (°) for $[\text{Cd}(\text{HL}^2)_2(\text{py})_2] \cdot \text{py}_2$

<i>Bond lengths</i>			
Cd(1)-N(2)	2.321(5)	Cd(1)-S(3)	2.5791(16)
Cd(1)-N(5)	2.324(5)	S(1)-C(10)	1.727(6)
Cd(1)-N(8)	2.522(5)	S(3)-C(27)	1.731(6)
Cd(1)-N(7)	2.542(5)	N(3)-C(10)	1.305(8)
Cd(1)-S(1)	2.5768(17)	N(6)-C(27)	1.297(7)
<i>Bond angles</i>			
N(2)-Cd(1)-N(5)	173.73(17)	N(8)-Cd(1)-S(1)	88.81(13)
N(2)-Cd(1)-N(8)	91.90(17)	N(7)-Cd(1)-S(1)	87.50(12)
N(5)-Cd(1)-N(8)	94.30(17)	N(2)-Cd(1)-S(3)	102.72(12)
N(2)-Cd(1)-N(7)	88.37(17)	N(5)-Cd(1)-S(3)	76.34(12)
N(5)-Cd(1)-N(7)	85.50(16)	N(8)-Cd(1)-S(3)	90.24(13)
N(8)-Cd(1)-N(7)	176.13(17)	N(7)-Cd(1)-S(3)	93.46(12)
N(2)-Cd(1)-S(1)	76.39(12)	S(1)-Cd(1)-S(3)	178.68(6)
N(5)-Cd(1)-S(1)	104.65(13)		

2.2.7 Crystal structure of $[\text{Cd}(\text{HL}^3)_2(\text{py})_2]$

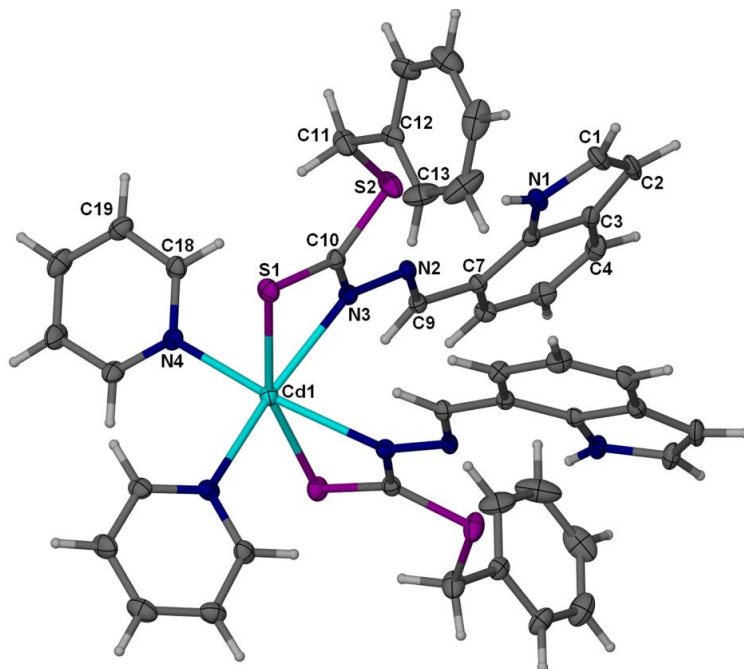


Figure 2-10 The molecular structure of $[\text{Cd}(\text{HL}^3)_2(\text{py})_2]$ with thermal ellipsoids drawn at the 30% probability level. The unlabelled atoms are generated by the symmetry operation $(-x+1/2, -y+1/2, z)$.

The structure of the complex is represented in Figure 2-10 and the selected bond lengths and angles are compiled in Table 2-5. The cadmium ion lies on a crystallographic 2-fold rotational axis of symmetry and is six-coordinated by two ligands HL^3 and two *cis*-positioned pyridine ligands in a highly distorted octahedral geometry. Similar to HL^1 and HL^2 , the ligand HL^3 coordinated to the metal center as a monoanionic *N,S*-bidentate chelate, but unlike them, the coordination occurred through the iminothiolate nitrogens and sulfurs to form two four-membered chelate rings with bite angle of $61.09(6)^\circ$. The azomethine nitrogen is hydrogen bonded to the indole N-H.

Table 2-5 Selected bond lengths (Å) and bond angles (°) for [Cd(HL³)₂(py)₂]

<i>Bond lengths</i>			
Cd-N(4)	2.365(3)	S(1)-C(10)	1.710(4)
Cd-N(3)	2.409(3)	N(3)-C(10)	1.318(4)
Cd-S(1)	2.6732(10)		
<i>Bond angles</i>			
N(4)-Cd-N(4)#1	101.31(15)	N(3)-Cd-S(1)#1	102.43(7)
N(4)-Cd-N(3)	93.22(10)	N(4)-Cd-S(1)	89.83(8)
N(4)#1-Cd-N(3)	158.49(9)	N(3)-Cd-S(1)	61.10(7)
N(3)-Cd-N(3)#1	77.85(14)	S(1)#1-Cd-S(1)	160.16(5)
N(4)-Cd-S(1)#1	102.79(7)		

Symmetry transformations used to generate equivalent atoms: #1 -x+1/2, -y+1/2, z

The preference for four over five-membered chelate ring is unusual among the complexes of S-alkyl/aryldithiocarbazonates and thiosemicarbazones, however there are few reports on this mode of coordination [41-46]. The Cd-S, Cd-N_{iminothiolate} and Cd-N_{py} bond distances are 2.6732(9), 2.409(3) and 2.366(3) Å respectively which are similar to those in [Cd(C₇H₄NS₂)₂(py)₂], the closest analogous structure [47].

2.2.8 Crystal structure of [Ni(L³)(py)]

A solution of [Ni(L³)(Et₃N)(H₂O)] in a mixture of DMSO and pyridine gave red crystals of [Ni(L³)(py)]. The structure of the complex is depicted in Figure 2-11 and the selected bond lengths and angles are listed in Table 2-6. The crystal studied was a racemic twin and the twin parameter refined to 0.18(3). As the structure shows, L³ is coordinated to the metal ion as a dianionic *N,N,S*-tridentate ligand through the indole nitrogen, azomethine nitrogen and iminothiolate sulfur atoms, forming two five-membered and six-membered

rings with the metal atom. The pyridine nitrogen atom occupied the fourth position, giving rise to a distorted square planar nickel(II) complex with the metal center being 0.019(4) Å out of the coordination plane, N1-N2-N4-S1. The pyridine ring makes a dihedral angle of 74.99(15)° with the mean plane passing through the coordination plane.

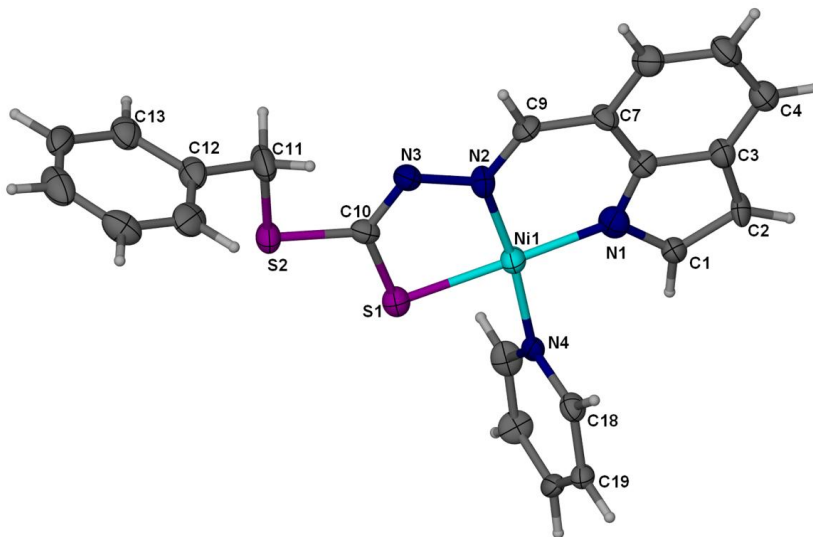


Figure 2-11 The molecular structure of [Ni(L³)(py)] with thermal ellipsoids drawn at the 50% probability level.

Table 2-6 Selected bond lengths (Å) and bond angles (°) for [Ni(L³)(py)]

<i>Bond lengths</i>			
Ni(1)-N(2)	1.884(7)	Ni(1)-S(1)	2.170(3)
Ni(1)-N(1)	1.891(8)	S(1)-C(10)	1.718(9)
Ni(1)-N(4)	1.904(6)	N(3)-C(10)	1.287(10)
<i>Bond angles</i>			
N(2)-Ni(1)-N(1)	94.4(3)	N(2)-Ni(1)-S(1)	86.5(2)
N(2)-Ni(1)-N(4)	171.0(3)	N(1)-Ni(1)-S(1)	177.4(3)
N(1)-Ni(1)-N(4)	93.2(3)	N(4)-Ni(1)-S(1)	86.2(2)

2.2.9 NMR analysis of $[\text{Cd}(\text{HL}^3)_2]$

The formation of four-membered chelate ring observed in $[\text{Cd}(\text{HL}^3)_2(\text{py})_2]$, poses the question of the driving force behind such an unusual coordination mode. Two factors which might be responsible for this observation are the steric bulk of the two pyridine ligands, and intramolecular hydrogen bonding between the indole NH and the azomethine nitrogen atom. The first effect is absent in $[\text{Cd}(\text{HL}^3)_2]$, therefore the elucidation of its structure can help us to find out the origin of the coordination mode. To do that, a detailed 2D-NMR spectroscopy study, using NOESY, COSY and HMQC techniques, was undertaken which allowed us to assign most of the ^1H and ^{13}C NMR signals unambiguously. Owing to the presence of the indole NH, five membered chelate ring formation can only take place when the azomethine C=N bond is directed away from the indole-NH (**1**, Figure 2-12). On the other hand, the conformation in which the C=N bond directed toward the indole-NH, stabilized by NH...H hydrogen bonding, leads to the four-membered ring (**2**, Figure 2-12).

The structure of $[\text{Cd}(\text{HL}^3)_2]$ was found to be **2** by 2D-NMR and NOE experiments, wherein the azomethine hydrogen at 8.66 ppm has an NOE correlation with the aromatic hydrogen at 7.18 ppm, and no NOE effect was observed between the azomethine hydrogen and the indole NH at 10.23 ppm. Therefore the unusual coordination mode observed in the crystal structure of $[\text{Cd}(\text{HL}^3)_2(\text{py})_2]$ is not the effect of steric bulk of the co-ligand pyridines, but most likely is a consequence of the intramolecular NH...N hydrogen bonding. This is in agreement with the five membered ring formation observed in $[\text{Cd}(\text{HL}^2)_2(\text{py})_2]$ in which two co-ligand pyridines exist, but the analogous intramolecular hydrogen bonding is prevented.

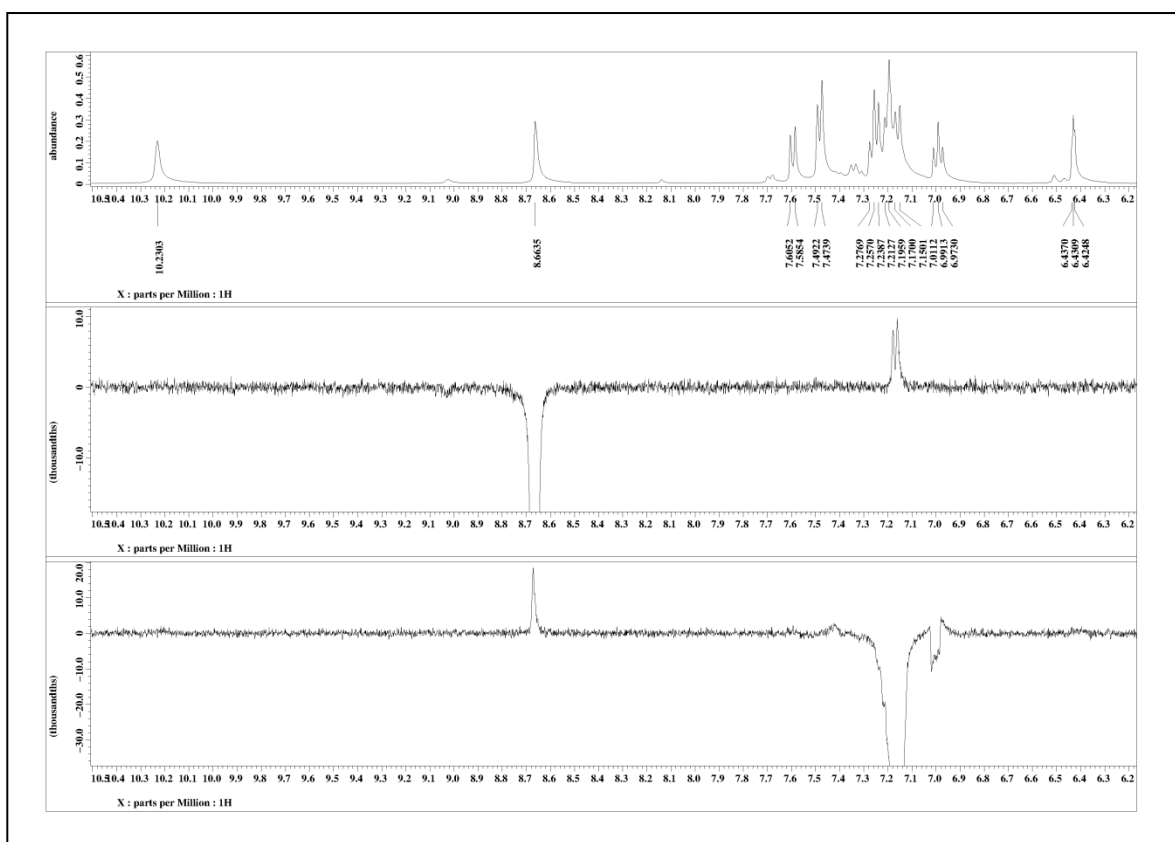
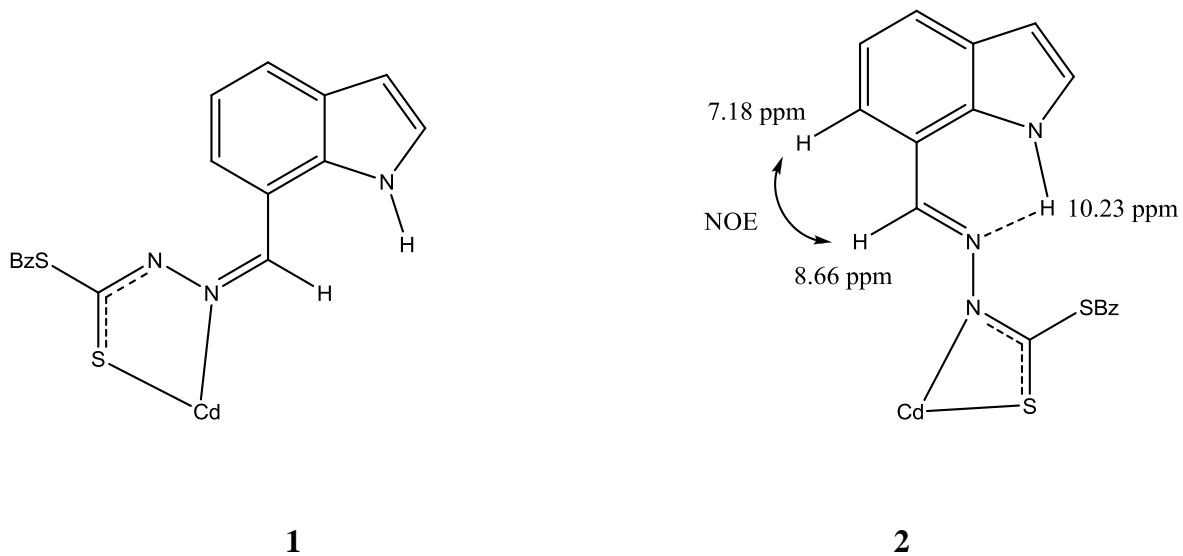


Figure 2-13 NOE correlation between the azomethine hydrogen and the phenyl hydrogen in $[\text{Cd}(\text{HL}^3)_2]$

2.3 Conclusions

The synthesized *S*-benzylthiocarbazones can coordinate to the metal ions in different ways (Figure 2-14). Like most dithiocarbazone esters, the ligands HL¹ and HL² with the imine link at positions 2 and 3 of the indole system coordinated to the metal ions through the azomethine nitrogen and thioamide sulfur atoms and created five-membered chelate rings (**3** and **4**). Similarly, the 7-imineindole (HL³) di-ligated the cadmium(II) as a monoanionic bidentate ligand, however in an unusual manner through the thioamide nitrogen and sulfur atoms, leading to the formation of four-membered rings with the metal center (**5**). It would appear that intramolecular NH...N hydrogen bonding is the responsible for such observed coordination mode. In the presence of KOH, the ligand L³ can act as a dianionic *N,N,S*-tridentate chelate (**6**) and mono-ligate the metal ions to afford complexes of the type [M(L³)(H₂O)].

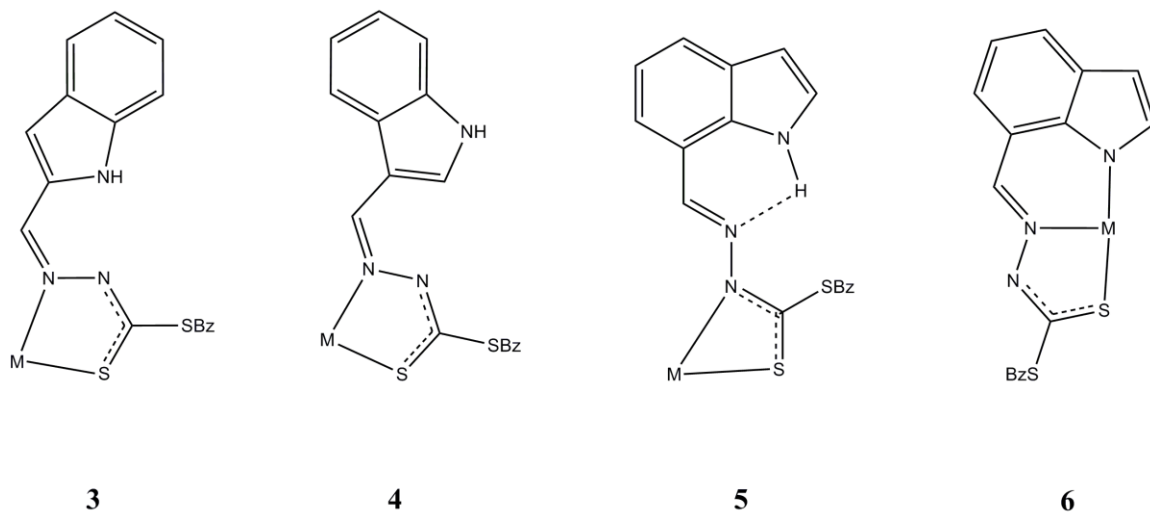


Figure 2-14 Coordination modes of the synthesized *S*-benzylthiocarbazone ligands.

2.4 Experimental

Indole carbaldehydes were purchased from the Aldrich–Sigma Company. Ethanol was distilled prior to use. Magnetic susceptibilities were measured with a Sherwood Scientific MSB-AUTO magnetic susceptibility balance at 298 K. Diamagnetic corrections were applied using Pascal’s constants. The IR spectra were recorded on a Perkin–Elmer RX1 FT-IR spectrometer with samples prepared as KBr pellets. The NMR spectra were recorded on a JEOL Lambda 400 MHz FT-NMR spectrometer. The electronic spectra were measured by means of a Shimadzu UV-3600 UV-VIS-NIR Spectrophotometer in the region 200–1100 nm.

2.4.1 Preparation of S-benzylthiocarbazate

This compound was synthesized as reported previously [48]. A mixture of hydrazine hydrate (10 g, 0.2 mol) and potassium hydroxide (11.4 g, 0.2 mol) in 90% ethanol (70 ml) was cooled in an ice bath. Carbon disulphide (15.2 g, 0.2 mol) was then added drop-wise with vigorous stirring. The temperature of the reaction mixture was not allowed to rise above 5 °C during the period of addition of carbon disulfide. To the mixture, 40% ethanol (60 ml) was added and the solution was cooled in ice. Benzyl chloride (25.3 g, 0.2 mol) was then added slowly with vigorous stirring. The white product was separated by filtration, washed with water and dried in air. The crude product was recrystallized from absolute ethanol; yield, 23 g (58%).

2.4.2 Preparation of the Schiff base ligands

A mixture of S-benzylthiocarbamate (1.98 g, 10 mmol) and the appropriate indole carbaldehyde (1.45 g, 10mmol) in ethanol (100 ml) was refluxed for 3 h. The mixture was then cooled to room temperature and the precipitated Schiff base was filtered off, washed with cold ethanol and dried over silica gel.

H₂L¹: 2.88 g, 89%. *Anal.* Calcd for C₂₀H₁₉N₃O₂S: C, 65.73; H, 5.24; N, 11.50. Found: C, 65.60; H, 5.24; N, 11.29%. ¹H NMR (DMSO-*d*₆): δ 4.49 (s, 2H, SCH₂); 6.91 (d, 1H, Ar-*H*); 7.00 (t, 1H, Ar-*H*); 7.17 (t, 1H, Ar-*H*); 7.26 (m, 1H, Ar-*H*); 7.33 (t, 2H, Ar-*H*); 7.43 (d, 3H, Ar-*H*); 7.55 (d, 1H, Ar-*H*); 8.27 (s, 1H, CHN); 11.30 (s, 1H, indole NH); 13.31 (s, 1H, NHCS). ¹³C NMR (DMSO-*d*₆): δ 37.99 (SCH₂); 108.91, 112.19, 119.88, 121.09, 124.10, 127.35, 127.71, 128.58, 129.40, 131.99, 136.71, 138.18 (*Ar*); 139.39 (CHN); 195.56 (NHCS). IR (KBr, cm⁻¹): 3443 s (νNH); 3119 s (νNH); 1600 s (νCN); 1332 (br); 1027 s (νCSS).

H₂L²: 2.96 g, 91%. *Anal.* Calcd for C₂₀H₁₉N₃O₂S: C, 65.73; H, 5.24; N, 11.50. Found: C, 65.33; H, 5.67; N, 11.29%. ¹H NMR (DMSO-*d*₆): δ 4.55 (s, 2H, SCH₂); 7.10 (t, 1H, Ar-*H*); 7.17 (t, 1H, Ar-*H*); 7.25 (m, 1H, Ar-*H*); 7.30 (t, 2H, Ar-*H*); 7.42 (dd, 3H, Ar-*H*); 7.91 (d, 1H, Ar-*H*, *J*=2.7); 8.15 (d, 1H, Ar-*H*); 8.42 (s, 1H, CHN); 11.74 (s, 1H, indole NH); 13.17 (s, 1H, NHCS). ¹³C NMR (DMSO-*d*₆): δ 37.12 (SCH₂); 108.86, 112.07, 121.09, 121.72, 122.96, 123.93, 127.08, 128.45, 129.13, 132.85, 137.13, 137.71 (*Ar*); 144.22 (CHN); 193.22 (NHCS). IR (KBr, cm⁻¹): 3405 s (νNH); 3272 s (νNH); 1610 s (νCN); 1490 m; 1314 s; 1022 s (νCSS).

H₂L³: 2.66 g, 82%. *Anal.* Calcd for C₂₀H₁₉N₃O₂S: C, 65.73; H, 5.24; N, 11.50. Found: C, 65.21; H, 5.73; N, 11.78%. ¹H NMR (DMSO-*d*₆): δ 4.65 (s, 2H, SCH₂); 6.59 (dd,

1H, Ar-*H*); 7.15 (t, 1H, Ar-*H*); 7.26 (m, 1H, Ar-*H*); 7.33 (t, 2H, Ar-*H*); 7.41 (d, 1H, Ar-*H*); 7.46 (d, 2H, Ar-*H*); 7.53 (t, 1H, Ar-*H*); 7.75 (d, 1H, Ar-*H*); 8.53 (s, 1H, CHN); 10.25 (s, 1H, indole NH); 13.57 (s, 1H, NHCS). ¹H NMR (THF-*d*₈): δ 4.67 (s, 2H, SCH₂); 6.53 (m, 1H, Ar-*H*); 7.10 (t, 1H, Ar-*H*); 7.20-7.34 (m, 5H, Ar-*H*); 7.45 (d, 2H, Ar-*H*); 7.69 (d, 1H, Ar-*H*); 8.31 (s, 1H, CHN); 10.16 (s, 1H, indole NH); 12.37 (s, 1H, NHCS). ¹³C NMR (DMSO-*d*₆): δ 37.21 (SCH₂); 102.37, 116.56, 119.50, 123.96, 125.47, 126.53, 127.16, 128.34, 128.43, 129.08, 131.74, 137.22 (*Ar*); 147.93 (CHN); 194.88 (NHCS). ¹³C NMR (THF-*d*₈): δ 37.74 (SCH₂); 101.64, 116.23, 118.51, 123.14, 124.75, 124.82, 126.37, 127.60, 128.13, 128.48, 131.73, 136.58 (*Ar*); 145.98 (CHN); 195.23 (NHCS). IR (KBr, cm⁻¹): 3426 s (νNH); 3107 m (νNH); 1593 m; 1578 m; 1523 s; 1322 s; 1028 s (νCSS).

2.4.3 Synthesis of the complexes [M(HL)₂]

A solution of the appropriate hydrated metal acetate salt (1.0 mmol) in ethanol was added to a hot ethanolic solution of the Schiff base (0.65 g, 2.0 mmol). The mixture was refluxed for 30 min and then cooled to the room temperature. The complex that separated out was filtered off, washed with ethanol and dried over silica gel.

[Zn(HL¹)₂]: 0.636 g, 89%. *Anal.* Calc. for C₃₄H₂₈N₆S₄Zn: C, 57.17; H, 3.95; N, 11.77. Found: C, 56.89; H, 4.11; N, 11.42%. ¹H NMR (DMSO-*d*₆): δ 4.66 (s, 2H, SCH₂); 7.06 (t, 1H, Ar-*H*); 7.22-7.42 (m, 6H, Ar-*H*); 7.49 (d, 2H, Ar-*H*) 7.62 (d, 1H, Ar-*H*); 7.86 (s, 1H, CHN); 11.36 (s, 1H, indole NH). ¹³C NMR (DMSO-*d*₆): δ 35.69 (SCH₂); 112.31, 112.50, 120.54, 122.12, 125.22, 127.31, 127.33, 128.68, 128.99, 129.95, 136.94, 137.53 (*Ar*); 143.71 (CHN); 182.14 (NCS). IR (KBr, cm⁻¹): 3384 m (νNH); 1597 s (νCN); 1444 s; 1334 m; 1128 s; 1037 m, 940 m (νCSS).

Suitable crystals for crystallographic analysis were obtained from a DMF solution of the complex at room temperature.

[Ni(HL¹)₂].H₂O: 0.624 g, 86%. *Anal. Calc.* for C₃₄H₃₀N₆NiO₄: C, 56.28; H, 4.17; N, 11.58. Found: C, 56.08; H, 4.18; N, 11.39%. ¹H NMR (DMSO-*d*₆): δ 4,54 (s, 2H, SCH₂); 7.10 (t, 1H, Ar-*H*); 7.21 (t, 1H, Ar-*H*); 7.30 (t, 1H, Ar-*H*); 7.37 (t, 2H, Ar-*H*); 7.49 (m, 3H, Ar-*H*); 7.62 (d, 1H, Ar-*H*); 8.20 (s, 1H, CHN); 8.41 (d, 1H, Ar-*H*); 12.28 (s, 1H, indole NH). IR (KBr, cm⁻¹): 3405 br (νNH, νOH); 1582 m; 1560 s; 1451 br; 1340 s; 1128 s; 1028 m, 1011 m (νCSS). μ_{eff} = 0.00 B.M.

[Ni(HL²)₂]: 0.64 g, 91%. *Anal. Calc.* for C₃₄H₂₈N₆NiS₄: C, 57.71; H, 3.99; N, 11.88. Found: C, 57.10; H, 4.29; N, 12.03 %. ¹H NMR (DMSO-*d*₆): δ 4,53 (s, 2H, SCH₂); 7.10 (t, 1H, Ar-*H*); 7.21 (t, 1H, Ar-*H*); 7.29 (t, 1H, Ar-*H*); 7.36 (t, 2H, Ar-*H*); 7.48 (m, 3H, Ar-*H*); 7.62 (d, 1H, Ar-*H*); 8.19 (s, 1H, CHN); 8.40 (d, 1H, Ar-*H*); 12.28 (s, 1H, indole NH). IR (KBr, cm⁻¹): 3422 br (νNH); 1590 m; 1460 s; 1234 m; 1131 w; 1045 s, 971 m (νCSS). UV-Vis [λ_{max} (nm) solid]: 256; 326; 372; 430; 632. μ_{eff} = 0.00 B.M.

The X-ray quality crystal of [Ni(HL²)₂].2DMF was obtained by slow evaporation of a DMF solution of the complex at room temperature.

[Cd(HL²)₂]: 0.72 g, 93%. *Anal. Calc.* for C₃₄H₂₈CdN₆S₄: C, 53.64; H, 3.71; N, 11.04. Found: C, 53.21; H, 3.37; N, 11.34%. ¹H NMR (DMSO-*d*₆): δ 4.53 (s, 2H, SCH₂); 7.11-7.32 (m, 5H, Ar-*H*); 7.43-7.49 (m, 3H, Ar-*H*); 7.68 (d, 1H, Ar-*H*); 8.17 (s, 1H, Ar-*H*); 8.45 (s, 1H, CHN); 11.92 (s, 1H, indole NH). ¹³C NMR (DMSO-*d*₆): δ 35.64 (SCH₂); 107.93, 112.34, 117.31, 120.93, 122.50, 126.84, 126.95, 128.43, 128.98, 132.94, 135.32, 137.37 (Ar); 145.35(CHN); 178.59 (NCS). IR (KBr, cm⁻¹): 3394 m (νNH); 1591 s (νCN); 1230 sh; 1025 m, 932 s (νCSS).

The X-ray quality crystal of $[\text{Cd}(\text{HL}^2)_2(\text{py})_2]$.py₂ was obtained by slow evaporation of a pyridine solution of the complex at room temperature

[Zn(HL²)₂]: 0.648 g, 91%. *Anal.* Calc. for C₃₄H₂₈N₆S₄Zn: C, 57.17; H, 3.95; N, 11.77. Found: C, 57.65; H, 3.68; N, 11.49%. ¹H NMR (DMSO-*d*₆): δ 4.58 (s, 2H, SCH₂); 7.19-7.29 (m, 3H, Ar-*H*); 7.32-7.37 (m, 2H, Ar-*H*); 7.47-7.52 (m, 3H, Ar-*H*); 7.85 (d, 1H, Ar-*H*); 8.08 (s, 1H, CHN); 8.56 (d, 1H, *J*=2.8 Hz, Ar-*H*); 12.12 (s, 1H, indole NH). ¹³C NMR (DMSO-*d*₆): δ 36.44 (SCH₂); 108.31, 113.07, 118.29, 121.95, 123.40, 127.36, 127.76, 129.11, 129.60, 134.91, 136.00, 137.39 (*Ar*); 146.69 (CHN); 179.04 (NCS). IR (KBr, cm⁻¹): 3399 br (νNH); 1600 s (νCN); 1231 sh; 1209 w, 945 m (νCSS).

[Cd(HL³)₂]: 0.542 g, 71%. *Anal.* Calc. for C₃₄H₂₈CdN₆S₄: C, 53.64; H, 3.71; N, 11.04. Found: C, 53.17; H, 3.44; N, 10.67%. ¹H NMR (THF-*d*₈): δ 4.71 (s, 2H, SCH₂); 6.43 (t, 1H, *J* = 2.3 Hz, Ar-*H*); 6.99 (t, 1H, Ar-*H*); 7.18 (d, 1H, Ar-*H*); 7.20-7.28 (m, 4H, Ar-*H*); 7.48 (d, 2H, Ar-*H*); 7.60 (d, 1H, Ar-*H*); 8.66 (s, 1H, CHN); 10.23 (s, 1H, indole NH). ¹³C NMR (THF-*d*₈): δ 39.14 (SCH₂); 101.99, 117.79, 119.03, 123.18, 125.16, 125.48, 126.95, 128.27, 128.52, 129.12, 132.93, 137.96 (*Ar*); 152.46 (CHN); 190.00 (NCS). IR (KBr, cm⁻¹): 3407 s (νNH); 1590 sh; 1573 s; 1440 s; 1344 s; 1234 m; 1040 m, 982 m (νCSS).

The X-ray quality crystal of $[\text{Cd}(\text{HL}^3)_2(\text{py})_2]$ was obtained by slow evaporation of a pyridine solution of the complex at room temperature.

2.4.4 Synthesis of the complexes $[\text{M}(\text{L}^3)(\text{H}_2\text{O})]$

An ethanolic solution (20 mL) of H₂L³ (0.325 g, 1 mmol) and KOH (0.14 g, 2.5 mmol) was added dropwise to a solution of the metal(II) acetate (1.2 mmol) in the same

solvent (10 mL) with constant stirring. The resulting solution was refluxed for 30 min and then cooled to the room temperature. The brown nickel(II) complex precipitated during the reaction. The zinc(II) and cadmium(II) complexes were separated out on addition of water to the cooled solution. The solids were filtered off, washed with water several times and dried over silica gel.

[Zn(L³)(H₂O)]: 0.328 g, 81%. *Anal.* Calc. for C₁₇H₁₅N₃OS₂Zn: C, 50.19; H, 3.72; N, 10.33. Found: C, 50.02; H, 3.90; N, 10.04%. ¹H NMR (DMSO-*d*₆): δ 4.41 (s, 2H, SCH₂); 6.47 (d, 1H, Ar-*H*); 6.95 (t, 1H, Ar-*H*); 7.23 (t, 1H, Ar-*H*); 7.31 (t, 3H, Ar-*H*); 7.44 (d, 2H, Ar-*H*); 7.54 (d, 1H, Ar-*H*); 7.70 (d, 1H, Ar-*H*); 8.86 (s, 1H, CHN). ¹³C NMR (DMSO-*d*₆): δ 34.39 (SCH₂); 100.75, 116.23, 116.98, 123.98, 125.76, 126.82, 128.34, 129.18, 131.39, 137.55, 138.39, 140.65 (*Ar*); 157.96 (CHN); 175.28 (NCS). IR (KBr, cm⁻¹): 3409 br (νOH); 1600 sh; 1577 sh; 1552 sh; 1453 br; 1335 s; 1228 m; 1021 m, 957 s (νCSS).

[Cd(L³)(H₂O)]: 0.222 g, 49%. *Anal.* Calc. for C₁₇H₁₅CdN₃OS₂: C, 44.99; H, 3.33; N, 9.26. Found: C, 45.22; H, 3.06; N, 9.20%. ¹H NMR (DMSO-*d*₆): δ 4.39 (s, 2H, SCH₂); 6.47 (d, 1H, Ar-*H*); 6.92 (t, 1H, Ar-*H*); 7.21 (t, 1H, Ar-*H*); 7.27-7.31 (m, 3H, Ar-*H*); 7.40-7.43 (m, 3H, Ar-*H*); 7.68 (d, 1H, Ar-*H*); 8.86 (s, 1H, CHN). ¹³C NMR (DMSO-*d*₆): δ 34.88 (SCH₂); 100.99, 116.32, 117.86, 124.24, 127.28, 127.37, 128.84, 129.71, 132.05, 138.08, 139.15, 141.89 (*Ar*); 160.76 (CHN); 173.67 (NCS). IR (KBr, cm⁻¹): 3402 br (νOH); 1595 sh; 1576 sh; 1452 br; 1344 s; 1227 m; 1041 w, 945 m (νCSS).

[Ni(L³)(H₂O)]: 0.366 g, 91%. *Anal.* Calc. for C₁₇H₁₅N₃NiOS₂: C, 51.03; H, 3.78; N, 10.50. Found: C, 50.70; H, 3.68; N, 10.75%. IR (KBr, cm⁻¹): 3421 br (νOH); 1601 m; 1585

w; 1533 s; 1460 m; 1232 s; 1049 m, 986 w (ν_{CSS}). UV-Vis [λ_{max} (nm) solid]: 274; 381; 464. $\mu_{\text{eff}} = 1.50$ B.M.

[Ni(L³)(Et₃N)(H₂O)]: The complex was prepared following the general procedure for preparation of [M(L³)(H₂O)], except for using a few drops of triethylamine instead of KOH. 0.351 g, 70%. *Anal.* Calc. for C₂₃H₃₀N₄NiOS₂: C, 55.10; H, 6.03; N, 11.18. Found: C, 55.59; H, 4.34; N, 11.53%. IR (KBr, cm⁻¹): 3386 br (ν_{OH}); 1602 m; 1534 s; 1459 m; 1233 s; 1050 m, 981 w (ν_{CSS}). $\mu_{\text{eff}} = 1.13$ B.M.

The X-ray quality crystal of [Ni(L³)(py)] was obtained by slow evaporation of a solution of the complex in a mixture of pyridine and DMSO.

2.4.5 Crystallography

Suitable crystals for crystallographic analysis were mounted on a glass fiber using perfluoropolyether oil and cooled rapidly to 100 K in a stream of cold N₂. Diffraction data were measured using a Bruker SMART Apex II CCD area-detector diffractometer (graphite-monochromated Mo K α radiation, $\lambda = 0.71073$ Å). The orientation matrix, unit cell refinement and data reduction were all handled by the Apex2 software (SAINT integration, SADABS absorption correction) [49]. The structures were solved using direct or Patterson methods in the program SHELXS-97 [50] and were refined by the full matrix least-squares method on F^2 with SHELXL-97. All the non-hydrogen atoms were refined anisotropically and all the C-bound hydrogen atoms were placed at calculated positions and refined isotropically. N-bound hydrogen atoms were located in difference Fourier maps and refined with distance restraint of N-H 0.88 Å. Drawings of the molecules were produced with XSEED [51]. Crystal data and refinement are summarized in Tables 2-7, 2-8, and 2-9.

Crystallography data for the structures in chapter II have been deposited with the Cambridge Crystallographic Data Centre, CCDC Nos. 712538 (for $\mathbf{H}_2\mathbf{L}^1 \cdot 0.5\mathbf{EtOH}$), 709349 (for $\mathbf{H}_2\mathbf{L}^2$), 787620 (for $[\mathbf{Zn}(\mathbf{HL}^1)_2]$), 712350 (for $[\mathbf{Ni}(\mathbf{HL}^2)_2] \cdot 2\mathbf{DMF}$), 787621 (for $[\mathbf{Cd}(\mathbf{HL}^2)_2(\mathbf{py})_2] \cdot \mathbf{py}_2$), 787622 (for $[\mathbf{Cd}(\mathbf{HL}^3)_2(\mathbf{py})_2]$), 787623 (for $[\mathbf{Ni}(\mathbf{L}^3)(\mathbf{py})]$). These data can be obtained free of charge from The Cambridge Crystallographic Data Centre via www.ccdc.cam.ac.uk/data_request/cif.

Table 2-7 Crystal data and refinement parameters for **H₂L¹. 0.5EtOH** and **H₂L²**.

	H₂L¹. 0.5EtOH	H₂L²
Empirical formula	C ₁₇ H ₁₅ N ₃ S ₂	C ₁₈ H ₁₈ N ₃ O _{0.50} S ₂
Formula weight	325.44	348.47
Crystal system , Space group	Monoclinic, <i>P 21/c</i>	Monoclinic, <i>C 2/c</i>
Unit cell dimensions		
<i>a</i> (Å)	15.4936(7)	13.4225(2)
<i>b</i> (Å)	9.8114(4)	15.4088(2)
<i>c</i> (Å)	10.2531(4)	16.8120(3)
α (°)		
β (°)	98.432(3)	102.6370(10)
γ (°)		
Volume (Å ³)	1541.77(11)	3392.90(9)
Z, Density (calculated) (g cm ⁻³)	4, 1.402	8, 1.364
Absorption coefficient (mm ⁻¹)	0.344	0.320
<i>F</i> (000)	680	1464
θ range for data collection (°)	1.33 to 27.49	2.04 to 27.50
Reflections collected / unique	8531 / 3383 (<i>R</i> _{int} = 0.0575)	14302 / 3897 (<i>R</i> _{int} = 0.0278)
Completeness	To θ = 27.49 : 95.5 %	To θ = 27.50° : 99.9 %
Data / restraints / parameters	3383 / 2 / 205	3897 / 5 / 230
Goodness-of-fit on <i>F</i> ²	1.016	1.023
Final <i>R</i> indices [<i>I</i> >2 σ (<i>I</i>)]	<i>R</i> ₁ = 0.0488, <i>wR</i> ₂ = 0.0953	<i>R</i> ₁ = 0.0329, <i>wR</i> ₂ = 0.0803
<i>R</i> indices (all data)	<i>R</i> ₁ = 0.0818, <i>wR</i> ₂ = 0.1126	<i>R</i> ₁ = 0.0405, <i>wR</i> ₂ = 0.0853
Largest diff. peak and hole (e.Å ⁻³)	0.479 and -0.323	0.349 and -0.391

Table 2-8 Crystal data and refinement parameters for compounds [Zn(HL¹)₂], [Ni(HL²)₂].2DMF and [Cd(HL²)₂(py)₂].py₂.

	[Zn(HL ¹) ₂]	[Ni(HL ²) ₂].2DMF	[Cd(HL ²) ₂ (py) ₂].py ₂
Empirical formula	C ₃₄ H ₂₈ N ₆ S ₄ Zn	C ₄₀ H ₄₂ N ₈ NiO ₂ S ₄	C ₅₄ H ₄₈ CdN ₁₀ S ₄
Formula weight	714.23	853.77	1077.66
Crystal system , Space group	Orthorhombic, <i>P c a 21</i>	Monoclinic, <i>P 21/c</i>	Triclinic, <i>P -1</i>
Unit cell dimensions			
<i>a</i> (Å)	29.2662(4)	10.3808(3)	10.2268(13)
<i>b</i> (Å)	5.46790(10)	20.0219(7)	13.0466(17)
<i>c</i> (Å)	20.0663(3)	10.7831(3)	19.321(3)
<i>α</i> (°)			100.495(2)
<i>β</i> (°)		117.921(2)	91.444(2)
<i>γ</i> (°)			101.803(2)
Volume (Å ³)	3211.10(9)	1980.31(11)	2476.0(6)
Z, Density (calculated) (g cm ⁻³)	4, 1.477	2, 1.432	2, 1.445
Absorption coefficient (mm ⁻¹)	1.061	0.748	0.659
<i>F</i> (000)	1472	892	1108
<i>θ</i> range for data collection (°)	1.72 to 27.49	2.03 to 25.00	1.07 to 25.01
Reflections collected / unique	29190/ 7277 [<i>R</i> _{int} = 0.0631]	13342 / 3481 [<i>R</i> _{int} = 0.0619]	11675/ 8504 [<i>R</i> _{int} = 0.0289]
Completeness	To <i>θ</i> = 25.25° : 100.0 %	To <i>θ</i> = 25.00 : 100.0 %	To <i>θ</i> = 25.01° : 97.4 %
Data / restraints / parameters	7277 / 3 / 413	3481 / 1 / 256	8504 / 416 / 628
Goodness-of-fit on <i>F</i> ²	1.009	1.027	1.030
Final <i>R</i> indices [<i>I</i> > 2σ (<i>I</i>)]	<i>R</i> ₁ = 0.0463, <i>wR</i> ₂ = 0.1025	<i>R</i> ₁ = 0.0397, <i>wR</i> ₂ = 0.0819	<i>R</i> ₁ = 0.0564, <i>wR</i> ₂ = 0.1308
<i>R</i> indices (all data)	<i>R</i> ₁ = 0.0640, <i>wR</i> ₂ = 0.1122	<i>R</i> ₁ = 0.0606, <i>wR</i> ₂ = 0.0908	<i>R</i> ₁ = 0.0966, <i>wR</i> ₂ = 0.1585
Largest diff. peak and hole (e.Å ⁻³)	2.063 and -0.338	0.503 and -0.289	0.902 and -0.553

Table 2-9 Crystal data and refinement parameters for compounds [Cd(HL³)₂(py)₂] and [Ni(L³)(py)].

	[Cd(HL ³) ₂ (py) ₂]	[Ni(L ³)(py)]
Empirical formula	C ₄₄ H ₃₈ CdN ₈ S ₄	C ₂₂ H ₁₈ N ₄ NiS ₂
Formula weight	919.46	461.23
Crystal system , Space group	Orthorhombic, <i>Pccn</i>	Monoclinic, <i>Pc</i>
Unit cell dimensions		
<i>a</i> (Å)	9.8897(18)	5.9660(4)
<i>b</i> (Å)	20.836(4)	15.0622(12)
<i>c</i> (Å)	20.652(4)	11.2428(9)
α (°)		
β (°)		94.441(6)
γ (°)		
Volume (Å ³)	4255.6(14)	1007.26(13)
Z, Density (calculated) (g cm ⁻³)	4, 1.435	2, 1.521
Absorption coefficient (mm ⁻¹)	0.751	1.187
<i>F</i> (000)	1880	476
θ range for data collection (°)	1.97 to 25.25	2.26 to 25.99
Reflections collected / unique	15959/ 3842 [<i>R</i> _{int} = 0.0686]	8122/ 3902 [<i>R</i> _{int} = 0.1155]
Completeness	To $\theta = 25.25^\circ$: 99.6 %	To $\theta = 25.00^\circ$: 99.9 %
Data / restraints / parameters	3842 / 169 / 261	3902 / 2 / 263
Goodness-of-fit on <i>F</i> ²	1.016	1.018
Final <i>R</i> indices [<i>I</i> > 2 σ (<i>I</i>)]	<i>R</i> ₁ = 0.0377, <i>wR</i> ₂ = 0.0705	<i>R</i> ₁ = 0.0668, <i>wR</i> ₂ = 0.1307
<i>R</i> indices (all data)	<i>R</i> ₁ = 0.0760, <i>wR</i> ₂ = 0.0830	<i>R</i> ₁ = 0.1076, <i>wR</i> ₂ = 0.1488
Largest diff. peak and hole (e.Å ⁻³)	0.397 and -0.417	0.859 and -0.617

CHAPTER III

*Indole-based gallic acid derivatives:
antioxidant, cytotoxic activities, and
structure-activity relationship*

3.1 Introduction

The generation of reactive oxygen species (ROS) and reactive nitrogen species (RNS) has been considered to be a possible mediator of cellular damage in many diseases [52]. Human bodies are constantly exposed to ROS and RNS generated from endogenous and some exogenous sources. Antioxidants, both enzymatic and non-enzymatic, prevent oxidative damage to biological molecules by various mechanisms. Polyphenols constitute an important class of chemopreventive agents because they can quench or prevent the formation of ROS and RNS [53]. The ability of phenolic compounds to quench free radicals arises because of both their acidity (ability to donate protons) and their delocalized π -electrons (ability to transfer electrons while remaining relatively stable) characteristic of benzene rings. Among polyphenols, gallic acid (3,4,5-trihydroxybenzoic acid) derivatives are a well-known group of naturally occurring compounds which have been found in many phytochemicals. In recent years, a number of their biological and pharmacological activities have been described which has stimulated much interests in the development of synthetic gallic acid derivatives [54-62]. These compounds have been proven to have various biological properties including neuroprotective, antioxidant [63] and anticancer activities [64]. Several studies have demonstrated that gallic acid and its derivatives can selectively induce cancer cell death by apoptosis without harming healthy cells [65-67].

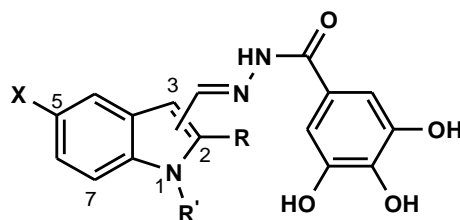
Indole derivatives are biologically important chemicals with a wide range of therapeutic properties. Antibacterial [15], antifungal [16], antiviral [17], antimalarial [18], anti-HIV [19], anticancer [20-22] and antioxidant [23,24] properties have been reported to be associated with the indolic nucleus. Indolic compounds are very efficient antioxidants, protecting both lipids and proteins from peroxidation, and it is known that the indole structure influences the antioxidant efficacy in biological systems [68].

In the design of new drugs, the development of hybrid molecules through the combination of different pharmacophores in one frame may lead to compounds with interesting pharmacological properties. The co-administration of the moieties, acting by different mechanisms may have a synergistic effect, resulting in a higher activity than each of the components separately. In the light of interesting biological activities associated with gallic acid derivatives and indolic compounds, it was considered worthwhile to synthesize some hybrid molecules incorporating both indole and 3,4,5-trihydroxy benzoyl nucleus. The synthesized compounds were investigated for their antioxidant and cytotoxic activities.

3.2 Results

3.2.1 Chemistry

The structures of the synthesized compounds are presented in Table 3-1. The gallic hydrazide moiety is connected *via* an imine link on the indole nucleus, at different position (2, 3 or 7). Compounds differentiate also in substitution at position 1, 2 and 5 of the indole nucleus. The compounds were synthesized upon the reaction of the appropriate indole carboxaldehydes with gallic hydrazide which had itself been prepared from the reaction between methyl 3,4,5-trihydroxybenzoate and hydrazine. The synthetic route is depicted in Scheme 1. All the compounds were characterized by elemental analysis and spectroscopic methods. The structures of compounds **3a**, **3e** and **3f** were further established by X-ray crystallographic analysis.

Table 3-1 Structure of the synthesized indole gallic hydrazones

Compound	Position of the Gallic hydrazone moiety	X	R	R'
2a	2	H	-	H
3a	3	H	H	H
3b	3	H	H	CH ₃
3c	3	H	CH ₃	H
3d	3	CH ₃	H	H
3e	3	Cl	H	H
3f	3	Br	H	H
7a	7	H	H	H

3.2.2 *In vitro* antioxidant activities

The synthesized compounds were subjected to DPPH radical scavenging and lipid peroxidation inhibitory assays to determine their antioxidant activity. The results were compared with Ascorbic acid and α -tocopherol. All the tested compounds showed noticeable DPPH radical scavenging activity, with IC₅₀ values of 0.17- 0.37mM, when compared to the reference compounds, ascorbic acid and α -tocopherol with IC₅₀ values of 0.98 and 0.91mM, respectively (Table 3-2). Among them, compounds **3e** and **3f** with a

halogen group in position 5 of the indole ring showed the highest activity. All the compounds under study also possessed inhibitory effect of lipid peroxidation. The effect of the test compounds and α -tocopherol (positive control) on their reaction with lipid is shown in Table 3-2. The results show a very similar trend to the one of DPPH radical scavenging assay. The halogenated compounds, **3e** and **3f**, showed strong inhibitory activity, with the lowest IC₅₀ values, and comparable to α -tocopherol.

Table 3-2 DPPH radical scavenging activity and anti-lipid peroxidation (LP) activities of **2a-7a**¹.

Compound	DPPH IC₅₀ (μM)	LP IC₅₀ (nM)
2a	357 \pm 12 ^{a,b}	403 \pm 8 ^a
3a	259 \pm 4 ^{c,d}	344 \pm 9 ^b
3b	303 \pm 10 ^{a,d}	621 \pm 4 ^c
3c	216 \pm 9 ^{c,e}	179 \pm 4 ^d
3d	358 \pm 10 ^{a,b}	713 \pm 18 ^e
3e	189 \pm 8 ^e	29 \pm 3 ^f
3f	172 \pm 9 ^e	50 \pm 3 ^f
7a	373 \pm 12 ^b	657 \pm 16 ^c
Ascorbic acid	981 \pm 7 ^f	–
α-tocopherol	911 \pm 19 ^g	38 \pm 6 ^f

¹The values represent the mean \pm S.E.M. of three determinations. Values in a column with the same superscript letter are not significantly different, $P < 0.05$ (ANOVA and Tukey's test).

3.2.3 Cytotoxic activities

The synthesized compounds were tested for their cytotoxic activity on HCT-116 and MCF-7 cell lines by the MTT assay. As shown in Table 3.3, all the compounds have comparable activities with the positive control, curcumin. The highest activities against MCF-7 cell line were found for the halogenated compounds **3e** and **3f** with IC₅₀ values of 19.2 μM and 13.3 μM respectively. A similar trend was observed with HCT-116 cell line, with the halogenated compounds **3e** and **3f** yielding the lowest IC₅₀ values, 6.7 μM. Figure 3-1 displays the effect of increasing concentrations of the compounds on the cancer lines. It is apparent that the cell viability decreased almost linearly as a function of the log concentration of the compounds.

Table 3-3 Cytotoxic activity of **2a-7a**¹.

Compound	IC ₅₀ (μM)	
	MCF-7	HCT116
2a	40.0±2.5 ^{a,b}	29.4±1.6 ^a
3a	46.9±3.1 ^b	29.2±2.8 ^a
3b	35.1±2.8 ^{a,b}	30.0±3.7 ^a
3c	27.9±3.1 ^{a,c}	21.0±1.5 ^{a,b}
3d	39.0±2.1 ^{a,b}	29.4±3.0 ^a
3e	19.2±1.1 ^{c,d}	6.7±0.1 ^c
3f	13.3±0.9 ^d	6.7±0.2 ^c
7a	44.4±1.6 ^b	29.9±0.1 ^a
Curcumin	34.7±3.5 ^{a,b}	13.7 ± 0.9 ^{b,c}

¹The values represent the mean ± S.E.M. of three determinations. Values in a column with the same superscript letter are not significantly different, $P < 0.05$ (ANOVA and Tukey's test).

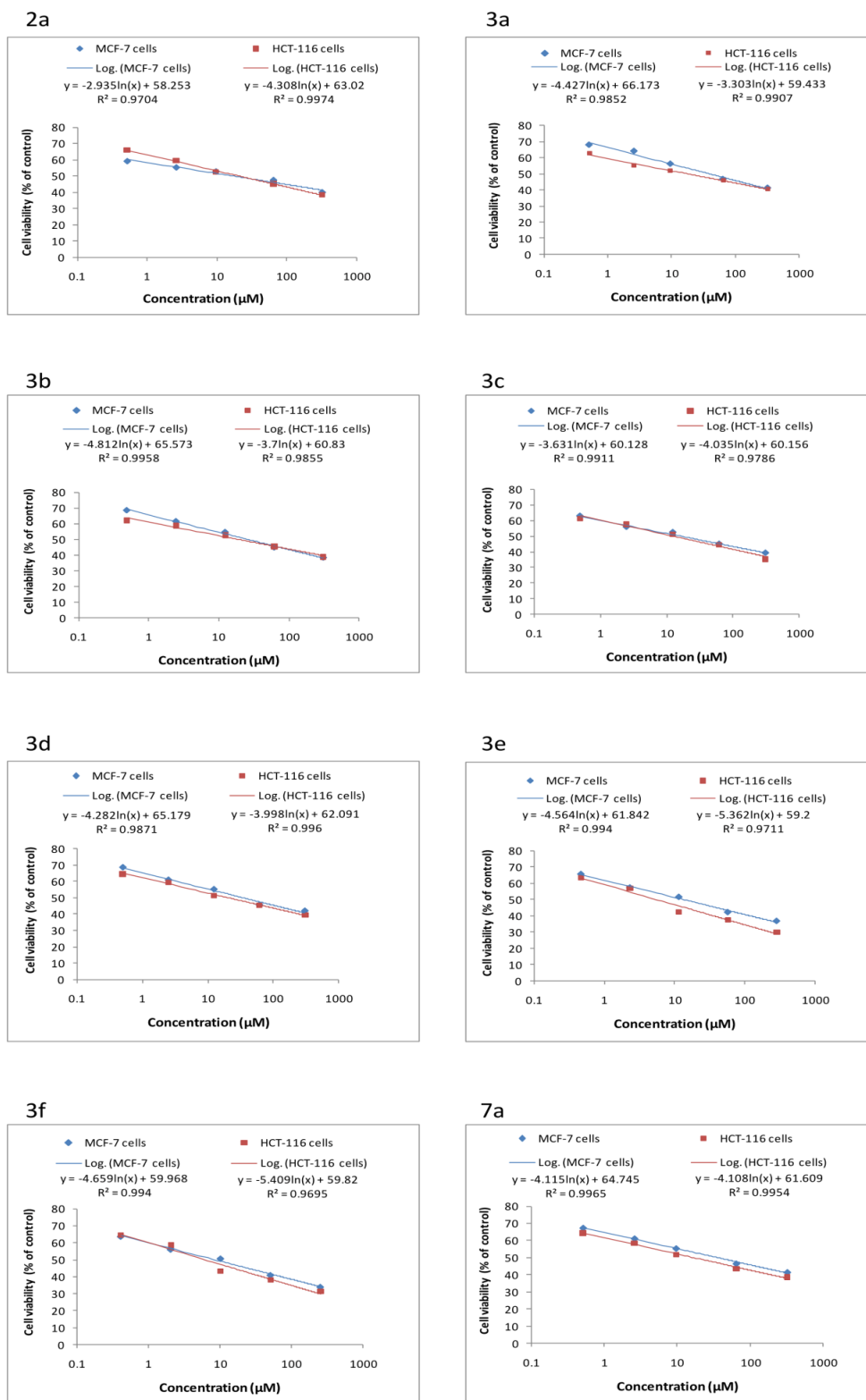


Figure 3-1 Dose-response curves of MCF-7 and HCT-116 cells to varying concentrations of compounds **2a-7a**.

3.3 Discussion

The present study was conducted to investigate structure-activity relationship for the antioxidant and cytotoxic activities of hybrid molecules containing indole and gallic hydrazone moieties. Eight different indole gallic hydrazones were synthesized and tested for their antioxidant potency by well known *in vitro* well known antioxidant assays, DPPH radical scavenging ability and lipid peroxidation inhibitory. It is well established that gallic acid derivatives possess antioxidant properties. The antioxidant activity of these phenolic compounds is mainly due to their redox properties, which can play an important role in the absorption and neutralization of free radicals, the quenching of singlet and triplet oxygen, or the decomposition of peroxides [69]. Likewise, indolic compounds are known to have antioxidant properties. The active redox center of indoles is the nitrogen atom. Replacement of the nitrogen by oxygen significantly reduces antioxidant activity [70]. Delocalization of the nitrogen electron pair over the aromatic system seems to be of great importance for antioxidant activity of indole derivatives. It is reasonable to conclude that multiple mechanisms regulate antioxidant action of the hybrid molecules, although they may contribute to the antioxidant activity to different degrees.

All the tested compounds showed significant DPPH radical scavenging activity and with a very similar trend, inhibitory effect on lipid peroxidation. Comparison of the activity of compounds **2a**, **3a** and **7a** shows the importance of the attachment position of the imine link, while the activities of the other compounds reveal the effect of the substitution patterns of the halogen or methyl group. The higher antioxidant activity of compound **3a** compared to **2a** and **7a** can be explained by the fact that the attachment of the gallic hydrazone at the 3-position permits stabilization of the indolyl cation radical intermediate by the conjugated imine side chain without disruption of the benzene

aromaticity. Introduction of a chlorine or bromine atom in position 5 of the indole moiety significantly enhances the antioxidant activity. Thus, compounds **3e** and **3f** show the highest activities among all the target compounds. This might be ascribed to the electron donating properties of the halogens by resonance, making the lone pair electron on the indole nitrogen atom more available to a plausible electron transfer. However, some other factors may be involved, as there are some reports which show different influences by halogens in the 5-position of indole [23,71]. The effect of a methyl substituent depends on its attached position. Compound **3c**, with a methyl group in 2-position, has a higher activity than the unsubstituted compound **3a**, whereas introduction of a methyl group on the indole nitrogen or at the 5-position diminishes the antioxidant activity.

For further assessment, the compounds were subjected to cytotoxicity assay against HCT-116 and MCF-7 cell lines. In a previously reported study on cytotoxic and antioxidant activities of some phenolic systems (hydroxycinnamic acid derivatives), a positive structure-activity-property relationship between the activities was observed. It was suggested that the antitumor activity of phenolic derivatives is highly dependent upon their conformational characteristics, which, in turn determine their antioxidant properties [65]. The considerable antioxidant activities of our synthesized molecules intrigued us to know how relevant these results are to their cytotoxic activity. According to the *in vitro* results, the target compounds have comparable activities with the positive control, curcumin. In excellent agreement with antioxidant efficiency, the halogenated compounds, **3e** and **3f**, showed the highest activities against both cell lines with IC₅₀ values lower than curcumin. Furthermore, consistent with the antioxidant activity results, the replacement of the hydrogen in position 2 by a methyl group enhanced the cytotoxicity, thus, compound **3c** is more active than **3a**. To a lesser extent, introduction of a methyl group on the indole

nitrogen (**3b**) or at position 5 of the indole moiety (**3d**) also increased the activity against MCF-7 cells, while it did not show any obvious effects on HCT-116 cell line (**3a** ~ **3b** ~ **3d**). A discrepancy was also observed with the effect of the position of the imine link on the indole system. While the 3-imineindole **3a** showed higher antioxidant activity compared to the 2-imineindole, **2a**, and the 7-imineindole, **7a**, the cytotoxicity effectiveness against MCF-7 cell line followed the order of **2a** > **7a** > **3a**. These three compounds showed almost the same effect on HCT-116 cells. Overall, the results obtained from this study showed a limited correlation between the antioxidant and cytotoxic properties of the synthesized compounds.

3.4 Conclusions

In conclusion, we have designed a series of hybrid molecules on the basis of the biological significance of indole and gallic acid. With a high degree of consistency, the compounds showed significant antioxidant activities in DPPH radical scavenging and inhibitory of lipid peroxidation assays. The compounds also exhibited noticeable cytotoxicity against HCT-116 and MCF-7 cell lines. A limited degree of agreement was observed between cytotoxic and antioxidant activities. The activities are dependant on the position of the imine link and different substituents on indole moiety. Among all, the halogenated compounds, **3e** and **3f**, are the most efficient compounds. Further study is required to understand the mechanisms of action of this class of compounds.

3.5 Experimental

Melting points were determined using a MEL-TEMP II melting point instrument and were not corrected. Microanalyses were carried out on a Perkin-Elmer 2400 elemental analyzer. $^1\text{H-NMR}$ and $^{13}\text{C-NMR}$ spectra were determined with a JEOL Lambda 400 MHz FT-NMR (^1H : 400 MHz and ^{13}C : 100.4 MHz) spectrometer. Chemical shifts are given in δ values (ppm) using TMS as the internal standard. X-ray diffraction data were collected on a Bruker APEX II CCD diffractometer using Mo $K\alpha$ radiation. The structures were solved by direct methods and refined by a full-matrix least-squares procedure based on F^2 .

3.5.1 Synthesis of 3,4,5-trihydroxybenzoic hydrazide (gallic hydrazide)

A mixture of methyl 3,4,5-trihydroxybenzoate (9.2 g, 50 mmol) and hydrazine hydrate (45 ml) was stirred at room temperature for 30 minutes until the ester was dissolved completely. Ethanol (250 ml) was added to the mixture and it was stirred under reflux for 6 h and then at room temperature overnight. The white solid was filtered, washed with ethanol and dried over silica gel to give 5.13 g, 56% gallic hydrazide.

3.5.2 Synthesis of gallic acid hydrazones 2a-7a

An equimolar (5 mmol) mixture of indole carboxaldehyde and 3,4,5-trihydroxybenzoylhydrazine in the presence of acetic acid (1 ml) was heated in ethanol (70 ml) for 6 h. The solution was then cooled and filtered to remove the unreacted hydrazide. The hydrazide was washed with ethanol and the filtrates added together, evaporated partially and poured to water (400 ml). The solid product formed was filtered off, washed

with diethyl ether and dried over silica gel to give the related indole gallic hydrazone with 57-77% yield.

3,4,5-Trihydroxy-N'-[(1H-indol-2-yl)methylidene]benzohydrazide (2a). Yield 68%, mp 261-263 °C; ¹H NMR (DMSO-*d*₆): δ 6.77 (s, 1H, Ar-*H*), 6.93 (s, 2H, Ar-*H*), 6.99 (t, 1H, Ar-*H*), 7.13 (t, 1H, Ar-*H*), 7.42 (d, 1H, Ar-*H*), 7.54 (d, 1H, Ar-*H*), 8.43 (s, 1H, CHN), 9.13 (br, 3H, OH), 11.50 (s, 1H, NH), 11.53 (s, 1H, NH); ¹³C NMR (DMSO-*d*₆): 106.26, 107.17, 111.92, 120.66, 123.16, 123.36, 127.68, 133.50, 136.96, 137.72, 139.34 (CHN), 145.57, 163.16 (CONH); Anal. Calcd for C₁₆H₁₃N₃O₄: C, 61.73; H, 4.21; N, 13.50%. Found: C, 61.20; H, 4.98; N, 13.10%.

3,4,5-Trihydroxy-N'-[(1H-indol-3-yl)methylidene]benzohydrazide (3a). Yield 73%, mp 238-240°C; ¹H NMR (DMSO-*d*₆): δ 6.92 (s, 2H, Ar-*H*), 7.16 (t, 1H, Ar-*H*), 7.20 (t, 1H, Ar-*H*), 7.43 (d, 1H, Ar-*H*), 7.76 (s, 1H, Ar-*H*), 8.28 (d, 1H, Ar-*H*), 8.57 (s, 1H, Ar-*H*), 8.75 (s, 1H, OH), 9.13 (s, 2H, OH), 11.21 (s, 1H, indole NH), 11.53 (s, 1H, CONH); ¹³C NMR (DMSO-*d*₆): 107.45, 112.22, 112.33, 120.97, 122.41, 123.22, 124.34, 124.76, 130.39, 137.14, 137.41, 144.92 (CHN), 145.95, 163.57 (CONH); Anal. Calcd for C₁₆H₁₃N₃O₄: C, 61.73; H, 4.21; N, 13.50%. Found: C, 61.44; H, 4.75; N, 13.17%.

The solid state structure of **3a** was established by X-ray crystallographic analysis. CCDC 712568 contains the crystallographic data for the structure.

3,4,5-Trihydroxy-N'-[(1-methyl-1H-indol-3-yl)methylidene]benzohydrazide (3b). Yield 65%, mp 256-258 °C; ¹H NMR (DMSO-*d*₆): δ 3.81 (s, 3H, CH₃), 6.92 (s, 2H, Ar-*H*), 7.17 (t, 1H, Ar-*H*), 7.26 (t, 1H, Ar-*H*), 7.48 (d, 1H, Ar-*H*), 7.75 (s, 1H, Ar-*H*), 8.28 (d, 1H, Ar-*H*), 8.54 (s, 1H, Ar-*H*), 8.72 (s, 1H, OH), 9.10 (s, 2H, OH), 11.19 (s, 1H, CONH); ¹³C NMR (DMSO-*d*₆): 32.76 (CH₃), 107.04, 110.14, 110.99, 120.55, 122.18, 122.67, 124.11,

124.79, 133.48, 136.59, 137.54, 143.38 (CHN), 145.56, 162.70 (CONH); Anal. Calcd for C₁₇H₁₅N₃O₄: C, 62.76; H, 4.65; N, 12.92%. Found: C, 63.01; 4.89; N, 12.57%.

3,4,5-Trihydroxy-N'-(2-methyl-1H-indol-3-yl)methylidene]benzohydrazide (3c).

Yield 77%, mp 284-286 °C; ¹H NMR (DMSO-*d*₆): δ 2.50 (s, 3H, CH₃), 6.69 (s, 2H, Ar-*H*), 7.10 (m, 2H, Ar-*H*), 7.32 (d, 1H, Ar-*H*), 8.21 (d, 1H, Ar-*H*), 8.66 (s, 1H, Ar-*H*), 8.76 (s, 1H, OH), 9.12 (s, 2H, OH), 11.10 (s, 1H, indole NH), 11.41 (s, 1H, CONH); ¹³C NMR (DMSO-*d*₆): 11.50 (CH₃), 106.98, 107.78, 110.79, 120.13, 121.27, 121.75, 124.20, 125.47, 135.72, 136.53, 139.54, 143.57 (CHN), 145.59, 162.46 (CONH); Anal. Calcd for C₁₇H₁₅N₃O₄: C, 62.76; H, 4.65; N, 12.92. Found: C, 62.51; H, 5.05; N, 13.00%.

3,4,5-Trihydroxy-N'-(5-methyl-1H-indol-3-yl)methylidene]benzohydrazide (3d).

Yield 65%, mp 259-260 °C; ¹H NMR (DMSO-*d*₆): δ 2.41 (s, 3H, CH₃), 6.91 (s, 2H, Ar-*H*), 7.01 (d, 1H, Ar-*H*), 7.30 (d, 1H, Ar-*H*), 7.69 (s, 1H, Ar-*H*), 8.05 (s, 1H, Ar-*H*), 8.54 (s, 1H, Ar-*H*), 8.70-9.10 (br, 3H, OH), 11.15 (s, 1H, indole NH), 11.41 (s, 1H, CONH); ¹³C NMR (DMSO-*d*₆): 21.58 (CH₃), 107.28, 111.65, 111.76, 121.85, 124.29, 124.48, 124.86, 129.41, 130.33, 135.63, 136.90, 144.88 (CHN), 145.79, 163.18 (CONH); Anal. Calcd for C₁₇H₁₅N₃O₄: C, 62.76; H, 4.65; N, 12.92. Found: C, 62.35; H, 4.98; N, 13.06%.

3,4,5-Trihydroxy-N'-(5-chloro-1H-indol-3-yl)methylidene]benzohydrazide (3e).

Yield 67%, mp 274-276 °C; ¹H NMR (DMSO-*d*₆): δ 6.89 (s, 2H, Ar-*H*), 7.18 (dd, 1H, Ar-*H*), 7.42 (d, 1H, Ar-*H*), 7.82 (d, 1H, Ar-*H*), 8.28 (s, 1H, Ar-*H*), 8.52 (s, 1H, Ar-*H*), 8.77 (s, 1H, OH), 9.13 (s, 2H, OH), 11.26 (s, 1H, indole NH), 11.69 (s, 1H, CONH); ¹³C NMR (DMSO-*d*₆): δ 107.52, 112.22, 113.90, 121.71, 123.08, 124.44, 125.46, 125.87, 131.93, 136.02, 137.14, 143.84 (CHN), 146.05, 163.25 (CONH); Anal. Calcd for C₁₆H₁₂ClN₃O₄: C, 55.58; H, 3.50; N, 12.15. Found: C, 55.76; H, 3.89; N, 11.96%.

The solid state structure of **3e** was established by X-ray crystallographic analysis. CCDC 717359 contains the crystallographic data for the structure.

3,4,5-Trihydroxy-N'-[(5-bromo-1H-indol-3-yl)methylidene]benzohydrazide (3f).

Yield 71%, mp 273-275 °C; ¹H NMR (DMSO-*d*₆): δ 6.89 (s, 2H, Ar-*H*), 7.29 (dd, 1H, Ar-*H*), 7.38 (d, 1H, Ar-*H*), 7.81 (d, 1H, Ar-*H*), 8.42 (s, 1H, Ar-*H*), 8.51 (s, 1H, Ar-*H*), 8.77 (s, 1H, OH), 9.13 (s, 2H, OH), 11.26 (s, 1H, indole NH), 11.70 (s, 1H, CONH); ¹³C NMR (DMSO-*d*₆): δ 107.51, 112.11, 113.51, 114.37, 124.43, 124.72, 125.63, 126.51, 131.79, 136.27, 137.14, 143.88 (CHN), 146.05, 163.45 (CONH); Anal. Calcd for C₁₆H₁₂BrN₃O₄: C, 49.25; H, 3.10; N, 10.77. Found: C, 49.70; H, 3.43; N, 10.70%

The solid state structure of **3f** was established by X-ray crystallographic analysis. CCDC 709350 contains the crystallographic data for the structure.

3,4,5-Trihydroxy-N'-[(1H-indol-7-yl)methylidene]benzohydrazide (7a). Yield 57%, mp 237-240 °C; ¹H NMR (DMSO-*d*₆): δ 6.56 (m, 1H, Ar-*H*), 6.98 (s, 2H, Ar-*H*), 7.12 (t, 1H, Ar-*H*), 7.31 (d, 1H, Ar-*H*), 7.53 (s, 1H, Ar-*H*), 7.68 (d, 1H, Ar-*H*), 8.63 (s, 1H, CHN), 8.88 (s, 1H, OH), 9.22 (s, 2H, OH), 10.91 (s, 1H, indole NH), 11.81 (s, 1H, CONH); ¹³C NMR (DMSO-*d*₆): 102.3, 107.30, 118.10, 119.23, 122.73, 123.07, 124.04, 126.21, 128.23, 131.89, 137.26, 145.72, 147.55 (CHN), 163.44 (CONH); Anal. Calcd for C₁₆H₁₃N₃O₄: C, 61.73; H, 4.21; N, 13.50%. Found: C, 62.2; H, 5.11; N, 13.77%.

3.5.3 DPPH free radical scavenging activity

Radical scavenging activity was determined by a spectrophotometric method based on the reduction of an ethanol solution of 1,1-diphenyl-2-picrylhydrazyl (DPPH) [72].

Briefly, to a solution of DPPH (200 μ M) in absolute ethanol, the compound dissolved in DMSO was added at various concentrations. All the samples were incubated in dark for 30 minutes at room temperature. When DPPH reacts with an antioxidant, it will be reduced. The change in color (from purple to yellow) was measured spectrophotometrically at 517 nm for each sample after incubation. Ascorbic acid and α -tocopherol were used as positive controls. The free radical scavenging activity of the compounds was calculated as a percentage of radical reduction. Each experiment was carried out in triplicates and each experiment was performed three times. IC₅₀ values were determined from a calibration curve for each compound. The radical scavenging activity was obtained from the equation:

$$\text{Percentage of scavenging activity (\%)} = [1 - (A_s/A_c)] \times 100$$

where A_c is the absorbance of control (DPPH solution + DMSO) and A_s is the absorbance of compound/positive control.

3.5.4 Lipid Peroxidation Assay

The lipid peroxidation assay was carried out following the previously described method [73]. Fowl egg yolk, comprising mainly of phospholipids, triacylglycerols and proteins, was used as an alternative to rat liver microsomes and linoleic acid. The reactive mixture for inducing lipid peroxidation contained 1ml egg yolk emulsified with phosphate buffer saline (0.1 M, pH 7.4), to obtain a final concentration of 12.5 g/l and 200 μ l of 3000 μ M FeSO₄. 40-43 mg (1×10^{-4} M) of each test compound was dissolved in 1ml DMSO (100%). This stock solution was then diluted to final extraction concentration 1×10^{-4} , 1×10^{-5} , 1×10^{-6} , 1×10^{-7} , 1×10^{-8} , 1×10^{-9} and 1×10^{-10} M. Each assay was carried out in triplicates. The mixture was incubated at 37°C for 1 hour, after which it was treated with 0.5 ml of

freshly prepared 15% TCA and 1.0 ml of 1% TBA. The reaction tubes were kept in boiling water bath for 10 minutes. Upon cooling, the tubes were centrifuged at 3500 g for 10 minutes to remove precipitated protein. LP was measured spectrometrically by estimation of thiobarbituric reactive substances (TBARS). The formation of TBARS was measured by removing 100 μ l of supernatant and measuring the absorbance at 532 nm. α -Tocopherol ranging from 1×10^{-4} to 1×10^{-10} M was used as the standard reference. The control was buffered egg with FeSO₄ only. The percentage of inhibition was calculated from the following equation:

$$\% \text{ inhibition} = [1 - (A_s/A_0)] \times 100$$

where A_0 refers to the absorbance of the control and A_s is the absorbance of the sample. To determine the concentration required to achieve 50% inhibition (IC₅₀) of phospholipid oxidation in egg yolk, the percentage of lipid peroxidation inhibition was plotted against extract concentration.

3.5.5 Cell culture

The human colon carcinoma HCT-116 and hormone-dependent breast carcinoma MCF7 were purchased from the American Type Culture Collection (ATCC, USA). HCT 116 and MCF 7 cells in RPMI 1640 Medium (Sigma), supplemented with 10 % (v/v) heat-inactivated fetal bovine serum (FBS, PAA Lab, Austria), 100 μ g/ml streptomycin and 100 unit/ml penicillin (PAA Lab, Austria) and 50 μ g/ml fungizone (PAA Lab, Austria). The media were filter sterilized using a 0.22 μ m filter membrane (Minisart, Sartorius stedim). The cells were cultured in 5 % CO₂ incubator at 37° C in a humidified atmosphere. The culture was subcultured every 2 or 3 days and routinely checked under an inverted

microscope (Motic) for any contamination. Cells in the exponential growth phase were used for all experiments. The cells were harvested from culture flasks by accutase (Innovative Cell Technologies) and the viable cell count was determined using trypan blue exclusion assay with a hemocytometer.

3.5.6 MTT cytotoxicity assay

MTT [3-(4,5-dimethylthiazol-2-yl)-2,5-diphenyltetrazolium bromide] assay was modified from Mossmann [74]. Cells were seeded at density of 5,000 cells/well into a 96-well flat-bottomed culture plates (Orange Scientific) and allowed to adhere overnight. The experimental compounds were predissolved in dimethyl sulphoxide (DMSO) and diluted to the required concentration (five concentrations, 0.1-100 µg/ml), such that the total DMSO concentration did not exceed 0.5%. At this concentration, DMSO was found to be nontoxic to the cells tested. Vehicle DMSO was used as a control. Cells were incubated with the samples (three wells on a plate for each concentration) for 72 hours. Treated and untreated cells were inspected qualitatively using an inverted light microscope (x 20). Then, 20 µl of MTT (5 mg/ml) (Sigma) was added to each well and the plates were incubated at 37 °C for 4 hour. The media was then gently aspirated, and 150µl DMSO was added to dissolve the formazan crystals. The amount of formazan product was measured spectrophotometrically at 570 nm and 650nm as a background using a microplate reader (Oasys UVM340).

The percentage of viability = (absorbance of treated cells/ absorbance of untreated cells) x 100.

CHAPTER IV

*Coordination behavior of
2-(diformylmethylene)-3,3-dimethylindole
towards late-transition-metal ions*

4.1 Introduction

The combination of coordinate bonding with intermolecular interactions, such as hydrogen bonding and π - π interactions, in metal complexes of multidentate organic ligands provides intriguing prospects for the design of novel metal-organic supramolecular architectures. In this context, the geometries of the metal centers and certain features of the ligands, such as flexibility, versatile bonding modes, and the ability to undertake hydrogen bonding, can heavily control the self-assembly process, thus the structure and properties of the products. The architecture of the products can be predictable to a high degree when rigid ligands are used [75-77] whereas, utilizing ligands with more flexibility reduces the structure predetermination and may afford unique frameworks with interesting properties [78-80].

Some years ago, Helliwell and coworkers described the synthesis and crystal structure of 2-(diformylmethylidene)-3,3-dimethylindole [81]. The structure of this aminomethylene-malonaldehyde offers an interesting potential ambidentate ligand owing to the presence of disparate coordination sites, capable of showing ketoamine-enolimine tautomerism (Figure 4-1).

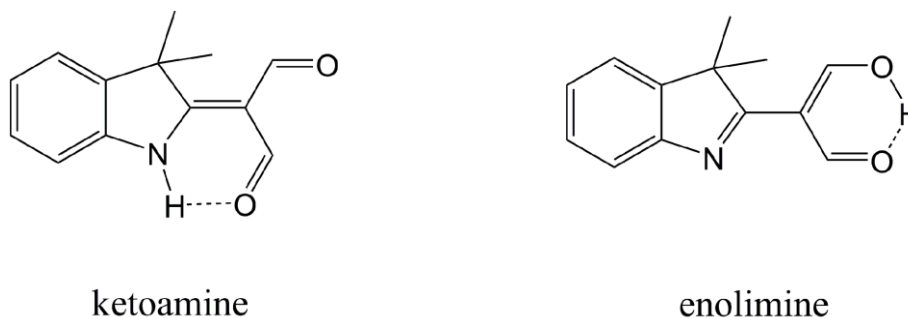


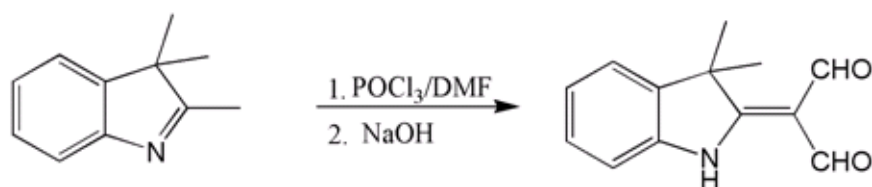
Figure 4-1 Tautomeric forms of 2-(diformylmethylidene)-3,3-dimethylindole.

Herein, we report the results of our studies on coordination behavior of the diformyl ligand towards Co^{II} , Ni^{II} , Cu^{II} , Zn^{II} , Cd^{II} and Pd^{II} ions. To gain a deeper insight into the coordination chemistry of the ligand, where possible, the initial complexes were further modified by ancillary ligands.

4.2 Results and discussion

4.2.1 Syntheses and general characterizations

2-(Diformylmethylidene)-3,3-dimethylindole is the diformylation product of the reaction of 2,3,3-trimethylindolenine with Vilsmeier reagent (DMF/ POCl_3).



Scheme 4-1.

The compound may, in principle, exist in the two tautomeric forms depicted in Figure 4-1. In the solid state, as revealed by X-ray crystallography, the compound presents the ketoamine form. Figure 4-2 represents the molecular structures of two polymorphs of diformyl obtained by Helliwell *et al.* (a) and us (b). The molecular conformations of these polymorphs differ by a 180° rotation of one formyl group. The NMR spectroscopic data suggest that in CDCl_3 solution also, the ketoamine tautomer is preferred over the enolimine

form. The ^1H NMR spectrum shows the two formyl protons at 9.79 and 9.77 ppm and the NH signal at 13.56 ppm, while the ^{13}C signals of the formyl carbons appear at δ 192.43 and 187.85. These values are indicative of the ketoamine form as discussed earlier by Neuvonen *et al.* [82].

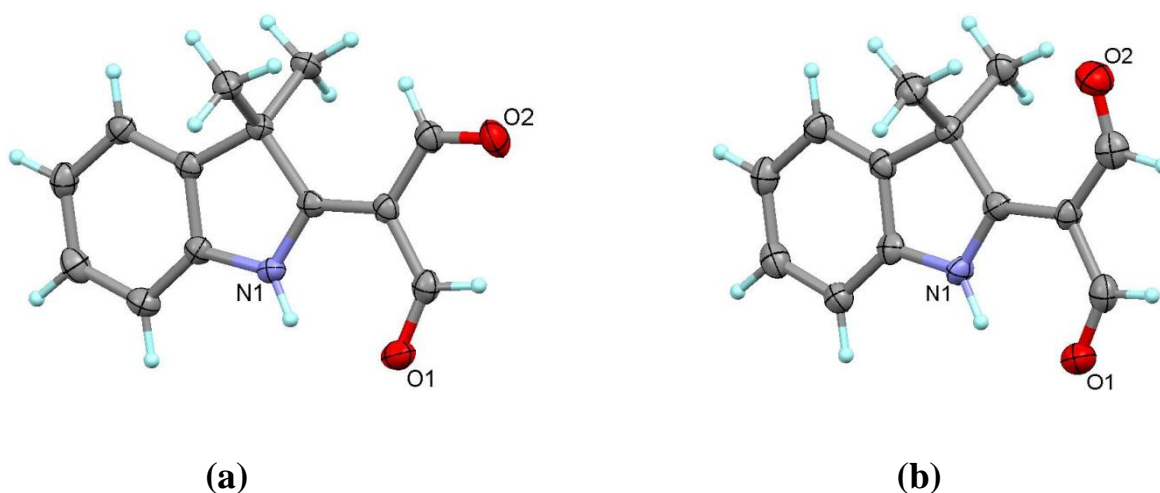


Figure 4-2 The X-ray crystal structures of two polymorphs of the diformyl compound.

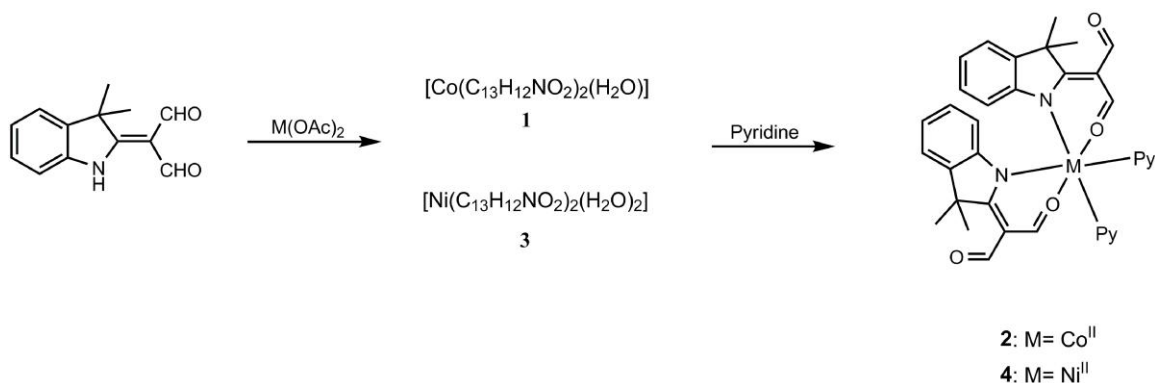
Upon the reaction with $\text{M}(\text{OAc})_2$ ($\text{M} = \text{Co}^{\text{II}}$, Ni^{II} , Cu^{II} , Zn^{II} , Cd^{II} , or Pd^{II}) in ethanol and in the presence of triethylamine, the diformyl compound loses its amino proton to ligate the metal ions as a monoanionic ligand. This is reflected in omission of the $\nu(\text{N-H})$ band of the ligand at 3146 cm^{-1} in the IR spectra of the obtained metal complexes. The elemental analyses for complexes of Cu^{II} (**5**), Zn^{II} (**6**), Cd^{II} (**8**) and Pd^{II} (**10**) ions are consistent with the formula $[\text{M}(\text{C}_{13}\text{H}_{12}\text{NO}_2)_2]$ while for the Co^{II} (**1**) and Ni^{II} (**3**) complexes suggest the presence of one and two molecules of water. The magnetic susceptibility value

of $[\text{Co}(\text{C}_{13}\text{H}_{12}\text{NO}_2)_2(\text{H}_2\text{O})]$ (**1**) (5.41 B.M.) indicates a high spin configuration with significant orbital contribution, characteristic of an octahedral Co(II) complex. Similarly, the magnetic moment of $[\text{Ni}(\text{C}_{13}\text{H}_{12}\text{NO}_2)_2(\text{H}_2\text{O})_2]$ (**3**) (2.97 B.M.) is typical of a high spin octahedral nickel(II) complex. Regrettably, no suitable single crystals could be obtained from these two compounds; however, on treatment with pyridine, $[\text{Co}(\text{C}_{13}\text{H}_{12}\text{NO}_2)_2(\text{py})_2]$ (**2**) and $[\text{Ni}(\text{C}_{13}\text{H}_{12}\text{NO}_2)_2(\text{py})_2]$ (**4**) were obtained as proper crystals for X-ray analysis. Our attempt to react the Cu^{II} (**5**), Zn^{II} (**6**), Cd^{II} (**8**) complexes with pyridine were unsuccessful, nevertheless the zinc and cadmium complexes reacted with methanol to give the corresponding methanol adducts with the formula $[\text{M}(\text{C}_{13}\text{H}_{12}\text{NO}_2)_2(\text{MeOH})_2]$ (**7** and **9**). The IR spectra of **7** and **9** show the $\nu(\text{O-H})$ as broad bands ($2700\text{-}3400\text{ cm}^{-1}$) and the $\nu(\text{C-O})$ of the methanol moieties at 1034 and 1033 cm^{-1} . The palladium(II) complex **10**, is diamagnetic and soluble in chloroform. The ^1H NMR spectrum of **10**, when compared to that of diformyl, shows a significant upfield shift (~ 2 ppm) of one of the *CHO* signals upon the complexation, while the position of the other *CHO* is little altered. Moreover the *NH* resonance of the ligand is absent in the spectrum of the palladium complex. Compound **10** reacted with pyridine in DMF to give the crystalline compounds of **11** and **12**. In a similar way, treatment of **10** with 4,4'-bipyridine in DMF led to the formation of **13**.

Except for compounds **1** and **3**, the three-dimensional structures of the complexes were fully determined by X-ray crystallographic analysis.

4.2.2 Crystal structures of cobalt(II) and nickel(II) complexes (2 and 4)

Recrystallization of **1** and **3** in the presence of pyridine afforded the crystals of **2** and **4**, respectively, (Scheme 4-2) whose structures are isomorphous and consist of discrete mononuclear molecules.



Scheme 4-2.

The structure of the Co complex (**2**) is shown in Figure 4-3. In the molecules, the deprotonated diformyl ligands act as *N,O*-bidentate chelates to form six-membered rings with the metal centers. While one of the carbonyl oxygen atoms of the diformyl ligand is involved in the coordination, the other one remains uncoordinated and engaged in intra and intermolecular C-H...O hydrogen bonding interactions. The Co^{II} and Ni^{II} ions are six-coordinated by two diformyl ligands and two *cis*-located pyridine molecules in a distorted octahedral geometry. The Co-N_{py} bond distances, 2.214(2) and 2.180 (2) Å, are somewhat longer than those observed in similar coordination systems [83,84] whereas the Ni-N_{py} bond distances, 2.144(3) and 2.148(3) Å, are in agreement with the values reported in the literature [85,86]. Selected values of bond lengths and bond angles for **2** and **4** are shown in Table 4-1.

Table 4-1 Selected bond lengths (Å) and bond angles (°) for **2** and **4**.

[Co(C ₁₃ H ₁₂ NO ₂) ₂ (py) ₂] (2)		[Ni(C ₁₃ H ₁₂ NO ₂) ₂ (py) ₂] (4)	
<i>Bond lengths</i>			
M-O(1)	2.0322(18)	M-O(1)	2.001(3)
M-O(3)	2.0278(18)	M-O(3)	2.019(3)
M-N(1)	2.110(2)	M-N(1)	2.073(3)
M-N(2)	2.115(2)	M-N(2)	2.077(3)
M-N(3)	2.214(2)	M-N(3)	2.148(3)
M-N(4)	2.180(2)	M-N(4)	2.144(3)
<i>Bond angles</i>			
O(3)-M-O(1)	170.58(8)	O(3)-M-O(1)	172.72(11)
O(3)-M-N(1)	100.32(8)	O(3)-M-N(2)	86.21(12)
O(1)-M-N(1)	84.88(8)	O(1)-M-N(2)	98.17(12)
O(3)-M-N(2)	85.56(8)	O(3)-M-N(1)	98.88(11)
O(1)-M-N(2)	101.84(8)	O(1)-M-N(1)	86.59(12)
N(1)-M-N(2)	95.60(8)	N(2)-M-N(1)	95.01(12)
O(3)-M-N(4)	89.54(8)	O(3)-M-N(3)	84.50(12)
O(1)-M-N(4)	84.77(8)	O(1)-M-N(3)	91.07(13)
N(1)-M-N(4)	169.25(8)	N(2)-M-N(3)	170.70(13)
N(2)-M-N(4)	89.39(8)	N(1)-M-N(3)	86.57(12)
O(3)-M-N(3)	83.00(8)	O(3)-M-N(4)	89.24(12)
O(1)-M-N(3)	89.64(8)	O(1)-M-N(4)	84.99(13)
N(1)-M-N(3)	85.42(8)	N(2)-M-N(4)	89.51(12)
N(2)-M-N(3)	168.51(8)	N(1)-M-N(4)	170.93(13)
N(4)-M-N(3)	91.59(8)	N(3)-M-N(4)	90.23(13)

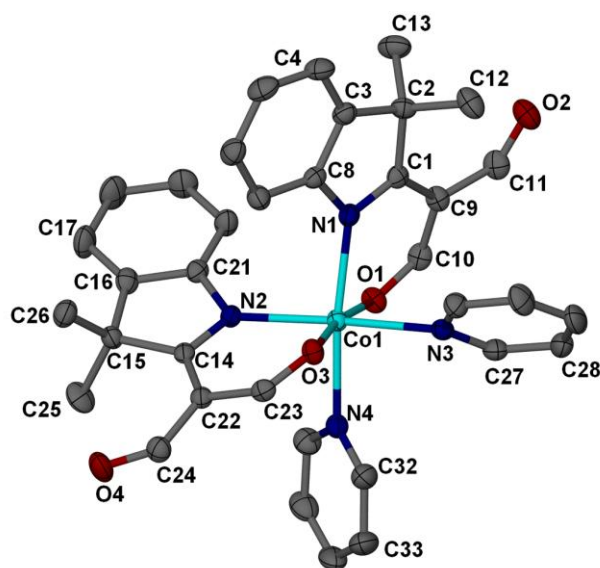
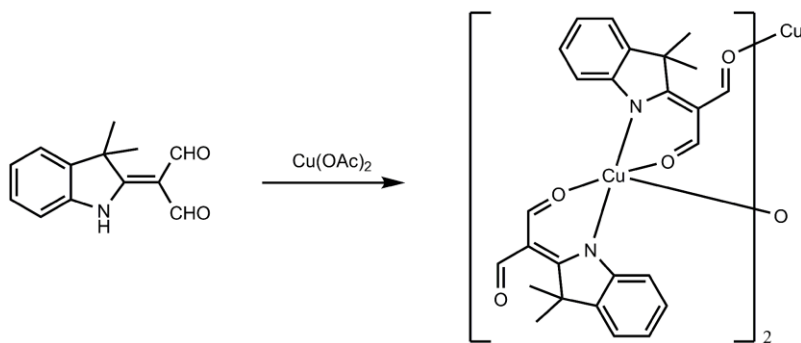


Figure 4-3 The molecular structures and labeling schemes of cobalt(II) complex **2** (50% probability ellipsoids). The H-atoms have been omitted for clarity.

4.2.3 Crystal structure of copper(II) complex **5**

In the copper(II) complex **5** the deprotonated diformyl ligand behaves in two fashions, *i.e.*, *N,O*-bidentate chelating and *N,O,O*-tridentate chelating-bridging, leading to discrete dinuclear complexes (Scheme 4-3).



Scheme 4-3

The crystal structure of **5** is shown in Figure 4-4. In the molecule, the copper atom is penta-coordinated. The coordination geometry around the metal ion can be determined by using the index $\tau = (\beta - \alpha)/60$, where β is the largest angle and α is the second one around the metal center. For an ideal square-pyramidal geometry τ is 0, while it is 1 in a perfect trigonal-bipyramid [87]. The two largest angles around the copper atom are $167.62(13)^\circ$ (O1—Cu1—O3) and $165.41(14)^\circ$ (N1—Cu1—N2) which give a τ value of 0.037. This value indicates a slightly distorted square pyramidal geometry in which the basal plane is defined by two nitrogen and two oxygen atoms afforded by two diformyl ligands, and the apical position is occupied by O4 atom from a symmetry related ligand with Cu-O4 distance of $2.580(4)$ Å. Within the resulting centrosymmetric dimer, the copper atoms are separated by $6.9404(14)$ Å. The uncoordinated carbonyl oxygen atom (O2) is involved in C-H...O hydrogen bonding interactions.

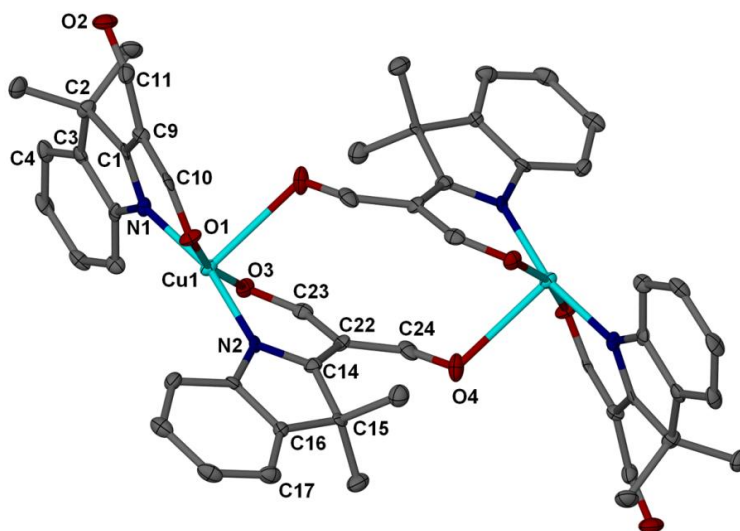


Figure 4-4 A perspective view of the dimeric structure of copper(II) complex **5** (50% probability ellipsoids). The H-atoms have been omitted for clarity

Selected geometrical parameters for the copper(II) complex are listed in Table 4-2. The Cu-O and Cu-N bond lengths are comparable to those in $[\text{Cu}_2\{(3,5\text{-}(\text{NO}_2)_2\text{sal})_2(2,2'\text{-bipy})_2\} \cdot 0.5\text{H}_2\text{O}]$, a dinuclear copper(II) complex with similar coordination environment [88].

Table 4-2 Selected bond lengths (Å) and bond angles (°) for $[\text{Cu}(\text{C}_{13}\text{H}_{12}\text{NO}_2)_2]_2$ (**5**).

<i>Bond lengths</i>			
M-O(1)	1.923(3)	M-N(2)	1.954(3)
M-O(3)	1.937(3)	M-O(4)#1	2.580(3)
M-N(1)	1.952(4)		
<i>Bond angles</i>			
O(1)-M-O(3)	167.62(13)	N(1)-M-N(2)	165.41(14)
O(1)-M-N(1)	90.78(13)	O(1)-M-O(4)#1	85.19(12)
O(3)-M-N(1)	93.27(13)	O(3)-M-O(4)#1	82.90(12)
O(1)-M-N(2)	90.12(13)	N(1)-M-O(4)#1	93.31(13)
O(3)-M-N(2)	88.89(13)	N(2)-M-O(4)#1	101.27(12)

Symmetry transformations used to generate equivalent atoms: #1 -x+1, -y+1, -z+2

4.2.4 Crystal structures of zinc(II) and cadmium(II) complexes

The anionic diformyl ligand showed the same behavior toward Zn^{II} and Cd^{II} ions, forming isostructural complexes $[\text{Zn}(\text{C}_{13}\text{H}_{12}\text{NO}_2)_2]$ (**6**) and $[\text{Cd}(\text{C}_{13}\text{H}_{12}\text{NO}_2)_2]$ (**8**). In these complexes, as shown in Figure 4-5 for the Zn complex, the ligand employs all three nitrogen and oxygen atoms in a chelating-bridging coordination fashion. The metal atoms, placed on inversion centers, are octahedrally coordinated by two nitrogen and two oxygen (O1) atoms provided by two diformyl chelates in the equatorial plane and two axially positioned oxygen (O2) atoms from two symmetry related ligands. The overall result is three-dimensional polymeric structures with cylindrical channels in the [1 1 1] direction (Figure 4-6). The total potential void volume of the unit cell is 219.4 \AA^3 (12.3% of the cell

volume) in the zinc complex and 263.5 \AA^3 (13.9% of the cell volume) in the cadmium complex, as estimated by PLATON [89].

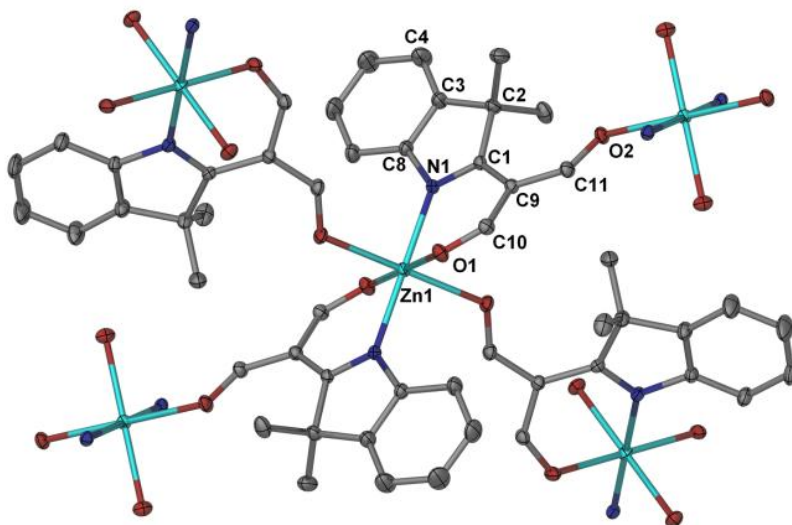


Figure 4-5 The molecular structure of zinc(II) complex **6** (30% probability ellipsoids). The H-atoms have been omitted for clarity.

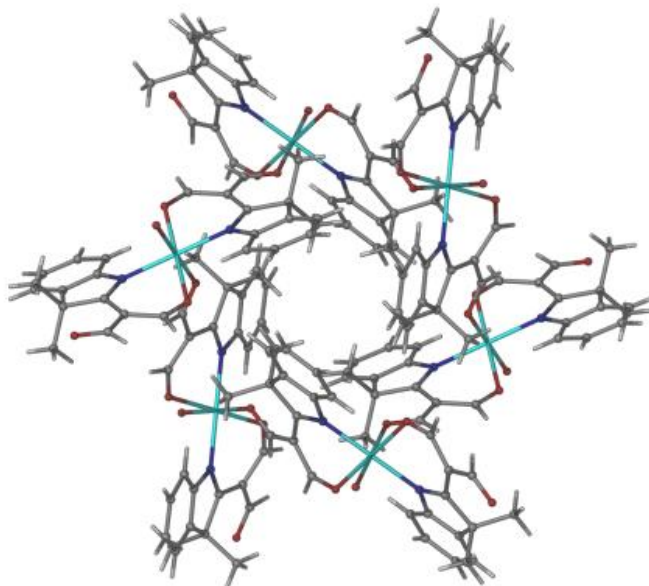


Figure 4-6 Packing view of zinc(II) complex **6** showing a cylindrical channel.

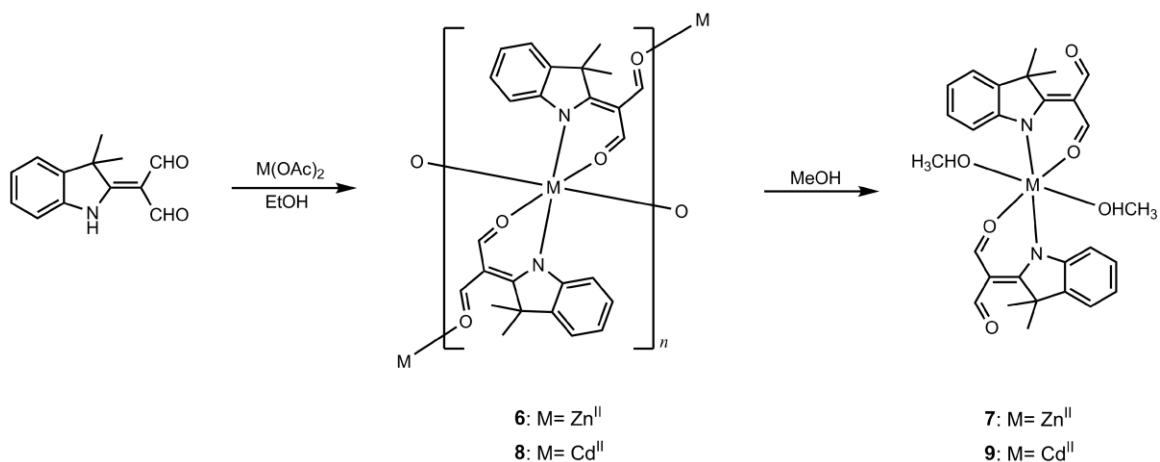
The coordination geometry of the zinc complex deviates slightly from an ideal octahedron as reflected by the cisoid angles of 83.36(5)-96.64(5)°. Similarly, but to a larger extent, the cadmium complex shows a distortion, the cisoid angles being 78.47(5)-101.53(5)°. Selected bond lengths and bond angles for the complexes **6** and **8** are listed in Table 4-3.

Table 4-3 Selected bond lengths (Å) and bond angles (°) for **6** and **8**.

$[\text{Zn}(\text{C}_{13}\text{H}_{12}\text{NO}_2)_2]_n$ (6)		$[\text{Cd}(\text{C}_{13}\text{H}_{12}\text{NO}_2)_2]_n$ (8)	
<i>Bond lengths</i>			
M-N(1)	2.1053(13)	M-N(1)	2.2693(14)
M-O(1)	2.0719(12)	M-O(1)	2.2733(12)
M-O(2)#1	2.2226(11)	M-O(2)#1	2.3344(12)
<i>Bond angles</i>			
N(1)-M-N(1)#2	180.0	N(1)-M-N(1)#2	180.0
N(1)-M-O(1)	83.36(5)	N(1)-M-O(1)	78.47(5)
O(1)-M-O(1)#2	180.0	O(1)-M-O(1)#2	180.0
O(1)-M-O(2)#1	90.25(5)	O(1)-M-O(2)#1	90.84(4)
N(1)-M-O(2)#1	91.24(5)	N(1)-M-O(2)#1	91.32(5)
O(2)#1-M-O(2)#3	180.0	O(2)#1-M-O(2)#3	180.0

Symmetry transformations used to generate equivalent atoms: #1 $x, y+1, z$; #2 $-x+1, -y+1, -z+2$; #3 $-x+1, -y+1, -z+1$

Coordination polymers **6** and **8** did not react with pyridine, however upon treatment with methanol, their three-dimensional networks were cleaved to form discrete mononuclear methanol adducts, **7** and **9** (Scheme 4-4).



Scheme 4-4

These two complexes are isostructural, wherein the anionic diformyl ligand acts as an *N,O*- bidentate chelate. The structure of the Zn complex is shown in Figure 4-7. The metal atom is located on a center of inversion and coordinated by two diformyl chelates and two *trans*-located methanol molecules in a distorted octahedral geometry. The uncoordinated formyl oxygens are hydrogen bonded to the methanol hydroxyl groups of the adjacent molecules, resulting in infinite hydrogen bonded chains along the crystallographic *b* axis. Table 4-4 summarizes the bond distances and angles for the zinc(II) and cadmium(II) complexes. The Zn-O and Zn-N bond distances are in agreement with the values reported for similar coordination systems [90, 91] as are the Cd-O and Cd-N bond lengths [92].

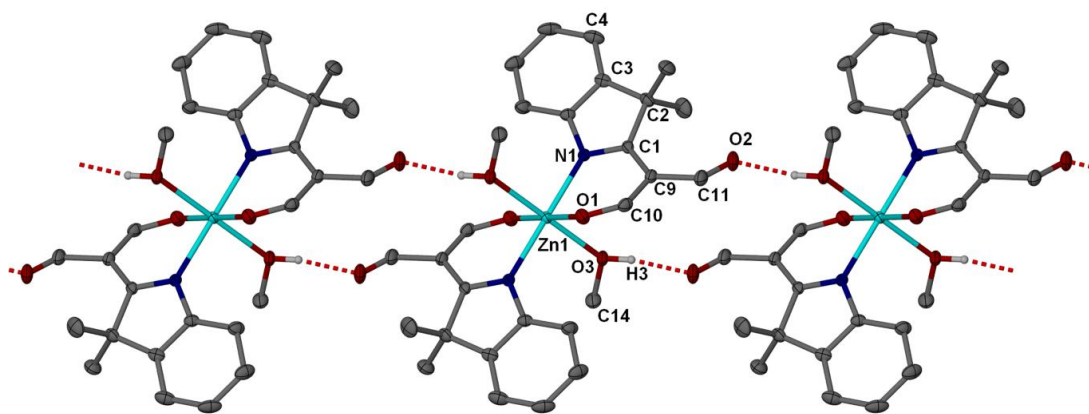


Figure 4-7 The crystal structure of zinc(II) complex **7** showing the atom labeling scheme and the O-H...O intermolecular hydrogen bonding (50% probability ellipsoids). The C-bound hydrogen atoms have been omitted for clarity.

Table 4-4 Selected bond lengths (Å) and bond angles (°) for **7** and **9**.

[Zn(C ₁₃ H ₁₂ NO ₂) ₂ (CH ₄ O) ₂] (7)		[Cd(C ₁₃ H ₁₂ NO ₂) ₂ (CH ₄ O) ₂] (9)	
<i>Bond lengths</i>			
M-N(1)	2.1060(15)	M-N(1)	2.2590(13)
M-O(1)	2.0804(14)	M-O(1)	2.2826(11)
M-O(3)	2.1968(13)	M-O(3)	2.3502(11)
<i>Bond angles</i>			
N(1)-M-N(1)#1	180.0	N(1)-M-N(1)#1	180.0
N(1)-M-O(1)	84.60(5)	N(1)-M-O(1)	79.14(4)
O(1)-M-O(1)#1	180.0	O(1)-M-O(1)#1	180.0
O(1)-M-O(3)	92.22(6)	O(1)-M-O(3)	90.66(4)
N(1)-M-O(3)	89.35(6)	N(1)-M-O(3)	89.63(4)
O(3)-M-O(3)#1	180.0	O(3)-M-O(3)#1	180.0

Symmetry transformations used to generate equivalent atoms: #1 -x+2, -y, -z

4.2.5 Crystal structures of palladium(II) complexes 10, 11, 12 and 13

The crystal of **10** suitable for X-ray analysis was obtained from a dioxane solution at room temperature. As depicted in Figure 4-8, the mono-anionic diformyl ligand acts as an *N,O*-bidentate chelate to form six-membered rings with the metal center in a distorted square planar coordination environment. The distortion is evident from the deviation (0.044 Å) of the palladium atom from the coordination plane (N1, N2, O1, O3) and also the N1-Pd1-N2 and O1-Pd1-O3 bond angles of $176.7(3)^\circ$ and $171.6(3)^\circ$ (Table 4-5).

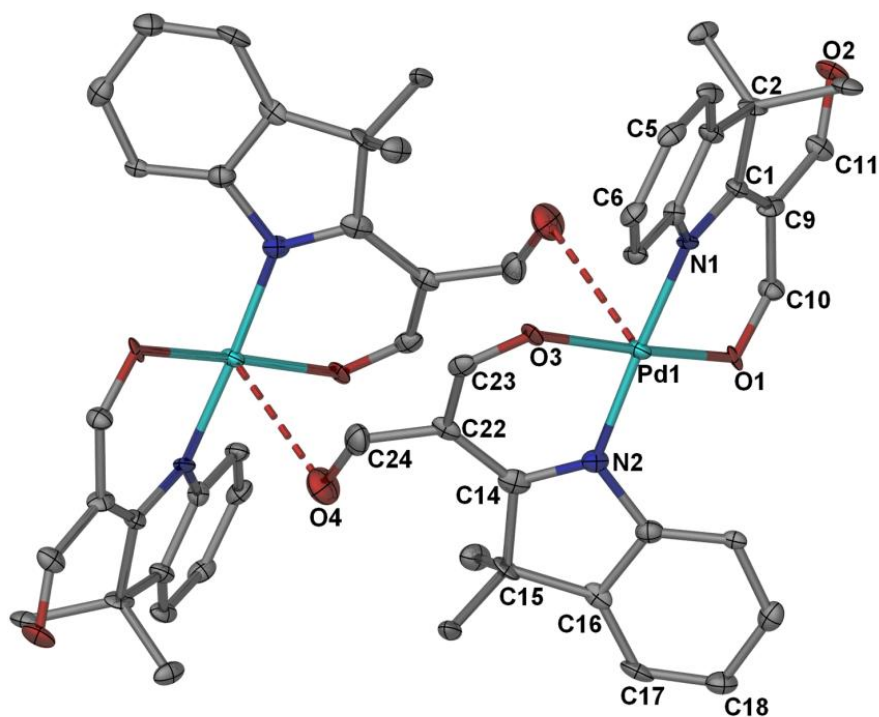


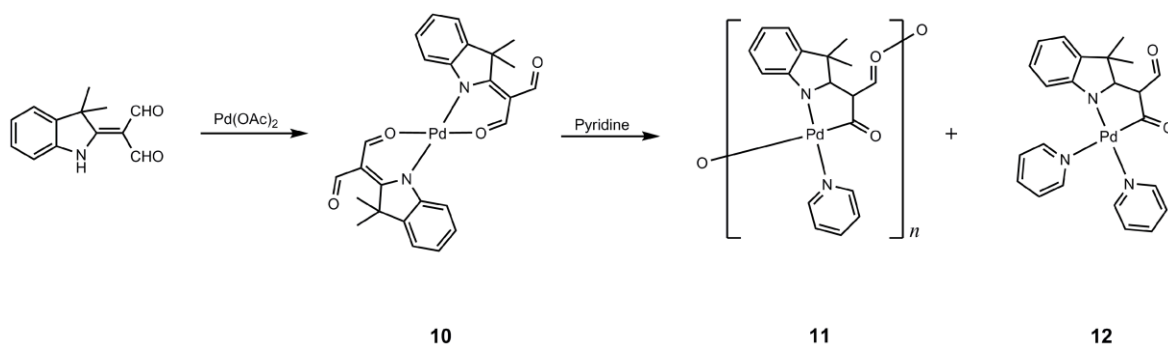
Figure 4-8 A perspective view of two molecules of palladium(II) complex **10** showing dimerization through Pd1...O4 interactions. Displacement ellipsoids are drawn at the 50% probability level.

Table 4-5 Selected bond lengths (Å) and bond angles (°) for [Pd(C₁₃H₁₂NO₂)₂] (**10**).

<i>Bond lengths</i>			
M-O(1)	1.998(6)	M-N(2)	2.002(8)
M-N(1)	2.002(8)	M-O(3)	2.016(7)
<i>Bond angles</i>			
O(1)-M-N(1)	90.7(3)	O(1)-M-O(3)	171.6(3)
O(1)-M-N(2)	88.9(3)	N(1)-M-O(3)	90.8(3)
N(1)-M-N(2)	176.7(3)	N(2)-M-O(3)	90.0(3)

Six-membered palladium(II) metallocycles with an *N,O*_{aldehyde}-bidentate chelate are unprecedented, however those with *N,O*_{ketone} ligands have been reported and have similar Pd-N and Pd-O bond lengths to those of the present structure [93-95]. The Pd cation is also involved in a long-range interaction with the apically placed O4 atom of a symmetry related molecule with Pd...O distance of 3.141(8) Å, leading to a dimeric, pseudo-square-pyramidal geometry around the palladium atom. This arrangement is similar to what was observed in dimeric copper(II) complex **5**, however the Pd...O4 distance is much longer than those usually considered as bonding interactions (*ca* 2.06 Å) and can only be indicative of a weak interaction. A similar interaction has been reported for a few palladium complexes with the Pd...O distances ranging between 2.734-3.303 Å [96-98]. The uncoordinated carbonyl oxygen atom O2 is engaged in intra and intermolecular C-H...O hydrogen bonding.

Treatment of the palladium(II) complex **10** with pyridine in DMF afforded concomitant crystallization of two different pyridine coordinated complexes, **11** and **12** (Scheme 4-5).



Scheme 4-5.

The ligand in these two complexes chelates the metal ion, not in the *N,O*-chelating mode observed in the former complexes, but in a *C,N*-chelating fashion. Interestingly, in the presence of pyridine, aldehyde C-H bond activation occurs at the Pd(II) center, thus the dianionic diformyl compound binds to the metal center via its carbonyl carbon C10 and the nitrogen donor atom to form a five-membered metallocycle. This type of cyclometalation of aldehyde functions is not without precedent and has been reported in palladium(II) complexes of quinoline-8-carbaldehyde and dimethylamino benzaldehyde [99,100]. Such organopalladium species have been utilized as intermediates in the double carbonylation of aromatic compounds to give α -keto amides [101].

In complex **11** the palladium ion is coordinated by the nitrogen and carbonyl C10 from one diformyl ligand and O2 of a symmetry related diformyl ligand into polymeric linear chains along the *c* axis (Figure 4-9). Thus, the doubly deprotonated diformyl behaves as a *C,N,O*-tridentate chelating-bridging agent. One coordinated pyridine molecule completes a distorted square planar environment around the palladium atom which is displaced 0.0398(9) Å out of the coordination plane (C10-N1-O2-N2). The distortion from

the ideal square planar geometry is also evident from the C10-Pd1-N1 bite angle of $80.95(8)^\circ$ and N1-Pd1-N2 angle of $174.52(6)^\circ$ (Table 4-6).

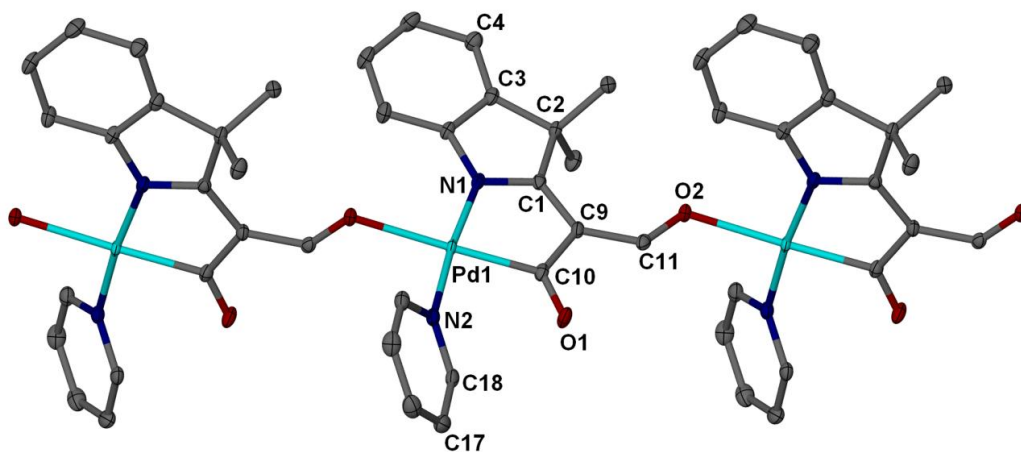


Figure 4-9 The crystal structure and atom labeling scheme of palladium(II) coordination polymer **11** (50% probability ellipsoids). The H-atoms have been omitted for clarity.

In contrast to the polymeric structure of **11**, the structure of complex **12** consists of discrete mononuclear units in which the doubly deprotonated diformyl ligand acts as a *C,N*-bidentate chelate. Both oxygen atoms of the ligand remain uncoordinated to the metal ion and are engaged in C-H...O hydrogen bonding interactions. The square planar geometry around the palladium(II) atom is completed by two pyridine ligands, the dihedral angle between them being $83.57(13)^\circ$. The deviation from the ideal geometry is reflected by the disposition of the metal center $0.0069(12) \text{ \AA}$ out of the coordination plane and coordination bond angles of $80.88(2)$ - $177.16(11)^\circ$ (Table 4-6). The Pd-C10 bond length of $1.997(3) \text{ \AA}$ is typical for Pd-acyl carbon distance and the Pd-N distances lie in the normal range. The longer bond length of Pd1-N3 than that of Pd1-N2 points to the large *trans* influence

associated with the acyl group, as has been observed in similar acyl palladium(II) complexes [102,103].

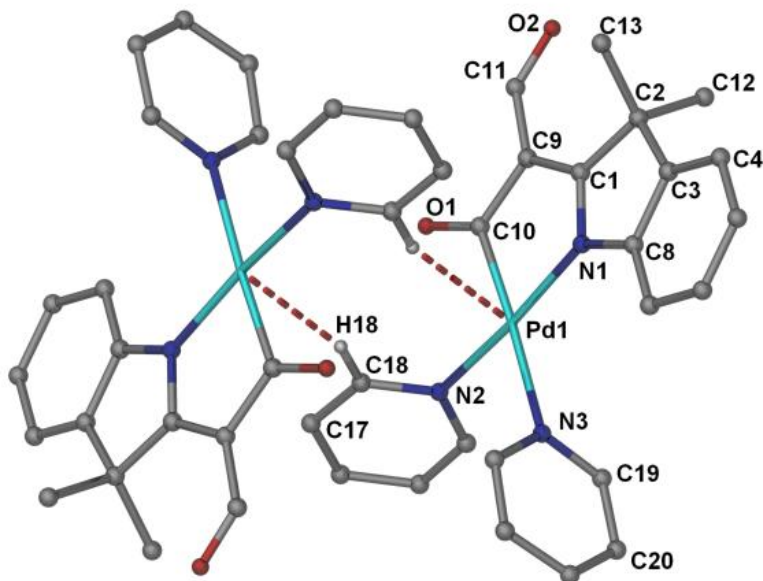


Figure 4-10 A perspective view of two molecules of palladium(II) complex **12** connected through Pd...H anagostic interactions.

An interesting feature of the structure is occurrence of a C-H...Pd interaction with Pd...H distance of 2.8017 Å and Pd-H-C angle of 162.53°, connecting two molecules into a centrosymmetric dimer (Figure 4-10). This interaction can best be regarded as an anagostic interaction which is characterized by an M...H distance of ~ 2.3-2.9 Å and M-H-C bond angle of 110-170° and is typically associated with square planar d⁸ metal centers [104]. The nature of this type of interaction is still ambiguous and may involve donation of filled d_{xz/yz} orbitals of the metal center into the C-H σ* orbital [105].

Table 4-6 Selected bond lengths (Å) and bond angles (°) for **11** and **12**.

[Pd(C ₁₃ H ₁₁ NO ₂)(py)] _n (11)		[Pd(C ₁₃ H ₁₁ NO ₂)(py) ₂] (12)	
<i>Bond lengths</i>			
M-C(10)	1.971(2)	M-C(10)	1.997(3)
M-N(1)	2.0322(17)	M-N(1)	2.032(2)
M-N(2)	2.0765(18)	M-N(2)	2.079(3)
M-O(2)#1	2.2355(14)	M-N(3)	2.232(3)
<i>Bond angles</i>			
C(10)-M-N(1)	80.95(8)	C(10)-M-N(1)	80.88(12)
C(10)-M-N(2)	93.72(8)	C(10)-M-N(2)	91.51(12)
N(1)-M-N(2)	174.52(6)	N(1)-M-N(2)	172.02(10)
C(10)-M-O(2)#1	176.96(7)	C(10)-M-N(3)	177.16(11)
N(1)-M-O(2)#1	99.65(6)	N(1)-M-N(3)	101.57(10)
N(2)-M-O(2)#1	85.61(6)	N(2)-M-N(3)	86.10(10)

Symmetry transformations used to generate equivalent atoms: #1 x, -y+1/2, z+1/2

From the formation of acyl-palladium(II) complexes **11** and **12**, one might expect that using 4,4'-bipyridine instead of pyridine in the reaction with the initial palladium complex, **10**, would lead to a bipyridine-bridged acyl-palladium complex. This presumption was confirmed by the crystal structure of **13**, obtained from a solution of **10** and 4,4'-bipyridine in DMF (Figure 4.11). In the structure, the Pd^{II} ion is four coordinated by the dianionic diformyl ligand as a *C,N*-bidentate chelate and two bridging 4,4'-bipy ligands in a square planar coordination environment.

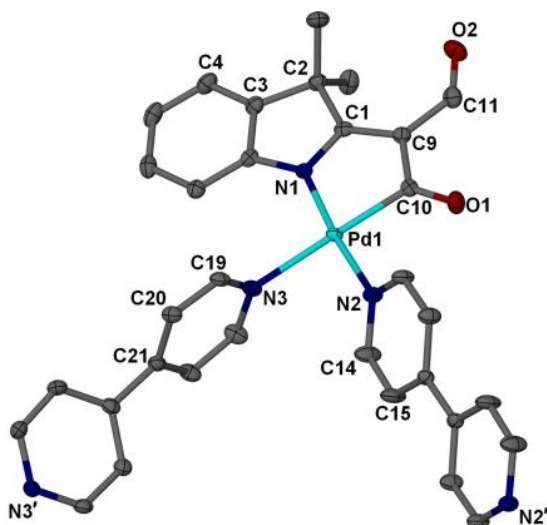


Figure 4-11 The crystal structures and atom labeling schemes of palladium(II) complex **13**. The co-crystallized DMF molecule and also hydrogen atoms have been omitted for clarity.

The deviation from the ideal geometry is reflected in cisoid angles [80.95(8)-99.95(7)°] and transoid angles [178.88(8)° and 174.36(7)°] (Table 4-7), and also the disposition of the palladium(II) atom 0.0106(10) Å out of the coordination plane. Similar to what was observed in complex **12**, the large *trans* influence of the acyl group is evident from the longer bond length of Pd1-N3 [2.2205(19) Å] than that of Pd1-N2 [2.0955(19) Å]. The adjacent palladium centers are bridged by two conformationally different 4,4'-bipy ligands, one of which is planar while the other one is significantly twisted [47.47(6)°] about the central C-C bond, resulting in an infinite looped chain running along the *c* axis (Figure 4-12). The crystal structure consists of the coordination polymer and half of the disordered DMF solvent molecule per each palladium atom. The DMF molecules are sandwiched between the metal centers and stabilize the loop structure by a weak Pd...O interaction [Pd1...O5 = 3.370(4) Å] and a Pd...H interaction. Once again, the geometric parameters of

the Pd...H interaction (Pd1...H26C = 2.5828 Å; Pd1-H26C-C26 = 131.50°) suggest its anagostic nature.

Table 4-7 Selected geometrical parameters for $\{[\text{Pd}(\text{C}_{13}\text{H}_{11}\text{NO}_2)(\text{bipy})]\cdot 0.5\text{DMF}\}_n$ (**13**).

<i>Bond lengths</i> (Å)			
M-C(10)	1.993(2)	M-N(2)	2.0955(19)
M-N(1)	2.0278(18)	M-N(3)	2.2205(19)
<i>Bond angles</i> (°)			
C(10)-M-N(1)	80.95(8)	C(10)-M-N(3)	178.88(8)
C(10)-M-N(2)	93.75(9)	N(1)-M-N(3)	99.95(7)
N(1)-M-N(2)	174.36(7)	N(2)-M-N(3)	85.38(7)

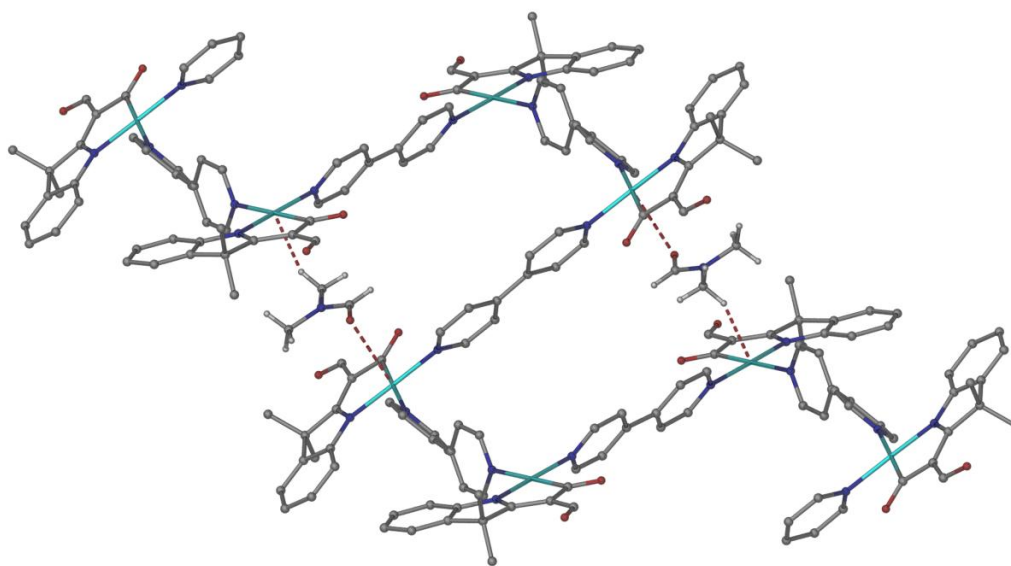


Figure 4-12 Infinite loop of palladium(II) coordination polymer **13**, showing Pd...O and anagostic Pd...H interactions with the co-crystallized DMF molecules.

4.3 Conclusions

2-(Diformylmethylidene)-3,3-dimethylindole can react with the selected transition metal ions to give the corresponding metal-organic compounds with a variety of structures. The structure of the complexes can be mononuclear, dinuclear or polynuclear, depending on the bonding mode of the ambidentate ligand, the geometry adopted by the metal centers and the presence and entity of ancillary ligands. Coordination environments vary from square-planar (Pd^{II}) to [4+1] distorted square-pyramidal (Cu^{II} and Pd^{II}) to octahedral (Co^{II} , Ni^{II} , Zn^{II} and Cd^{II}). In the resulting complexes, the diformyl ligand shows *N,O*-chelating or *N,O,O*-chelating-bridging modes when is monoanionic. Upon reaction with a pyridine-like ligand, the initial *N,O*-chelated palladium complex can undergo aldehyde C-H bond activation and gives the acyl-palladium complexes wherein the dianionic diformyl adopts *C,N*-chelating or *C,N,O*-chelating-bridging coordination fashion. Aside from the coordinating interactions, different non-covalent interactions (hydrogen bonding and anagostic interactions) were observed to define the architecture of the structures.

4.4 Experimental

2,3,3-trimethylindolenine was purchased from the Aldrich–Sigma Company. Ethanol was distilled prior to use. Magnetic susceptibilities were measured with a Sherwood Scientific MSB-AUTO magnetic susceptibility balance at 298 K. Diamagnetic corrections were applied using Pascal's constants. The IR spectra were taken on a Perkin Elmer Spectrum 400 ATR-FT-IR spectrometer. The NMR spectra were recorded on a JEOL Lambda 400 MHz FT-NMR spectrometer. The electronic spectra were measured by

means of a Shimadzu UV-3600 UV-VIS-NIR spectrophotometer in the region 200–1200 nm.

4.4.1 Synthesis of 2-(diformylmethylidene)-3,3-dimethylindole

A solution of trimethylindolenine, (5.57 g, 35 mmol), in anhydrous dimethylformamide (15 ml) was cooled in an ice bath. A solution of phosphoryl chloride (10 ml) in dimethylformamide (15 ml) was added dropwise with stirring over a period of 1 h at below 10° C. The cooling bath was removed and the reaction mixture was stirred at 90° C for 2 h. The resulting solution was poured onto ice water (400 ml), the pH was adjusted to 9.0 by the addition of aqueous NaOH (35%) whereupon the solid product was precipitated. It was filtered, washed with hot water, dried and recrystallized from n-hexane/ethyl acetate to give yellow prismatic crystals of diformyl. Yield: 4.35 g, 58%. IR (ATR): ν (cm⁻¹) 3146m, 2856w, 1661s, 1647s, 1629s, 1610s, 1509s, 1466s, 1218m, 1197m, 520m, 477m. ¹H NMR (CDCl₃): δ 13.56 (s, 1H, NH); 9.79 (s, 1H, CHO); 9.77 (s, 1H, CHO); 7.33-7.35 (m, 1H, Ar-H); 7.31 (dd, 1H, $J = 7.6, 1.3$ Hz, Ar-H); 7.25 (td, 1H, $J = 7.6, 1.3$ Hz, Ar-H); 7.19 (d, 1H, $J = 7.6$ Hz, Ar-H); 1.76 (s, 6H, CH₃). ¹³C NMR (CDCl₃): δ 192.43, 187.85 (CHO); 179.45 (OCHCCHO); 140.70, 139.45, 128.35, 125.74, 122.23, 112.78, 109.52 (Ar); 51.36 (CH₃CCH₃); 23.55 (CH₃CCH₃).

Further recrystallization from ethanol/water (3:1 v/v), led to a mixture of lath and prismatic habits. The unit cell dimensions of the prism crystal confirmed the form reported earlier by Helliwell *et al.* but the laths appeared new.

4.4.2 Synthesis of cobalt(II) complexes 1 and 2

A mixture of diformyl (0.43 g, 2.0 mmol) and cobalt(II) acetate tetrahydrate (0.25 g, 1.0 mmol) along with a few drops of triethylamine, in ethanol (10 mL) was refluxed for 1 hour and then cooled to room temperature. The resulting orange precipitate, $[\text{Co}(\text{C}_{13}\text{H}_{12}\text{NO}_2)_2(\text{H}_2\text{O})]$ (**1**), was filtered off, washed with ethanol and dried over silica-gel. Yields: 0.295 g, 58%. *Anal.* Calc. for $\text{C}_{26}\text{H}_{26}\text{CoN}_2\text{O}_5$: C, 61.78; H, 5.18; N, 5.54. Found: C, 61.75; H, 4.88; N, 5.44%. IR (ATR): ν (cm^{-1}) 3553w, 2822vw, 2782vw, 1635m, 1542vs, 1455s, 1201m, 503m, 480m. UV-Vis [λ_{max} (nm) solid]: 1080, 389, 271. $\mu_{\text{eff}} = 5.41$ B.M.

A solution of complex **1** in a mixture of chloroform and pyridine yielded orange crystals of $[\text{Co}(\text{C}_{13}\text{H}_{12}\text{NO}_2)_2(\text{py})_2]$ (**2**) after one week. *Anal.* Calc. for $\text{C}_{36}\text{H}_{34}\text{CoN}_4\text{O}_4$: C, 66.97; H, 5.31; N, 8.68. Found: C, 66.48; H, 5.09; N, 8.38%. IR (ATR): ν (cm^{-1}) 2748vw, 2720vw, 1655m, 1550vs, 1441s, 1193m, 499m, 468m, 428w. UV-Vis [λ_{max} (nm) solid]: 1017, 744, 635, 384, 268, 233. $\mu_{\text{eff}} = 4.91$ B.M.

4.4.3 Synthesis of nickel(II) complexes 3 and 4

A mixture of diformyl (0.43 g, 2.0 mmol) and nickel(II) acetate tetrahydrate (0.25 g, 1.0 mmol), along with a few drops of triethylamine in ethanol (10 mL), was refluxed for 1 hour and then left at room temperature overnight. The resulting green precipitate, $[\text{Ni}(\text{C}_{13}\text{H}_{12}\text{NO}_2)_2(\text{H}_2\text{O})_2]$ (**3**), was filtered off, washed with aqueous ethanol (50%) and dried over silica gel. Yields: 0.283 g, 54%. *Anal.* Calc. for $\text{C}_{26}\text{H}_{28}\text{N}_2\text{NiO}_6$: C, 59.69; H, 5.39; N, 5.35. Found: C, 59.83; H, 4.97; N, 5.40%. IR (ATR): ν (cm^{-1}) 3384br, 2862vw, 1622m, 1544vs, 1452s, 1206m, 499m, 480w. UV-Vis [λ_{max} (nm) solid]: 1023, 614, 395, 278, 223. $\mu_{\text{eff}} = 2.97$ B.M.

Slow evaporation of a solution of the complex **3** in a mixture of DMF and pyridine afforded dark green crystals of $[\text{Ni}(\text{C}_{13}\text{H}_{12}\text{NO}_2)_2(\text{py})_2]$ (**4**). *Anal.* Calc. for $\text{C}_{36}\text{H}_{34}\text{N}_4\text{NiO}_4$: C, 67.00; H, 5.31; N, 8.68. Found: C, 67.39; H, 5.12; N, 8.73%. IR (ATR): ν (cm^{-1}) 2778vw, 2720w, 1664m, 1559vs, 1440s, 1194m, 500m, 471m, 434m. UV–Vis [λ_{max} (nm) solid]: 974, 712, 566, 334, 264. $\mu_{\text{eff}} = 3.15$ B.M.

4.4.4 Synthesis of copper(II) complex **5**

A solution of copper(II) acetate monohydrate (0.2 g, 1.0 mmol) in ethanol (30 mL) was added to an ethanolic solution (30 mL) of diformyl (0.43 g, 2.0 mmol) followed by addition of a few drops of triethylamine. The mixture was refluxed for 15 minutes and then cooled to room temperature. The resulting green precipitate, $[\text{Cu}(\text{C}_{13}\text{H}_{12}\text{NO}_2)_2]_2$ (**5**), was washed with ethanol and dried over silica gel. Yields: 0.464 g, 94%. *Anal.* Calc. for $\text{C}_{26}\text{H}_{24}\text{CuN}_2\text{O}_4$: C, 63.47; H, 4.92; N, 5.69. Found: C, 63.48; H, 4.79; N, 5.63%. IR (ATR): ν (cm^{-1}) 2733w, 1673m, 1658m, 1552vs, 1438s, 1194m, 503m, 495m, 480m, 418m. UV–Vis [λ_{max} (nm) solid]: 637, 384, 290, 231. $\mu_{\text{eff}} = 1.96$ B.M.

The X-ray quality crystal of **5** was obtained from a DMSO solution at room temperature.

4.4.5 Synthesis of zinc(II) complexes **6** and **7**

An ethanolic solution (10 mL) of diformyl (0.43 g, 2.0 mmol) and zinc(II) acetate dihydrate (0.22 g, 1.0 mmol) in the presence of a few drops of triethylamine was refluxed for 1 hour and then cooled to room temperature. 1 mL water was added and the resulting

white precipitate was collected, washed with water and recrystallized from ethanol to give the colorless crystals of $[\text{Zn}(\text{C}_{13}\text{H}_{12}\text{NO}_2)_2]_n$ (**6**). Yields: 0.217 g, 44%. *Anal.* Calc. for $\text{C}_{26}\text{H}_{24}\text{N}_2\text{O}_4\text{Zn}$: C, 63.23; H, 4.90; N, 5.67. Found: C, 63.18; H, 4.66; N, 5.41%. IR (ATR): ν (cm^{-1}) 2814w, 2778w, 1639m, 1556vs, 1456s, 1205s, 502m, 478m.

Recrystallization of **6** from methanol afforded the colorless crystals of $[\text{Zn}(\text{C}_{13}\text{H}_{12}\text{NO}_2)_2(\text{CH}_4\text{O})_2]$ (**7**). *Anal.* Calc. for $\text{C}_{28}\text{H}_{32}\text{N}_2\text{O}_6\text{Zn}$: C, 60.27; H, 5.78; N, 5.02. Found: C, 59.99; H, 5.43; N, 5.11%. IR (ATR): ν (cm^{-1}) 2700-3400br, 1637m, 1549vs, 1445s, 1195m, 1034s, 498m, 466 m.

4.4.6 Synthesis of cadmium(II) complexes **8** and **9**

An ethanolic solution (10 mL) of diformyl (0.43 g, 2.0 mmol) and cadmium(II) acetate dihydrate (0.27 g, 1 mmol) along with a few drops of triethylamine was refluxed for 1 hour and then left at room temperature for a few hours whereupon the colorless crystals of $[\text{Cd}(\text{C}_{13}\text{H}_{12}\text{NO}_2)_2]_n$ (**8**) were obtained. Yields: 0.314 g, 58%. *Anal.* Calc. for $\text{C}_{26}\text{H}_{24}\text{CdN}_2\text{O}_4$: C, 57.73; H, 4.47; N, 5.18. Found: C, 57.44; H, 4.89; N, 5.32%. IR (ATR): ν (cm^{-1}) 2818w, 2774w, 1638m, 1559vs, 1456s, 1204s, 498m, 472 m.

Recrystallization of **8** from methanol led to the formation of $[\text{Cd}(\text{C}_{13}\text{H}_{12}\text{NO}_2)_2(\text{CH}_4\text{O})_2]$ (**9**) as colorless crystals. *Anal.* Calc. for $\text{C}_{28}\text{H}_{32}\text{CdN}_2\text{O}_6$: C, 55.59; H, 5.33; N, 4.63. Found: C, 55.42; H, 5.03; N, 4.61%. IR (ATR): ν (cm^{-1}) 2700-3400br, 1633m, 1545vs, 1445s, 1196m, 1033s, 495m, 465m.

4.4.7 Synthesis of palladium(II) complexes **10**, **11**, **12** and **13**

A solution of palladium(II) acetate (0.23 g, 1.0 mmol) in ethanol (20 mL) was added to an ethanolic solution (10 mL) of diformyl (0.43 g, 2.0 mmol) followed by addition of a few drops of triethylamine. The mixture was refluxed for 15 minutes and then cooled to room temperature. The precipitate, $[\text{Pd}(\text{C}_{13}\text{H}_{12}\text{NO}_2)_2]$ (**10**), was filtered off, washed with ethanol and dried over silica gel. Yields: 0.473 g, 88%. *Anal.* Calc. for $\text{C}_{26}\text{H}_{24}\text{N}_2\text{O}_4\text{Pd}$: C, 58.38; H, 4.52; N, 5.24. Found: C, 58.11; H, 4.58; N, 5.52%. IR (ATR): ν (cm^{-1}) 2743w, 2717w, 1674s, 1539vs, 1436s, 1189m, 508m, 493m, 439w. UV-Vis [λ_{max} (nm) solid]: 382, 321, 234. ^1H NMR (CDCl_3): δ 9.54 (s, 1H, CHO); 7.86 (d, 1H, $J = 7.2$ Hz, Ar-H); 7.73 (s, 1H, CHO); 7.27-7.32 (m, 3H, Ar-H); 1.66 (s, 6H, CH_3). ^{13}C NMR (CDCl_3): δ 188.91 (CHO); 185.27 (CHO); 178.19 (OCHCCHO); 147.23, 145.43, 127.42, 126.26, 121.14, 119.41, 116.76 (Ar); 52.57 (CH_3CCH_3); 23.01 (CH_3).

X-ray quality single crystals of **10** were obtained by slow evaporation of a dioxane solution at room temperature. Recrystallization of **10** from a mixture of DMF and pyridine at room temperature yielded the crystals of $[\text{Pd}(\text{C}_{13}\text{H}_{11}\text{NO}_2)(\text{py})]_n$ (**11**) and $[\text{Pd}(\text{C}_{13}\text{H}_{11}\text{NO}_2)(\text{py})_2]$ (**12**). Using 4,4'-bipyridine instead of pyridine led to the formation of $\{[\text{Pd}(\text{C}_{13}\text{H}_{11}\text{NO}_2)(\text{bipy})].0.5\text{DMF}\}_n$ (**13**).

4.4.8 Crystallography

Diffraction data were measured using a Bruker SMART Apex II CCD area-detector diffractometer (graphite-monochromated Mo $K\alpha$ radiation, $\lambda = 0.71073$ Å). The orientation matrix, unit cell refinement and data reduction were all handled by the Apex2 software (SAINT integration, SADABS absorption correction [49]). The structures were solved using

direct or Patterson methods in the program SHELXS-97 [50] and were refined by the full matrix least-squares method on F^2 with SHELXL-97. All the non-hydrogen atoms were refined anisotropically and all the C-bound hydrogen atoms were placed at calculated positions and refined isotropically. O-bound hydrogen atoms were located in difference Fourier maps and refined with distance restraint of O-H 0.84(2) Å. Drawings of the molecules were produced with XSEED [51]. Crystal data and refinement are summarized in Tables 4-8, 4-9, 4-10, 4-11 and 4-12. Crystallography data for the structures in chapter IV have been deposited with the Cambridge Crystallographic Data Centre, CCDC Nos. 750804 (for the diformyl), 805122 (for **2**), 805123 (for **4**), 805124 (for **5**), 805125 (for **6**), 805126 (for **7**), 805127 (for **8**), 805128 (for **9**), 805118 (for **10**), 805119 (for **11**), 805120 (for **12**), 805121 (for **13**). These data can be obtained free of charge from The Cambridge Crystallographic Data Centre via www.ccdc.cam.ac.uk/data_request/cif.

Table 4-8 Crystal data and refinement parameters for the cobalt(II), nickel(II) and copper(II) complexes.

	[Co(C ₁₃ H ₁₂ NO ₂) ₂ (py) ₂] (2)	[Ni(C ₁₃ H ₁₂ NO ₂) ₂ (py) ₂] (4)	[Cu(C ₁₃ H ₁₂ NO ₂) ₂] ₂ (5)
Empirical formula	C ₃₆ H ₃₄ CoN ₄ O ₄	C ₃₆ H ₃₄ N ₄ NiO ₄	C ₅₂ H ₄₈ Cu ₂ N ₄ O ₈
Formula weight	645.60	645.38	984.02
Temperature (K)	103(2)	296(2)	100(2)
Crystal system , Space group	Triclinic, <i>P</i> -1	Triclinic, <i>P</i> -1	Monoclinic, <i>P</i> 21/ <i>c</i>
Unit cell dimensions			
<i>a</i> (Å)	11.1749(10)	10.8259(7)	7.0057(14)
<i>b</i> (Å)	12.3090(11)	12.3814(9)	26.565(5)
<i>c</i> (Å)	13.7367(12)	13.8481(9)	11.849(2)
α (°)	81.537(2)	83.782(4)	
β (°)	71.2310(10)	81.876(4)	96.912(4)
γ (°)	64.2050(10)	64.616(4)	
Volume (Å ³)	1610.7(2)	1657.80(19)	2189.0(7)
Z, Density (calculated) (g cm ⁻³)	2, 1.331	2, 1.293	2, 1.493
<i>F</i> (000)	674	676	1020
θ range for data collection (°)	1.57 to 25.00	1.49 to 25.00	1.53 to 25.00
Reflections collected / unique	7623 / 5536 [<i>R</i> _{int} = 0.0200]	9403 / 5735 [<i>R</i> _{int} = 0.0734]	10109 / 3844 [<i>R</i> _{int} = 0.0705]
Completeness	To $\theta = 25.00^\circ$: 97.4 %	To $\theta = 25.00^\circ$: 98.1 %	To $\theta = 25.00^\circ$: 99.6 %
Data / restraints / parameters	5536 / 1 / 410	5735 / 2 / 410	3844 / 12 / 302
Goodness-of-fit on <i>F</i> ²	1.048	0.932	1.008
Final <i>R</i> indices [<i>I</i> > 2 σ (<i>I</i>)]	<i>R</i> ₁ = 0.0377, <i>wR</i> ₂ = 0.0975	<i>R</i> ₁ = 0.0537, <i>wR</i> ₂ = 0.1213	<i>R</i> ₁ = 0.0492, <i>wR</i> ₂ = 0.1027
<i>R</i> indices (all data)	<i>R</i> ₁ = 0.0503, <i>wR</i> ₂ = 0.1120	<i>R</i> ₁ = 0.0997, <i>wR</i> ₂ = 0.1390	<i>R</i> ₁ = 0.0926, <i>wR</i> ₂ = 0.1167
Largest diff. peak and hole (e.Å ⁻³)	0.313 and -0.272	0.916 and -0.365	0.378 and -0.517

Table 4-9 Crystal data and refinement parameters for the zinc(II) complexes.

	[Zn(C ₁₃ H ₁₂ NO ₂) ₂] _n (6)	[Zn(C ₁₃ H ₁₂ NO ₂) ₂ (CH ₄ O) ₂] (7)
Empirical formula	C ₂₆ H ₂₄ N ₂ O ₄ Zn	C ₂₈ H ₃₂ N ₂ O ₆ Zn
Formula weight	493.84	557.93
Temperature (K)	296(2)	113(2)
Crystal system , Space group	Rhombohedral, <i>R</i> ₋₃ : <i>r</i>	Monoclinic, <i>P</i> 21/ <i>c</i>
Unit cell dimensions		
<i>a</i> (Å)	12.6074(3)	11.402(6)
<i>b</i> (Å)	12.6074(3)	9.447(5)
<i>c</i> (Å)	12.6074(3)	12.139(6)
α (°)	104.04	
β (°)	104.04	94.409(9)
γ (°)	104.04	
Volume (Å ³)	1786.60(7)	1303.6(11)
Z, Density (calculated) (g cm ⁻³)	3, 1.377	2, 1.421
Absorption coefficient (mm ⁻¹)	1.065	0.987
<i>F</i> (000)	768	584
θ range for data collection (°)	1.76 to 27.49	1.79 to 25.25
Reflections collected / unique	10357 / 2743 [<i>R</i> _{int} = 0.0297]	5976 / 2354 [<i>R</i> _{int} = 0.0186]
Completeness	To $\theta = 27.49^\circ$: 100.0 %	To $\theta = 25.00^\circ$: 99.7 %
Data / restraints / parameters	2743 / 6 / 153	2354 / 1 / 175
Goodness-of-fit on <i>F</i> ²	1.027	1.075
Final <i>R</i> indices [<i>I</i> > 2 σ (<i>I</i>)]	<i>R</i> ₁ = 0.0289, <i>wR</i> ₂ = 0.0704	<i>R</i> ₁ = 0.0241, <i>wR</i> ₂ = 0.0635
<i>R</i> indices (all data)	<i>R</i> ₁ = 0.0389, <i>wR</i> ₂ = 0.0748	<i>R</i> ₁ = 0.0277, <i>wR</i> ₂ = 0.0659
Largest diff. peak and hole (e.Å ⁻³)	0.304 and -0.243	0.297 and -0.237

Table 4-10 Crystal data and refinement parameters for the cadmium(II) complexes.

	[Cd(C ₁₃ H ₁₂ NO ₂) ₂] _n (8)	[Cd(C ₁₃ H ₁₂ NO ₂) ₂ (CH ₄ O) ₂] (9)
Empirical formula	C ₂₆ H ₂₄ CdN ₂ O ₄	C ₂₈ H ₃₂ CdN ₂ O ₆
Formula weight	540.87	604.96
Temperature (K)	100(2)	100(2)
Crystal system , Space group	Rhombohedral, <i>R</i> ₋₃ : <i>r</i>	Monoclinic, <i>P</i> 21/ <i>c</i>
Unit cell dimensions		
<i>a</i> (Å)	12.8387(7)	11.5456(2)
<i>b</i> (Å)	12.8387(7)	9.62180(10)
<i>c</i> (Å)	12.8387(7)	11.9139(2)
<i>α</i> (°)	103.93	
<i>β</i> (°)	103.93	93.8480(10)
<i>γ</i> (°)	103.93	
Volume (Å ³)	1890.73(18)	1320.53(3)
<i>Z</i> , Density (calculated) (g cm ⁻³)	3, 1.425	2, 1.521
Absorption coefficient (mm ⁻¹)	0.899	0.872
<i>F</i> (000)	822	620
<i>θ</i> range for data collection (°)	1.72 to 26.99	2.72 to 27.50
Reflections collected / unique	2763 [<i>R</i> _{int} = 0.0463]	9378 / 3038 [<i>R</i> _{int} = 0.0216]
Completeness	To <i>θ</i> = 26.99° : 100.0 %	To <i>θ</i> = 26.00° : 99.9 %
Data / restraints / parameters	2763 / 0 / 153	3038 / 8 / 175
Goodness-of-fit on <i>F</i> ²	1.048	1.049
Final <i>R</i> indices [<i>I</i> > 2σ (<i>I</i>)]	<i>R</i> ₁ = 0.0247, <i>wR</i> ₂ = 0.0487	<i>R</i> ₁ = 0.0212, <i>wR</i> ₂ = 0.0499
<i>R</i> indices (all data)	<i>R</i> ₁ = 0.0293, <i>wR</i> ₂ = 0.0503	<i>R</i> ₁ = 0.0266, <i>wR</i> ₂ = 0.0520
Largest diff. peak and hole (e.Å ⁻³)	0.393 and -0.336	0.337 and -0.533

Table 4-11 Crystal data and refinement parameters for palladium(II) complexes **10** and **11**.

	[Pd(C ₁₃ H ₁₂ NO ₂) ₂] (10)	[Pd(C ₁₃ H ₁₁ NO ₂)(py)] _n (11)
Empirical formula	C ₂₆ H ₂₄ N ₂ O ₄ Pd	C ₁₈ H ₁₆ N ₂ O ₂ Pd
Formula weight	534.87	398.73
Temperature (K)	100(2)	100(2)
Crystal system , Space group	Monoclinic, <i>P 21/c</i>	Monoclinic, <i>P 21/c</i>
Unit cell dimensions		
<i>a</i> (Å)	7.0992(3)	6.5234(3)
<i>b</i> (Å)	26.6053(12)	17.4032(9)
<i>c</i> (Å)	11.6933(5)	14.0460(7)
<i>α</i> (°)		
<i>β</i> (°)	95.359(3)	91.6560(10)
<i>γ</i> (°)		
Volume (Å ³)	2198.93(17)	1593.95(14)
Z, Density (calculated) (g cm ⁻³)	4, 1.616	4, 1.662
Absorption coefficient (mm ⁻¹)	0.881	1.175
<i>F</i> (000)	1088	800
<i>θ</i> range for data collection (°)	2.32 to 25.04	2.34 to 27.00
Reflections collected / unique	15577 / 3885 [<i>R</i> _{int} = 0.1318]	19265 / 3481 [<i>R</i> _{int} = 0.0337]
Completeness	To <i>θ</i> = 25.00° : 99.7 %	To <i>θ</i> = 27.00° : 99.9 %
Data / restraints / parameters	3885 / 18 / 302	3481 / 0 / 210
Goodness-of-fit on <i>F</i> ²	1.182	1.040
Final <i>R</i> indices [<i>I</i> > 2σ (<i>I</i>)]	<i>R</i> ₁ = 0.0794, <i>wR</i> ₂ = 0.1627	<i>R</i> ₁ = 0.0214, <i>wR</i> ₂ = 0.0487
<i>R</i> indices (all data)	<i>R</i> ₁ = 0.1270, <i>wR</i> ₂ = 0.1763	<i>R</i> ₁ = 0.0254, <i>wR</i> ₂ = 0.0505
Largest diff. peak and hole (e.Å ⁻³)	1.694 and -1.350	0.432 and -0.405

Table 4-12 Crystal data and refinement parameters for palladium(II) complexes **12** and **13**.

	[Pd(C ₁₃ H ₁₁ NO ₂)(py) ₂] (12)	{[Pd(C ₁₃ H ₁₁ NO ₂)(bipy)].0.5 DMF} _n (13)
Empirical formula	C ₂₃ H ₂₁ N ₃ O ₂ Pd	C ₄₉ H ₄₅ N ₇ O ₅ Pd ₂
Formula weight	477.83	1024.72
Temperature (K)	296(2)	100(2)
Crystal system , Space group	Monoclinic, <i>P</i> 21/ <i>n</i>	Monoclinic, <i>C</i> 2/ <i>c</i>
Unit cell dimensions		
<i>a</i> (Å)	9.58720(10)	15.4998(2)
<i>b</i> (Å)	17.4169(2)	17.2185(2)
<i>c</i> (Å)	12.6524(2)	16.5477(2)
α (°)		
β (°)	93.0040(10)	93.954(2)
γ (°)		
Volume (Å ³)	2109.79(5)	4405.79(9)
Z, Density (calculated) (g cm ⁻³)	4, 1.504	4, 1.545
Absorption coefficient (mm ⁻¹)	0.903	0.873
<i>F</i> (000)	968	2080
θ range for data collection (°)	1.99 to 25.25	2.11 to 25.50
Reflections collected / unique	12337 / 3820 [<i>R</i> _{int} = 0.0199]	17779 / 4088 [<i>R</i> _{int} = 0.0299]
Completeness	To $\theta = 25.00^\circ$: 99.9 %	To $\theta = 25.00^\circ$: 100.0 %
Data / restraints / parameters	3820 / 2 / 264	4088 / 0 / 275
Goodness-of-fit on <i>F</i> ²	1.057	1.039
Final <i>R</i> indices [<i>I</i> > 2 σ (<i>I</i>)]	<i>R</i> ₁ = 0.0328, <i>wR</i> ₂ = 0.0925	<i>R</i> ₁ = 0.0246, <i>wR</i> ₂ = 0.0572
<i>R</i> indices (all data)	<i>R</i> ₁ = 0.0381, <i>wR</i> ₂ = 0.0968	<i>R</i> ₁ = 0.0282, <i>wR</i> ₂ = 0.0593
Largest diff. peak and hole (e.Å ⁻³)	1.573 and -0.504	0.771 and -0.515

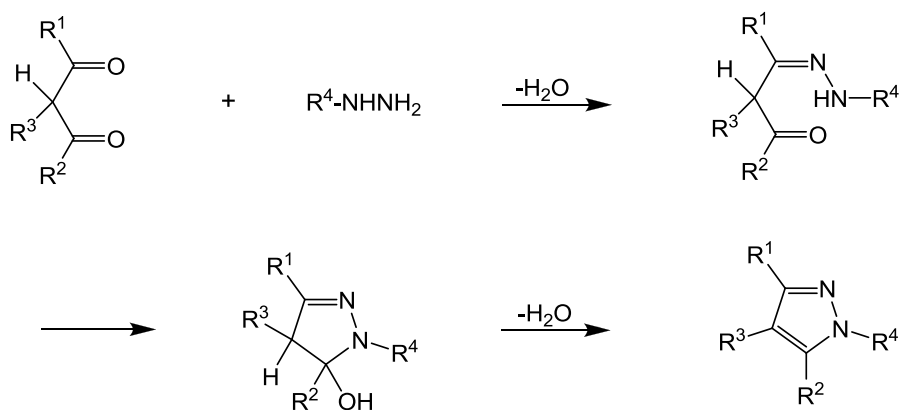
CHAPTER V

Reactions of

*2-(diformylmethyldene)-3,3-dimethylindole with
hydrazides: synthesis of new pyrazolyndolenine
derivatives*

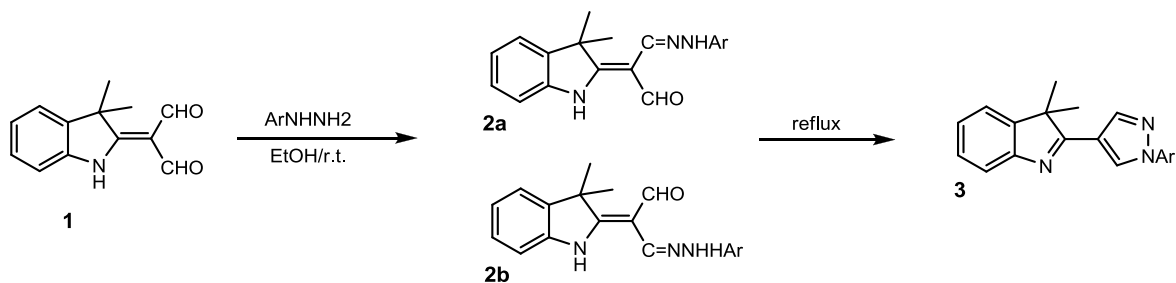
5.1 Introduction

Pyrazole derivatives constitute an important class of therapeutic agents in medicinal chemistry owing their effectiveness as antitumor [106], anti-inflammatory [107], antihypertensive [108], antipsychotic [109], and neuroprotective [110] agents. So far, a number of synthetic methods have been developed for formation of pyrazole skeleton [111], including the cyclization of 1,3-dicarbonyl with hydrazine derivatives [112-117], 1,3-dipolar cycloaddition of diazoalkanes with alkynes [118], the reaction of hydrazines with α,β -unsaturated ketones [119-121], the reaction of N-monosubstituted hydrazones with nitroolefins [122] and tandem coupling-cyclocondensation of acid chlorides, terminal alkynes and hydrazines [123]. Among those, the cyclization of 1,3-dicarbonyl with hydrazine derivatives, known as Knorr pyrazole synthesis [124], is one of the most common and widely-used methods in organic syntheses (Scheme 5-1). The reaction proceeds by the initial formation of the monohydrazones which are then converted to the pyrazoles by the action of heat or acids.



Scheme 5-1. Knorr pyrazole synthesis

Some years ago, Baradarani *et al.* have described the reaction of 2-(diformylmethylidene)-3,3-dimethylindole, **1**, with arylhydrazines to produce the related pyrazolyndolenines [125]. As they reported, the initial products of the reaction, separated at room temperature, were mono-hydrazones **2a** or **2b**, although it was not possible to ascertain which carbonyl group had reacted. Heating the mono-hydrazones in refluxing ethanol produced 4-(3,3-dimethylindol-2-yl)-substituted pyrazoles **3**, with migration of the double bond into the dihydropyrrole ring (Scheme 5-2).



Scheme 5-2.

We have now been able to determine the structure of the reported mono-hydrazone **2**. Moreover, we report the result of our investigation on the reaction of the diformyl **1** with hydrazides. Crystal structures of the synthesized compounds were also determined using single-crystal X-ray diffraction data.

5.2 Results and discussion

The ^1H NMR spectrum of the mono-hydrazone obtained from the reaction of the diformyl and phenylhydrazine shows the gem-dimethyl hydrogens at δ 1.73, the imine hydrogen at δ 8.31 and the aldehyde hydrogen at δ 10.00 ppm. To elucidate the structure of the compound, we have examined the possible NOE correlation between these hydrogens. The compound showed no NOE effect between the gem-methyl hydrogens and the imine hydrogen, whereas the effect was observed between the aldehyde and the methyl hydrogens (Figure 5-1). Therefore, the structure of the monohydrazone is unambiguously **2b**. This was further established by X-ray crystallographic analysis. Figure 5-2(a) shows the solid state structure of **2b** in which the imine link adopts the *trans* configuration stabilized by $\text{NH}\cdots\text{N}$ hydrogen bonding.

The greater reactivity of the C(13) in the diformyl **1** in comparison to C(12) may be due to the Bürgi-Dunitz direction of approach of the hydrazine which would be blocked by the gem-dimethyl group if nucleophilic attack took place at the C12 [126,127]. Attack at the C13, activated by intramolecular H-bonding, takes place away from the geminal methyl groups.

The hydrazone is then converted to pyrazolyindolenine **3** by the action of heat. The X-ray crystal structure of **3** shows that the indolenine and the pyrazole components are nearly coplanar, attesting to conjugation between these two heterocycles. This system and the third aromatic ring, *i.e.* the phenyl group are not coplanar (Figure 1b). The selected bond distances and bond angles of **2b** and **3** are given in Table 5-1.

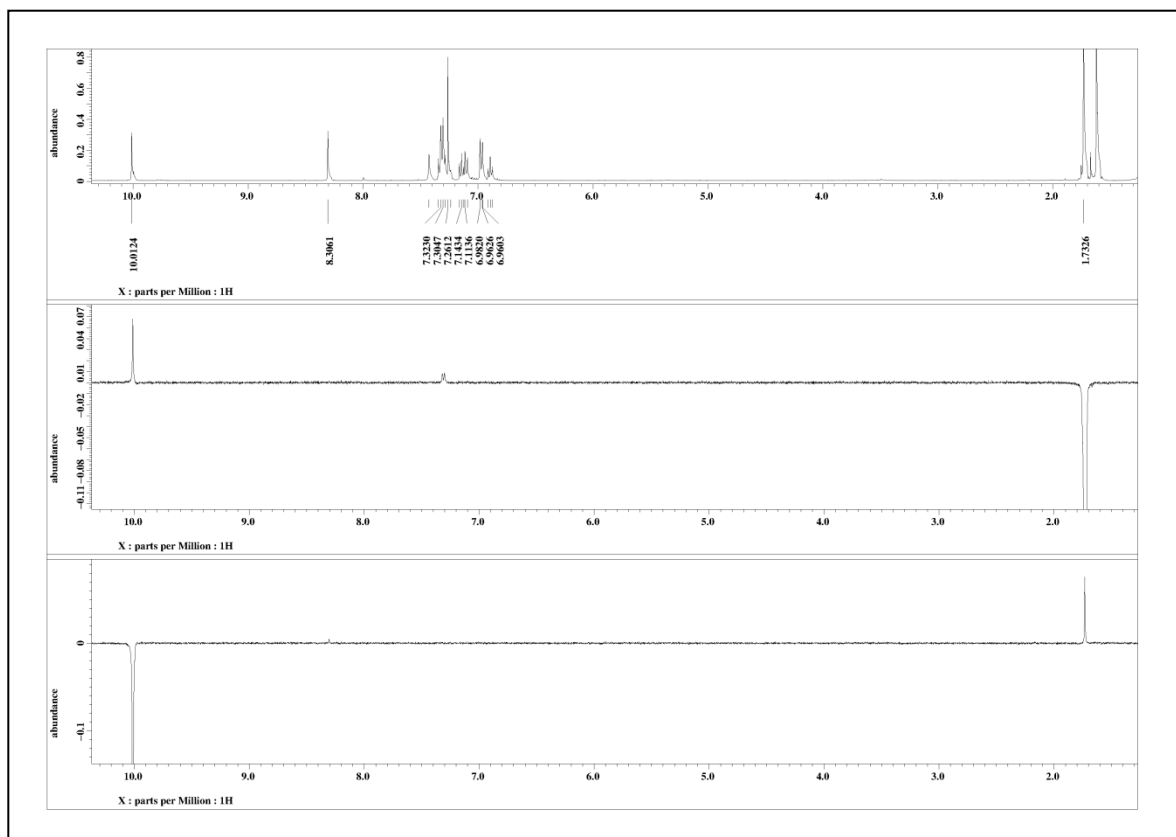
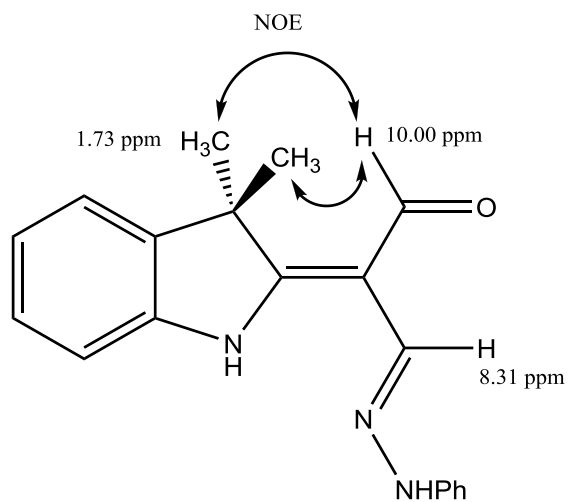


Figure 5-1 NOE correlation between the aldehyde hydrogen and the gem-dimethyl groups in

2b.

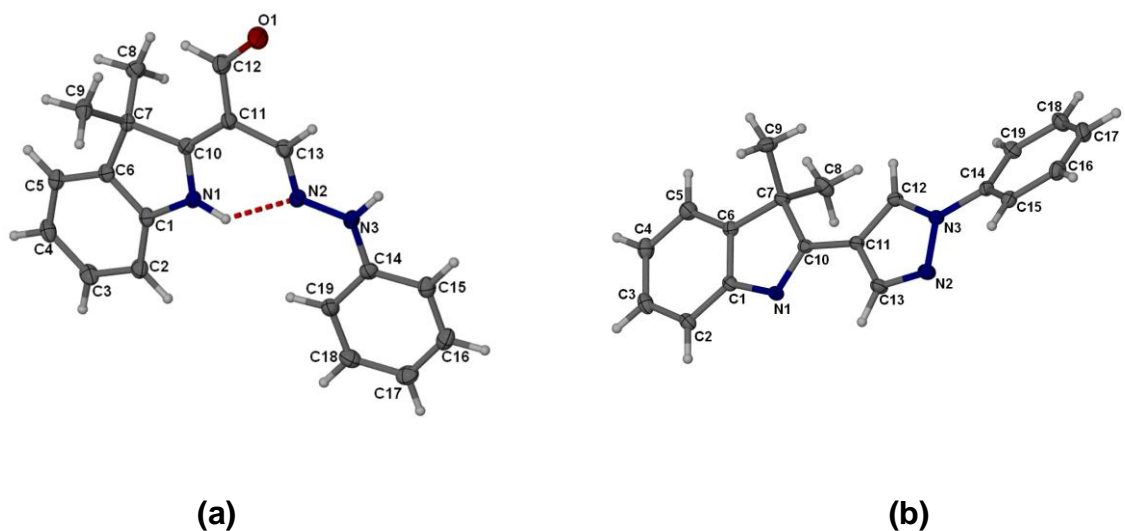
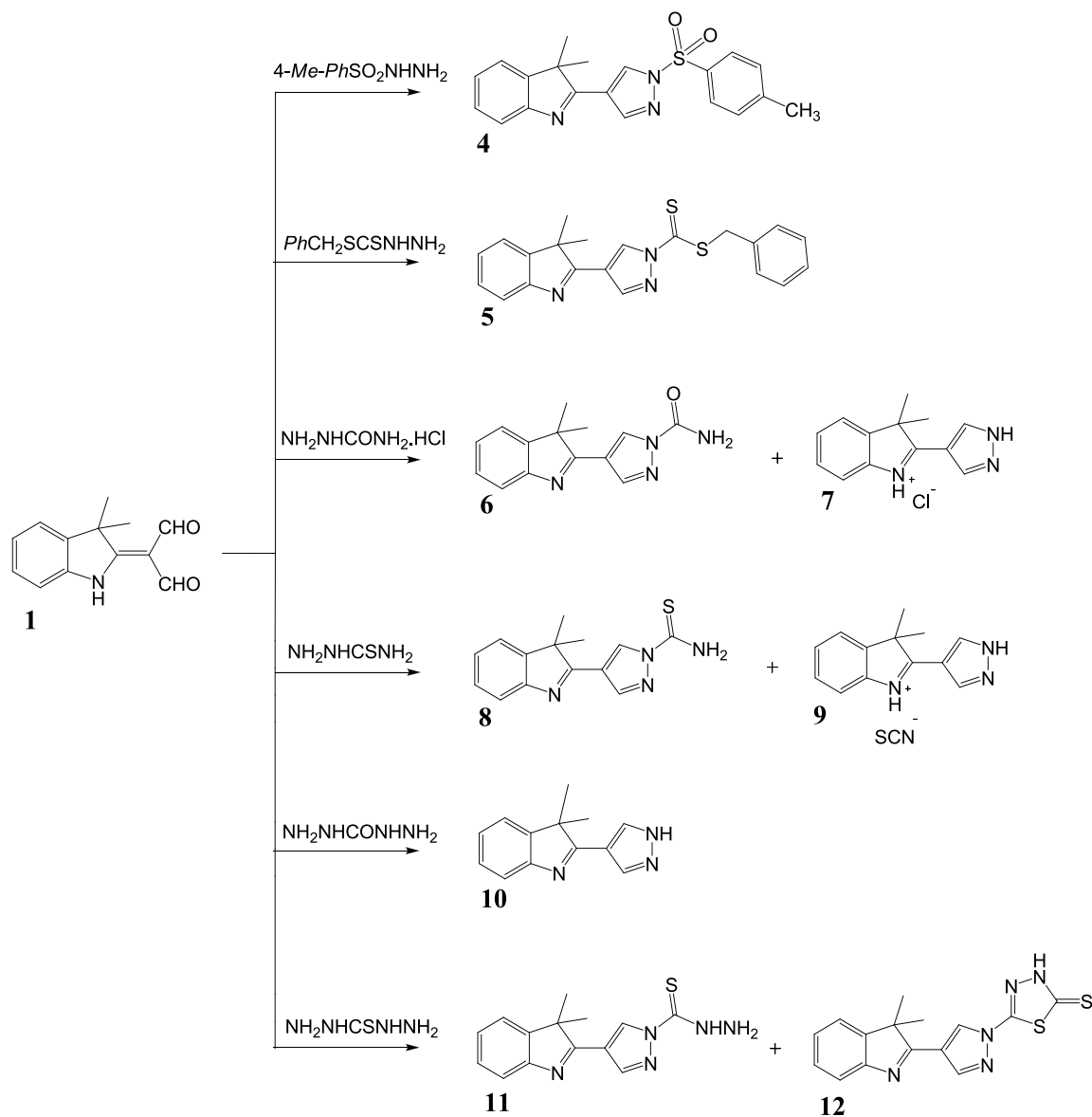


Figure 5-2 The crystal structure of compounds (a) **2b** and (b) **3**.

Table 5-1 Selected bond lengths (Å) and bond angles (°) for **2b** and **3**.

Compound 2b		Compound 3b	
<i>Bond lengths</i>			
O(1)-C(12)	1.2344(19)	N(1)-C(10)	1.2995(16)
N(1)-C(10)	1.344(2)	N(1)-C(1)	1.4189(17)
N(1)-C(1)	1.402(2)	N(2)-C(13)	1.3158(18)
N(2)-C(13)	1.288(2)	N(2)-N(3)	1.3606(15)
N(2)-N(3)	1.3652(19)	N(3)-C(12)	1.3437(16)
N(3)-C(14)	1.387(2)	N(3)-C(14)	1.4261(17)
C(10)-C(11)	1.391(2)	C(10)-C(11)	1.4503(19)
C(11)-C(12)	1.430(2)	C(11)-C(12)	1.3751(18)
C(11)-C(13)	1.452(2)	C(11)-C(13)	1.4010(19)
<i>Bond angles</i>			
C(13)-N(2)-N(3)	117.29(13)	N(2)-N(3)-C(14)	119.49(11)
C(9)-C(7)-C(8)	110.85(13)	C(9)-C(7)-C(8)	111.58(12)
C(12)-C(11)-C(13)	116.51(14)	N(1)-C(10)-C(11)	120.38(12)

To explore further aspects of the chemistry of this polyfunctional compound, we studied the reactions of the diformyl **1** with different hydrazides (Scheme 5-3).



Scheme 5-3.

The reaction of *p*-toluenesulfonylhydrazide was carried out in refluxing ethanol in the presence of acetic acid to give compound **4** as the sole product. The IR spectrum of **4** exhibited $\nu_s(\text{SO}_2)$ at 1180 cm^{-1} and $\nu_{as}(\text{SO}_2)$ at 1377 cm^{-1} . The X-ray crystal structure of **4** is depicted in Figure 5-3 and the selected bond lengths and angles are given in Table 5-2.

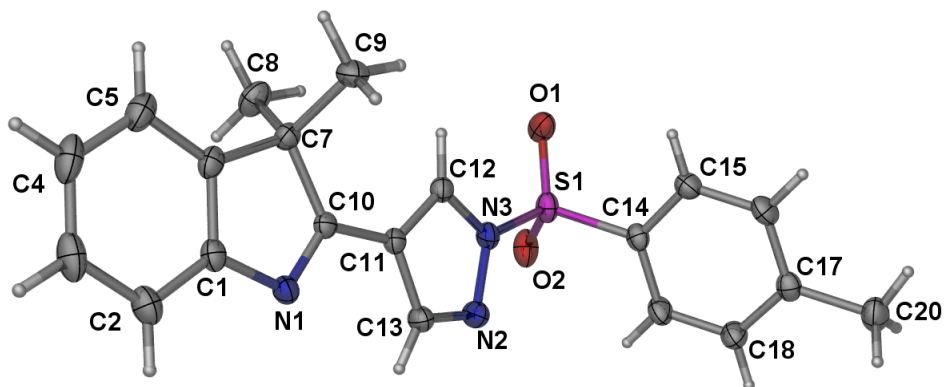


Figure 5-3 The crystal structure of compound **4** (30% probability ellipsoids).

Table 5-2 Selected bond lengths (Å) and bond angles (°) for **4**.

<i>Bond lengths</i>			
S(1)-O(2)	1.4196(15)	N(2)-N(3)	1.363(2)
S(1)-O(1)	1.4219(15)	N(3)-C(12)	1.361(2)
S(1)-N(3)	1.6919(14)	C(10)-C(11)	1.459(2)
S(1)-C(14)	1.7428(18)	C(11)-C(12)	1.363(2)
N(1)-C(10)	1.289(2)	C(11)-C(13)	1.414(2)
N(2)-C(13)	1.307(2)		
<i>Bond angles</i>			
O(2)-S(1)-O(1)	121.51(10)	O(1)-S(1)-C(14)	110.92(9)
O(2)-S(1)-N(3)	106.19(8)	N(3)-S(1)-C(14)	103.70(8)
O(1)-S(1)-N(3)	103.48(8)	N(2)-N(3)-S(1)	119.39(12)
O(2)-S(1)-C(14)	109.28(9)	N(3)-C(14)-S(1)	120.33(12)

Under the same reaction conditions S-benzylthiocarbamide [48] reacted efficiently with the diformyl **1** to form the pyrazole **5**. The structure of **5** is shown in Figure 5-4. It is noteworthy that neither the *p*-toluenesulfonyl nor the S-benzylthiocarbonyl groups were cleaved under the applied conditions.

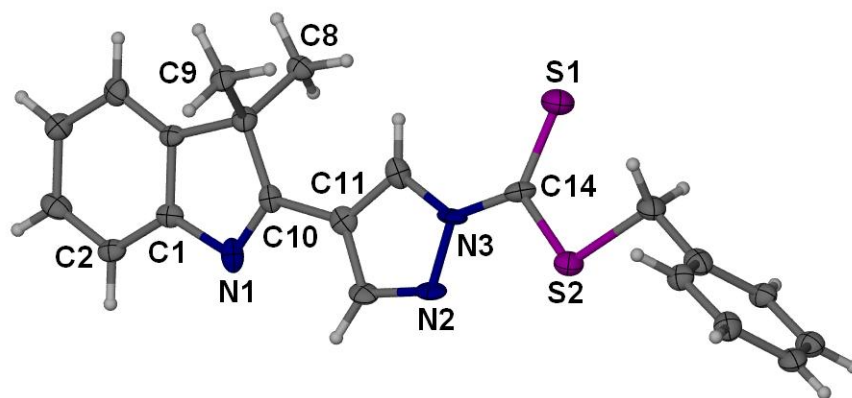


Figure 5-4 The crystal structure of compound **5**.

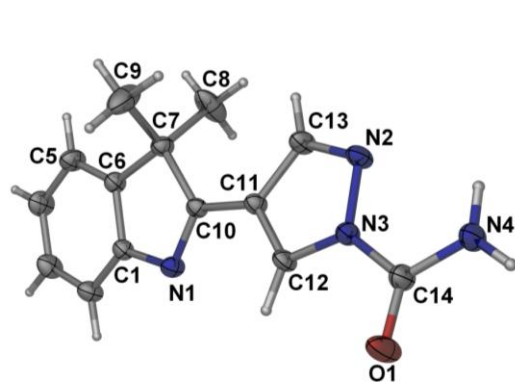
Diformyl **1** reacted with semicarbazide hydrochloride in ethanol at room temperature to form the 1-carbamoylpyrazole **6**. However, conducting the reaction in refluxing ethanol resulted in loss of carbamoyl group, leading to the indolium chloride salt **7**. $^1\text{H-NMR}$ spectrum of **6** shows the two amide hydrogens at δ 8.18 and 8.23 ppm which disappear by addition of D_2O . Figure 5-5 depicts the crystal structures of **6** and **7**.

Similarly, the reaction of thiosemicarbazide with diformyl **1** afforded the 1-thiocarbamoylpyrazole **8** and (after loss of thiocarbamoyl group) the indolium thiocyanate salt **9**, as a mixture. The IR spectrum of **9** displays the thiocyanate absorption as a strong band at 2078 cm^{-1} , and the $^{13}\text{C-NMR}$ has a peak at 207.11 ppm, related to the thiocyanate carbon. Our attempts to prevent the loss of the thiocarbamoyl moiety were unsuccessful;

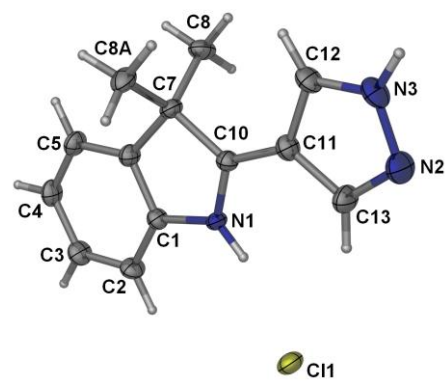
however, the pure products were easily obtained by sequential crystallization. The solid state structures of **8** and **9** are illustrated in Figure 5-6. 1-(Thio)carbamoylpyrazole derivatives are an intriguing class of chelating ligands and important intermediates in synthesis a variety of heterocyclic compounds [128-132]. It is well known that their (thio)carbamoyl groups tend to split off upon heating and also by the action of bases. In fact this cleavage can lead to an interesting series of metal complexes in coordination chemistry [133-134]. Evidently the indolenine nitrogen of compound **6** and **8** acts as base and is then converted to the related indolium salts, facilitating the cleavage of the (thio)carbamoyl group. The X-ray crystal structures of **7** and **9** confirm the formation of indolium salts. The selected interatomic distances and bond angles for compound **6-9** are listed in Tables 5-3 and 5-4.

Table 5-3 Selected bond lengths (Å) and bond angles (°) for **6** and **7**.

Compound 6		Compound 7	
<i>Bond lengths</i>			
O(1)-C(14)	1.215(3)	N(1)-C(10)	1.287(4)
N(1)-C(10)	1.302(3)	N(2)-C(13)	1.323(5)
N(2)-C(13)	1.312(3)	N(2)-N(3)	1.363(5)
N(2)-N(3)	1.364(3)	N(3)-C(12)	1.320(5)
N(3)-C(12)	1.343(3)	C(10)-C(11)	1.412(5)
N(3)-C(14)	1.415(3)	C(11)-C(12)	1.406(5)
N(4)-C(14)	1.318(4)	C(11)-C(13)	1.418(5)
C(10)-C(11)	1.457(4)		
C(11)-C(12)	1.356(4)		
C(11)-C(13)	1.417(4)		
<i>Bond angles</i>			
O(1)-C(14)-N(4)	126.2(3)	N(1)-C(10)-C(11)	122.2(3)
O(1)-C(14)-N(3)	118.5(3)	C(11)-C(10)-C(7)	126.9(3)

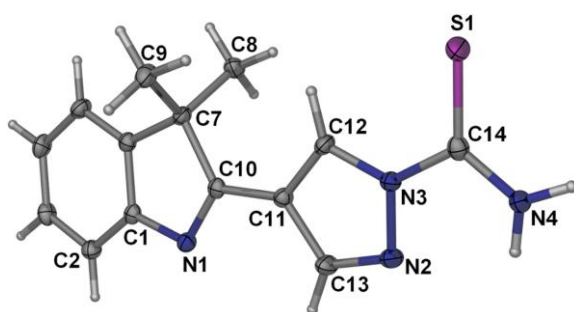


(a)

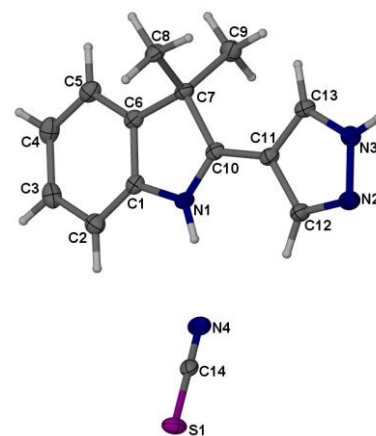


(b)

Figure 5-5 The crystal structures of compounds (a) **7** and (b) **8**.



(a)



(b)

Figure 5-6 The crystal structures of compounds (a) **8** and (b) **9**.

Table 5-4 Selected bond lengths (Å) and bond angles (°) for **8** and **9**.

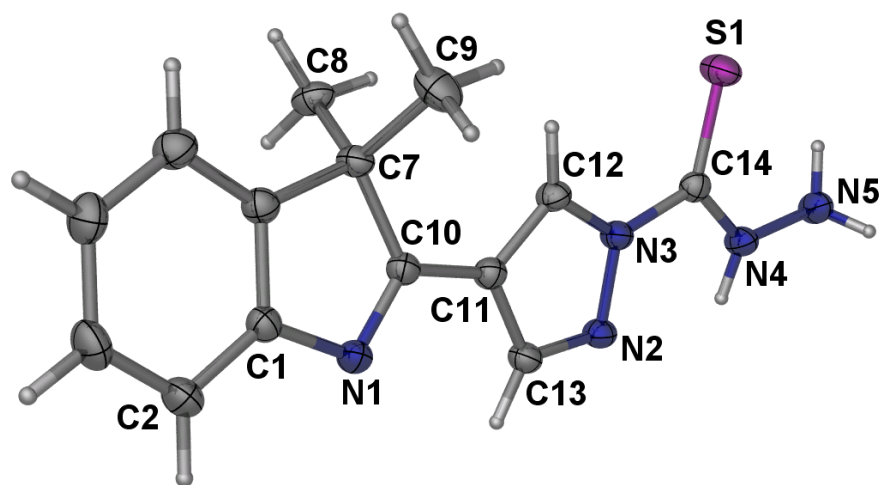
Compound 8		Compound 9	
<i>Bond lengths</i>			
S(1)-C(14)	1.6530(17)	S(1)-C(14)	1.648(2)
N(1)-C(10)	1.300(2)	N(1)-C(10)	1.300(2)
N(2)-C(13)	1.312(2)	N(2)-C(13)	1.324(2)
N(2)-N(3)	1.3723(18)	N(2)-N(3)	1.370(2)
N(3)-C(12)	1.360(2)	N(3)-C(12)	1.321(2)
N(3)-C(14)	1.413(2)	N(4)-C(14)	1.162(2)
N(4)-C(14)	1.318(2)	C(10)-C(11)	1.427(3)
C(10)-C(11)	1.454(2)	C(11)-C(12)	1.398(3)
C(11)-C(12)	1.372(2)	C(11)-C(13)	1.420(3)
C(11)-C(13)	1.423(2)		
<i>Bond angles</i>			
N(2)-N(3)-C(14)	120.17(13)	N(1)-C(10)-C(11)	122.14(17)
N(1)-C(10)-C(11)	121.09(15)	N(4)-C(14)-S(1)	178.79(17)
C(11)-C(10)-C(7)	124.33(14)		
N(4)-C(14)-S(1)	126.73(13)		
N(3)-C(14)-S(1)	120.33(12)		

Lastly, the reactions of the dialdehyde with carbohydrazide and thiocarbohydrazide were investigated. Regardless of the experimental conditions, the only product obtained from the reaction with carbohydrazide was (1*H*-pyrazole-4-yl)-3*H*-indole **10**, which was also obtained from the reaction of hydrazine and the diformyl [125]. Apparently the initial product is very unstable and immediately decomposes to compound **10**. The interaction of the dialdehyde with thiocarbohydrazide led to the formation of the pyrazole-*N*-thiocarbohydrazide **11** and the thiadiazole-2-thione **12**. To the best of our knowledge this protocol for formation of thiadiazole ring is unprecedented as is this arrangement of

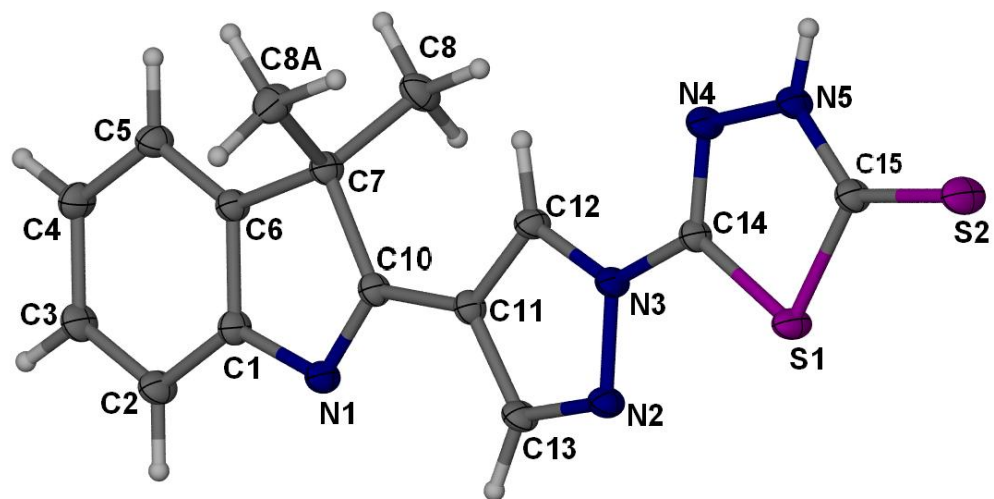
heterocyclic systems *i.e.* pyrazole-*N*-yl-1,3,4-thiadiazole-2-thione. Although thiadiazole-2-thione fused to the C atom of pyrazoles are known [135-137], analogous fusion to the N atom of pyrazoles is not. The crystal structure of compounds **11** and **12** are depicted in Figure 5-7 and selected bond lengths and bond angles are given in Table 5-5. The structure of **12** shows the three heterocyclic rings are coplanar, indicating conjugation between them, in contrast to compound **3**. This presumption is supported by the shorter bond length of N(3)-C(14) in **12** (1.39 Å) compared to the one in **3** (1.43 Å), attesting its significant double bond character.

Table 5-5 Selected bond lengths (Å) and bond angles (°) for **11** and **12**.

Compound 11		Compound 12	
<i>Bond lengths</i>			
S(1)-C(14)	1.6522(17)	S(1)-C(14)	1.722(3)
N(1)-C(10)	1.297(2)	S(1)-C(15)	1.751(3)
N(2)-C(13)	1.316(2)	S(2)-C(15)	1.657(3)
N(2)-N(3)	1.3729(19)	N(5)-C(15)	1.338(3)
N(3)-C(12)	1.351(2)	N(5)-N(4)	1.376(3)
N(3)-C(14)	1.410(2)	N(3)-C(12)	1.353(3)
N(4)-C(14)	1.313(2)	N(3)-N(2)	1.370(3)
N(4)-N(5)	1.414(2)	N(3)-C(14)	1.387(3)
C(10)-C(11)	1.450(2)	N(2)-C(13)	1.320(3)
C(11)-C(12)	1.366(2)	N(1)-C(10)	1.300(3)
C(11)-C(13)	1.425(2)	C(12)-C(11)	1.373(4)
		C(11)-C(13)	1.419(4)
		C(11)-C(10)	1.456(3)
<i>Bond angles (°)</i>			
N(2)-N(3)-C(14)	122.07(13)	N(2)-N(3)-C(14)	119.1(2)
C(14)-N(4)-N(5)	122.15(16)	S(2)-C(15)-S(1)	124.15(16)
N(1)-C(10)-C(11)	121.97(15)	N(1)-C(10)-C(11)	122.0(2)
C(13)-C(11)-C(10)	128.72(16)		
N(4)-C(14)-S(1)	125.03(14)		



(a)

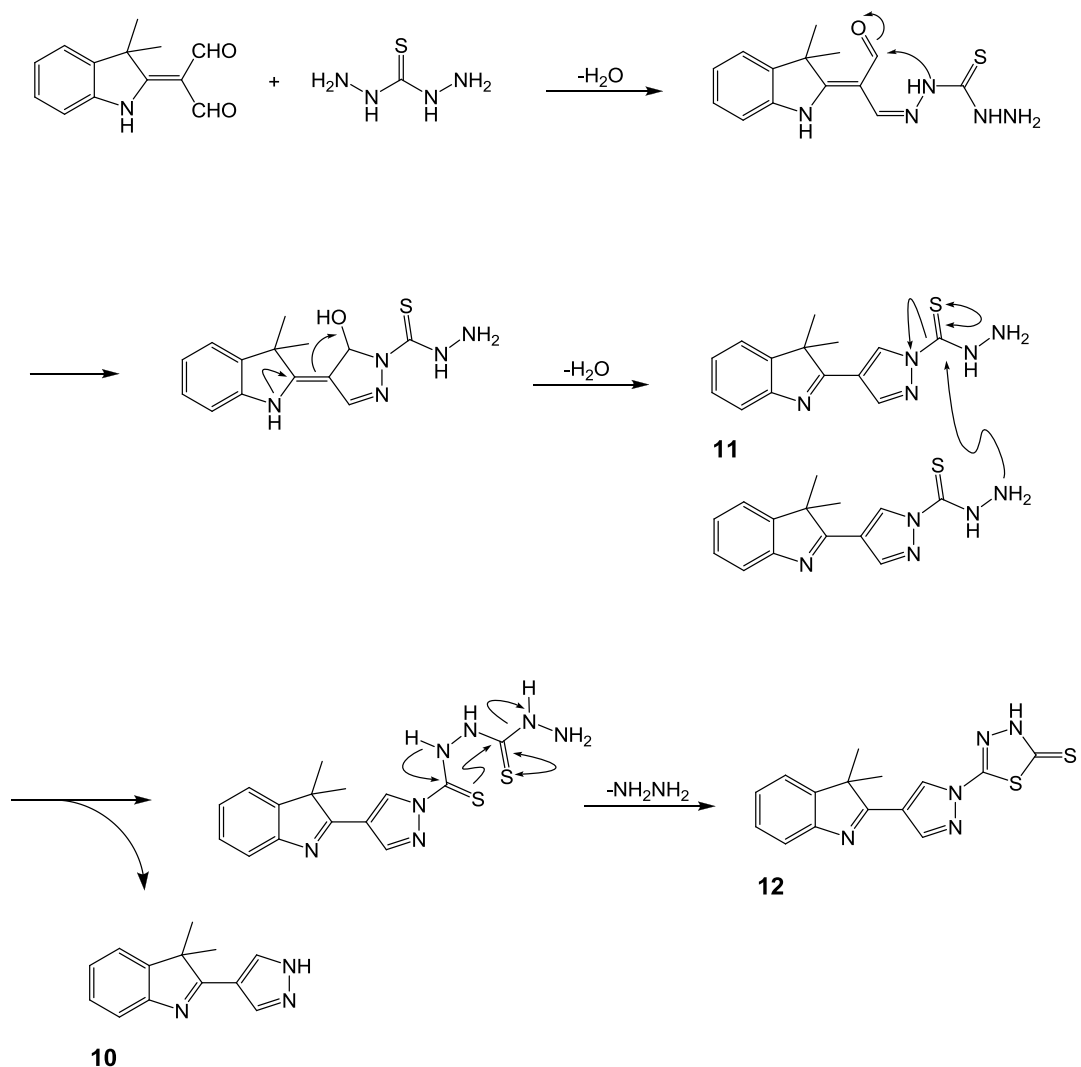


(b)

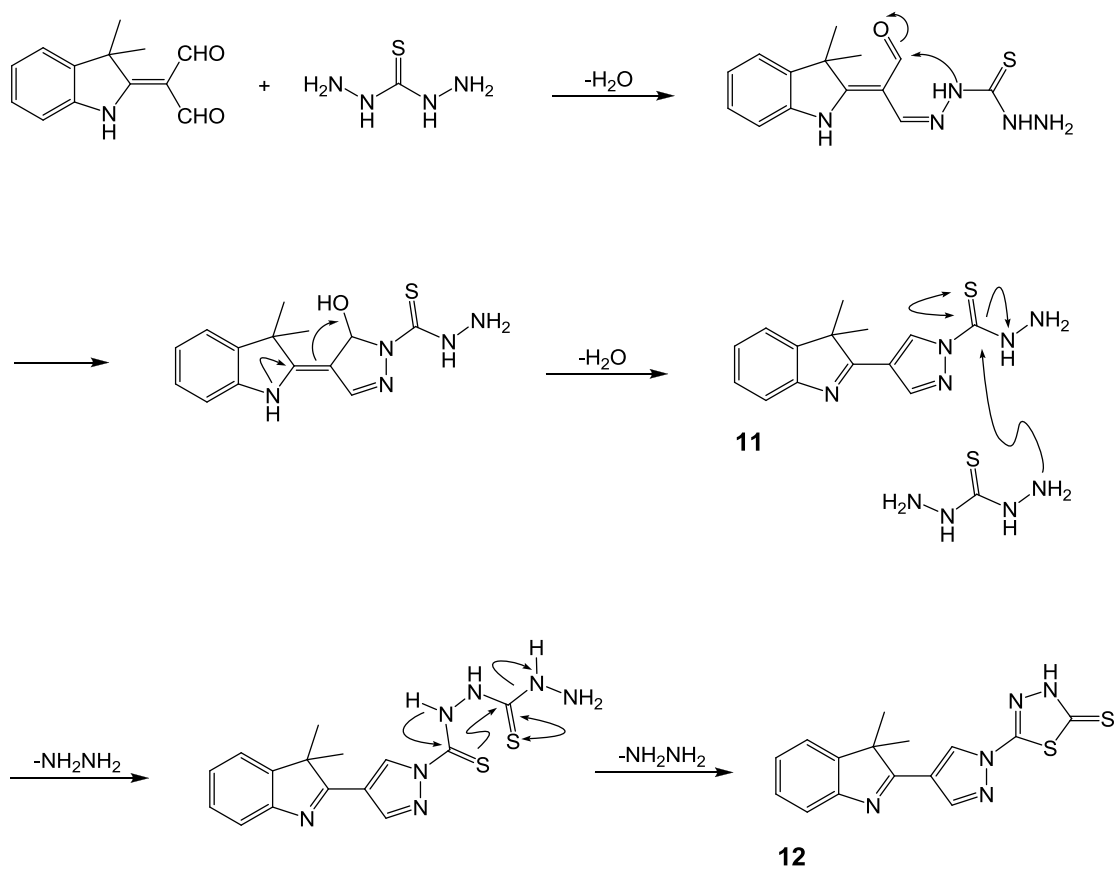
Figure 5-7 The crystal structures of compounds (a) **11** and (b) **12**.

The reaction mechanism for the formation of pyrazolyndolenine **11** is fundamentally the same as that for the formation of the other pyrazolyndolenines. To explain the formation of compound **12** two possible mechanisms were considered (Scheme 5-4). One involves intermolecular reaction of two molecules of compound **11** (i). The second one requires the nucleophilic attack of a second molecule of thiocarbohydrazide on compound **11** (ii).

(i)



(ii)



Scheme 5-4.

The intermediate then undergoes cyclocondensation to form the five member ring of 1,3,4-thiadiazole. The first mechanism may be ruled out since it would lead to formation of pyrazolylindolenine **10** which was not detected under reaction conditions. Moreover, refluxing an ethanolic solution of pyrazole-*N*-thiocarbohydrazide **11** in the presence of acetic acid did not give any of compound **12**. Therefore the path (ii) is assumed as the mechanism of the reaction.

It is also important to mention that in spite of some reports about the synthesis of pyrazoles using benzoic hydrazide and analogues [132, 138], our efforts to react benzoic hydrazide with the dialdehyde **1** under different conditions were unsuccessful. In fact the only product obtained was 1,2-dibenzoylhydrazine [139], the product of transacylation of benzoic hydrazide.

5.3 Conclusions

Cyclo-condensation of 2-(diformylmethylidene)-3,3-dimethylindole with the hydrazides led to the formation of a new set of indolenine-based pyrazoles. A unique pyrazole–thiadiazole double annulation was observed in the reaction of the diformyl compound with thiocarbohydrazide.

5.4 Experimental

Melting points were determined using a MEL-TEMP II melting point instrument and were not corrected. Microanalyses were carried out on a Perkin-Elmer 2400 elemental analyzer. ¹H-NMR and ¹³C-NMR spectra were determined with a Lambda JEOL 400 MHz FT-NMR (¹H: 400 MHz and ¹³C: 100.4 MHz) spectrometer. Chemical shifts are given in δ values (ppm) using TMS as the internal standard. The IR spectra were taken with a Perkin-Elmer RX1 FT-IR spectrophotometer. The mass spectra were taken on an Agilent 1200 LC/MS.

5.4.1 Reaction with *p*-toluenesulfonylhydrazide

A solution of the dialdehyde (**1**) (0.43 g, 2 mmol) and *p*-toluenesulfonylhydrazide (0.372 g, 2 mmol) in ethanol (20 mL) in the presence of acetic acid (0.2 mL) was refluxed for 4 h. The solution was evaporated to half of its volume and then set aside at room temperature overnight whereupon pale yellow crystals of the compound **4** were obtained.

*3,3-Dimethyl-2-[1-(*p*-toluenesulfonyl)-1*H*-pyrazol-4-yl]-3*H*-indole* (**4**): 0.65 g, 89%. mp 160-162 °C; IR (KBr, cm⁻¹): 2961, 1594, 1575, 1454, 1377, 1324, 1180, 1094, 1075, 673, 585; ¹H NMR (DMSO-*d*₆): δ 1.43 (s, 6H, gem-CH₃), 2.39 (s, 3H, Ar-CH₃), 7.25 (m, 1H, Ar-H), 7.32 (m, 1H, Ar-H), 7.50-7.55 (m, 4H, Ar-H), 8.00 (d, 2H, *J* = 8.4 Hz, Ar-H), 8.49 (s, 1H, pyrazolyl-H), 9.11 (s, 1H, pyrazolyl-H); ¹³C NMR (DMSO-*d*₆): δ 21.16, 23.39, 52.90, 118.38, 120.08, 121.48, 125.73, 127.67, 128.05, 130.50, 131.06, 132.86, 144.75, 146.68, 146.78, 152.98, 176.68; MS: *m/z* 366 (MH⁺); Anal. Calcd for C₂₀H₁₉N₃O₂S: C, 65.73; H, 5.24; N, 11.50; O, 8.76; S, 8.77%. Found: C, 65.60; H, 5.24; N, 11.29; S, 8.69%.

5.4.2 Reaction with *S*-benzylthiocarbamate

A solution of the dialdehyde (**1**) (0.43 g, 2 mmol) and *S*-benzylthiocarbamate [48] (0.396 g, 2 mmol) in ethanol (30 mL) in the presence of acetic acid (1 mL) refluxed for 3 h and then cooled at room temperature. The yellow solid of the compound **5** was separated out on addition of water (30 mL) to the solution. It was collected and washed with cold ethanol and dried over silica gel. The crystal for X-ray analysis was obtained by slow evaporation of an ethanolic solution at room temperature.

4-(3,3-Dimethyl-3H-indol-2-yl)-pyrazole-1-carbodithioic acid benzyl ester (5): 0.52 g, 68%. mp 143-144 °C; IR (KBr, cm⁻¹): 3141, 2968, 1578, 1373, 1169, 1073, 843, 755; ¹H NMR (DMSO-*d*₆): δ 1.45 (s, 6H, CH₃), 4.61 (s, 2H, CH₂), 7.25—7.37 (m, 5H, Ar-H), 7.46 (d, 2H, *J* = 7.2 Hz, Ar-H), 7.52 (d, 1H, *J* = 7.2 Hz, Ar-H), 7.58 (d, 1H, *J* = 7.6 Hz, Ar-H), 8.66 (s, 1H, pyrazolyl-H), 9.17 (s, 1H, pyrazolyl-H); ¹³C NMR (DMSO-*d*₆): δ 23.52, 40.32, 52.90, 119.86, 120.27, 121.56, 125.97, 127.74, 127.79, 128.59, 128.62, 129.39, 134.66, 144.95, 146.82, 153.07, 176.56, 199.13; MS: *m/z* 378 (MH⁺); Anal. Calcd for C₂₁H₁₉N₃S₂: C, 66.81; H, 5.07; N, 11.13; S, 16.99%. Found: C, 66.07; H, 5.21; N, 10.96; S, 16.77%.

5.4.3 Reaction with semicarbazide hydrochloride

A solution of the dialdehyde (**1**) (0.43 g, 2 mmol) and semicarbazide hydrochloride (0.223 g, 2 mmol) was stirred in ethanol (15 mL) at room temperature for one day during which pale yellow solid of compound **6** was formed. The solid was filtered, washed with NaHCO₃ aqueous solution and cold ethanol and dried over silica gel. More solid was obtained from the filtrate. Suitable crystal for X-ray analysis was grown in EtOAc. Compound **7** was obtained as a colorless crystal by conducting the reaction in refluxing ethanol for 5 h and leaving the solution at room temperature for 2 days.

4-(3,3-Dimethyl-3H-indol-2-yl)-pyrazole-1-carboxamide (6): 0.36 g, 71%. mp 176-178 °C; IR (KBr, cm⁻¹): 3383, 3237, 2973, 1741, 1570, 1441, 1356, 1207, 965, 753; ¹H NMR (DMSO-*d*₆): δ 1.57 (s, 6H, CH₃), 7.37 (m, 1H, indolenine-H), 7.43 (m, 1H, indolenine-H), 7.62—7.65 (m, 2H, indolenine-H), 8.18 (s, 1H, NH₂), 8.23 (s, 1H, NH₂), 8.68 (s, 1H, pyrazolyl-H), 9.23 (s, 1H, pyrazolyl-H); ¹³C NMR (DMSO-*d*₆): 24.03, 52.98,

114.08, 117.53, 122.48, 127.23, 128.44, 132.22, 142.75, 144.65, 145.29, 149.16, 178.47;
MS: m/z 255 (MH^+); Anal. Calcd for $C_{14}H_{14}N_4O$: C, 66.13; H, 5.55; N, 22.03; O, 6.29%.
Found: C, 66.02; H, 5.69; N, 21.94%.

3,3-Dimethyl-2-(1H-pyrazol-4-yl)-3H-indolium chloride (7): 0.37 g, 75%. mp 266-268 °C; IR (KBr, cm^{-1}): 3084, 1611, 1593, 1244, 1154, 762; 1H NMR (DMSO- d_6): δ 1.68 (s, 6H, CH_3), 7.44—7.53 (m, 2H, indolenine-H), 7.66 (d, 1H, $J = 7.6$ Hz, indolenine-H), 7.76 (d, 1H, $J = 7.2$ Hz, indolenine-H), 9.06 (s, 2H, pyrazolyl-H); ^{13}C NMR (DMSO- d_6): δ 23.94, 52.57, 109.38, 115.56, 122.93, 127.46, 128.73, 138.52, 141.01, 142.86, 179.64; Anal. Calcd for $C_{13}H_{14}ClN_3$: C, 63.03; H, 5.70; N, 16.96%. Found: C, 62.90; H, 5.89; N, 16.81%.

5.4.4 Reaction with thiosemicarbazide

A solution of the dialdehyde (**1**) (0.43 g, 2 mmol) and thiosemicarbazide (0.182 g, 2 mmol) in ethanol (20 mL) in the presence of acetic acid (0.5 mL) refluxed for 1 h. The solvent was evaporated and the resulting solid was dissolved in EtOAc : Hexane (7:3) and set aside at room temperature. In a few hours the yellow crystals of the compound **9** were formed. The crystals were collected and the solution was set aside for one day whereupon the yellow crystals of compound **8** were separated out.

4-(3,3-Dimethyl-3H-indol-2-yl)-pyrazole-1-carbothioamide (8): 0.34 g, 63%. mp 152-154 °C; IR (KBr, cm^{-1}): 3377, 3256, 2964, 1621, 1576, 1455, 1370, 1186, 1100, 974, 872, 757, 632; 1H NMR (DMSO- d_6): δ 1.44 (s, 6H, CH_3), 7.25 (m, 1H, indolenine-H), 7.34 (m, 1H, indolenine-H), 7.52 (d, 1H, $J = 7.2$ Hz, indolenine-H), 7.56 (d, 1H, $J = 7.6$ Hz, indolenine-H), 8.52 (s, 1H, pyrazolyl-H), 9.15 (s, 1H, pyrazolyl-H), 9.72 (s, 1H, NH_2),

10.20 (s, 1H, NH₂); ¹³C NMR (CDCl₃): δ 24.51, 53.30, 119.86, 120.67, 121.06, 125.98, 127.98, 130.17, 143.57, 146.40, 153.39, 176.81, 177.69; MS: m/z 271 (MH⁺); Anal. Calcd for C₁₄H₁₄N₄S: C, 62.20; H, 5.22; N, 20.72; S, 11.86%. Found: C, 61.86; H, 5.08; N, 20.49; S, 11.71%.

3,3-Dimethyl-2-(1H-pyrazol-4-yl)-3H-indolium thiocyanate (9): 0.15 g, 28%. mp 177-180 °C; IR (KBr, cm⁻¹): 3105, 2078, 1610, 1594, 1249, 1163, 944, 761; ¹H NMR (DMSO-*d*₆): δ 1.65 (s, 6H, CH₃), 7.39—7.50 (m, 2H, indolenine-H), 7.58 (d, 1H, *J* = 7.3 Hz, indolenine-H), 7.74 (d, 1H, *J* = 7.3 Hz, indolenine-H), 8.85 (s, 2H, pyrazolyl-H); ¹³C NMR (DMSO-*d*₆): δ 25.49, 53.24, 110.14, 116.28, 123.50, 128.02, 129.35, 138.64, 141.96, 143.52, 180.75, 207.108; Anal. Calcd for C₁₄H₁₄N₄S: C, 62.20; H, 5.22; N, 20.72; S, 11.86%. Found: C, 61.91; H, 5.41; N, 20.42; S, 11.60%.

5.4.5 Reaction with thiocarbohydrazide

A mixture of the dialdehyde (**1**) (0.43 g, 2 mmol) and thiocarbohydrazide (0.318 g, 3 mmol) in ethanol (20 mL) in the presence of acetic acid (0.5 mL) was refluxed for 4 h during which the compound **12** was precipitated. It was filtered, washed with water and ethanol and dried over silica gel. Suitable crystal for X-ray analysis was obtained by recrystallization from DMSO. Compound **11** was separated out as a yellow solid on addition of water to the filtrate and recrystallized from ethyl acetate to give the suitable crystal for X-ray analysis.

4-(3,3-Dimethyl-3H-indol-2-yl)-pyrazole-1-carbothioic acid hydrazide (11): 0.31 g, 54%. mp 149-150 °C; IR (KBr, cm⁻¹): 3260, 2965, 1579, 1540, 1454, 1358, 1246, 1165, 1014, 896, 750; ¹H NMR (CDCl₃): δ 1.52 (s, 6H, CH₃), 4.76 (bs, 2H, NH₂), 7.25-7.39 (m,

3H, indolenine-H), 7.66 (d, 1H, $J = 7.2$ Hz, indolenine-H), 8.40 (s, 1H, pyrazolyl-H), 9.05 (s, 1H, pyrazolyl-H), 9.97 (bs, 1H, NH); ^{13}C NMR (CDCl_3): δ 24.56, 53.31, 118.98, 120.67, 121.07, 125.95, 128.01, 130.26, 143.19, 146.38, 153.49, 174.79, 176.90; MS: m/z 286 (MH^+); Anal. Calcd for $\text{C}_{14}\text{H}_{15}\text{N}_5\text{S}$: C, 58.92; H, 5.30; N, 24.54; S, 11.24%. Found: C, 58.49; H, 5.58; N, 24.23; S, 11.09%.

5-[4-(3,3-Dimethyl-3H-indol-2-yl)-pyrazol-1-yl]-3H-[1,3,4]thiadiazole-2-thione (12): 0.09 g, 14%. mp 312-314 °C; IR (KBr, cm^{-1}): 3076, 2965, 1583, 1431, 1257, 1192, 1059, 739; ^1H NMR ($\text{DMSO}-d_6$): δ 1.48 (s, 6H, CH_3), 7.27 (m, 1H, indolenine-H), 7.35 (m, 1H, indolenine-H), 7.53 (d, 1H, $J = 6.8$ Hz, indolenine-H), 7.58 (d, 1H, $J = 7.2$ Hz, indolenine-H), 8.58 (s, 1H, pyrazolyl-H), 9.14 (s, 1H, pyrazolyl-H), 10.58 (s, 1H, NH); ^{13}C NMR ($\text{DMSO}-d_6$): δ 23.43, 52.91, 119.14, 120.07, 121.52, 125.73, 127.48, 127.72, 143.59, 146.82, 152.95, 153.08, 176.86, 186.17; Anal. Calcd for $\text{C}_{15}\text{H}_{13}\text{N}_5\text{S}_2$: C, 55.02; H, 4.00; N, 21.39; S, 19.59%. Found: C, 54.77; H, 3.84; N, 21.75; S, 19.36%.

5.4.6 Crystallography

Diffraction data were measured using a Bruker SMART Apex II CCD area-detector diffractometer (graphite-monochromated Mo $\text{K}\alpha$ radiation, $\lambda = 0.71073$ Å). The orientation matrix, unit cell refinement and data reduction were all handled by the Apex2 software (SAINT integration, SADABS absorption correction) [49]. The structures were solved using direct or Patterson methods in the program SHELXS-97 [50] and were refined by the full matrix least-squares method on F^2 with SHELXL-97. All the non-hydrogen atoms were refined anisotropically and all the C-bound hydrogen atoms were placed at calculated positions and refined isotropically. N-bound hydrogen atoms were located in difference

Fourier maps and refined with distance restraint of N-H 0.88 Å. Drawings of the molecules were produced with XSEED [51]. Crystal data and refinement are summarized in Tables 5-6, 5-7, 5-8, 5-9 and 5-10. Crystallography data for the structures in chapter V have been deposited with the Cambridge Crystallographic Data Centre, CCDC Nos. 764076 (for **2b**), 764077 (for **3**), 764078 (for **4**), 764079 (for **5**), 823997 (for **6**), 764080 (for **7**), 764081 (for **8**), 764082 (for **9**), 764083 (for **10**), 764084 (for **11**), 764085 (for **12**). These data can be obtained free of charge from The Cambridge Crystallographic Data Centre via www.ccdc.cam.ac.uk/data_request/cif.

Table 5-6 Crystal data and refinement parameters for compounds **2b** & **3**.

	2b	3
Empirical formula	C ₁₉ H ₁₉ N ₃ O	C ₁₉ H ₁₇ N ₃
Formula weight	305.37	287.36
Temperature (K)	100(2)	296(2)
Crystal system , Space group	Orthorhombic, <i>Pbcn</i>	Orthorhombic, <i>Pbca</i>
Unit cell dimensions		
<i>a</i> (Å)	16.145(2)	9.7922(6)
<i>b</i> (Å)	10.8349(13)	17.0132(10)
<i>c</i> (Å)	17.910(2)	18.4438(11)
<i>α</i> (°)		
<i>β</i> (°)		
<i>γ</i> (°)		
Volume (Å ³)	3132.9(7)	3072.7(3)
Z, Density (calculated) (g cm ⁻³)	8, 1.295	8, 1.242
Absorption coefficient (mm ⁻¹)	0.082	0.075
<i>F</i> (000)	1296	1216
<i>θ</i> range for data collection (°)	2.26 to 27.50	2.21 to 27.50
Reflections collected / unique	16906 / 3595 (<i>R</i> _{int} = 0.0644)	16743 / 3534 (<i>R</i> _{int} = 0.0437)
Completeness	To <i>θ</i> = 27.50 : 99.9 %	To <i>θ</i> = 27.50 : 100.0 %
Data / restraints / parameters	3595 / 2 / 216	3534 / 0 / 201
Goodness-of-fit on <i>F</i> ²	1.011	0.876
Final <i>R</i> indices [<i>I</i> > 2σ (<i>I</i>)]	<i>R</i> ₁ = 0.0438, <i>wR</i> ₂ = 0.0982	<i>R</i> ₁ = 0.0397, <i>wR</i> ₂ = 0.0866
<i>R</i> indices (all data)	<i>R</i> ₁ = 0.0744, <i>wR</i> ₂ = 0.1144	<i>R</i> ₁ = 0.0869, <i>wR</i> ₂ = 0.0986
Largest diff. peak and hole (e.Å ⁻³)	0.260 and -0.216	0.133 and -0.199

Table 5-7 Crystal data and refinement parameters for compounds **4** & **5**.

	4	5
Empirical formula	C ₂₀ H ₁₉ N ₃ O ₂ S	C ₂₁ H ₁₉ N ₃ S ₂
Formula weight	365.44	377.51
Temperature (K)	296(2)	293(2)
Crystal system , Space group	Monoclinic, <i>P 21/c</i>	Orthorhombic, <i>P 21 21 21</i>
Unit cell dimensions		
<i>a</i> (Å)	11.3543(3)	7.6913(2)
<i>b</i> (Å)	15.0517(4)	10.3041(3)
<i>c</i> (Å)	11.0574(3)	23.7916(5)
α (°)		
β (°)	99.989(2)	
γ (°)		
Volume (Å ³)	1861.08(9)	1885.53(8)
Z, Density (calculated) (g cm ⁻³)	4, 1.304	4, 1.330
Absorption coefficient (mm ⁻¹)	0.193	0.292
<i>F</i> (000)	768	792
θ range for data collection (°)	1.82 to 30.53	1.71 to 27.50
Reflections collected / unique	18320 / 5341 (<i>R</i> _{int} = 0.0226)	11330 / 4121 (<i>R</i> _{int} = 0.0665)
Completeness	To $\theta = 25.00$: 100.0 %	To $\theta = 27.50$: 97.7 %
Data / restraints / parameters	5341 / 0 / 238	4121 / 252 / 244
Goodness-of-fit on <i>F</i> ²	1.026	1.196
Final <i>R</i> indices [<i>I</i> > 2 σ (<i>I</i>)]	<i>R</i> ₁ = 0.0432, <i>wR</i> ₂ = 0.1167	<i>R</i> ₁ = 0.1177, <i>wR</i> ₂ = 0.2712
<i>R</i> indices (all data)	<i>R</i> ₁ = 0.0724, <i>wR</i> ₂ = 0.1343	<i>R</i> ₁ = 0.1532, <i>wR</i> ₂ = 0.2958
Largest diff. peak and hole (e.Å ⁻³)	0.260 and -0.308	0.772 and -0.418

Table 5-8 Crystal data and refinement parameters for compounds **6** & **7**.

	6	7
Empirical formula	C ₁₄ H ₁₄ N ₄ O	C ₁₃ H ₁₄ ClN ₃
Formula weight	254.29	247.72
Temperature (K)	296(2)	295(2)
Crystal system , Space group	Orthorhombic, <i>P b c a</i>	Orthorhombic, <i>P n m a</i>
Unit cell dimensions		
<i>a</i> (Å)	14.8824(10)	12.6012(19)
<i>b</i> (Å)	10.9417(8)	7.0159(10)
<i>c</i> (Å)	16.1298(10)	14.146(2)
α (°)		
β (°)		
γ (°)		
Volume (Å ³)	2626.6(3)	1250.6(3)
Z, Density (calculated) (g cm ⁻³)	8, 1.286	4, 1.316
Absorption coefficient (mm ⁻¹)	0.085	0.286
<i>F</i> (000)	1072	520
θ range for data collection (°)	2.53 to 25.00	2.16 to 27.49
Reflections collected / unique	19205 / 2311 ($R_{int} = 0.1449$)	11586 / 1559 ($R_{int} = 0.0588$)
Completeness	To $\theta = 25.00$: 100.0 %	To $\theta = 27.49$: 100.0 %
Data / restraints / parameters	2311 / 2 / 182	1559 / 8 / 114
Goodness-of-fit on F^2	0.961	1.026
Final <i>R</i> indices [$I > 2\sigma(I)$]	$R_1 = 0.0529$, $wR_2 = 0.1011$	$R_1 = 0.0522$, $wR_2 = 0.1413$
<i>R</i> indices (all data)	$R_1 = 0.1350$, $wR_2 = 0.1308$	$R_1 = 0.0794$, $wR_2 = 0.1616$
Largest diff. peak and hole (e.Å ⁻³)	0.149 and -0.148	0.576 and -0.302

Table 5-9 Crystal data and refinement parameters for compounds **8** & **9**.

	8	9
Empirical formula	C ₁₄ H ₁₄ N ₄ S	C ₁₄ H ₁₄ N ₄ S
Formula weight	270.35	270.35
Temperature (K)	123(2)	100(2)
Crystal system , Space group	Monoclinic, <i>P</i> 21/ <i>c</i>	Triclinic, <i>P</i> -1
Unit cell dimensions		
<i>a</i> (Å)	8.0060(13)	8.0142(1)
<i>b</i> (Å)	14.749(2)	8.4005(2)
<i>c</i> (Å)	11.5700(17)	11.9997(4)
α (°)		99.109(2)
β (°)	91.620(3)	108.190(2)
γ (°)		107.4340(10)
Volume (Å ³)	1365.6(4)	703.40(3)
Z, Density (calculated) (g cm ⁻³)	4, 1.315	2, 1.276
Absorption coefficient (mm ⁻¹)	0.229	0.222
<i>F</i> (000)	568	284
θ range for data collection (°)	2.24 to 30.90	1.86 to 27.50
Reflections collected / unique	9589 / 3920 (<i>R</i> _{int} = 0.0431)	4935 / 3114 (<i>R</i> _{int} = 0.0166)
Completeness	To θ = 25.00 : 99.9 %	To θ = 25.25 : 98.0 %
Data / restraints / parameters	3920 / 0 / 174	3114 / 2 / 180
Goodness-of-fit on F ²	0.966	1.075
Final <i>R</i> indices [<i>I</i> > 2 σ (<i>I</i>)]	<i>R</i> ₁ = 0.0400, <i>wR</i> ₂ = 0.0947	<i>R</i> ₁ = 0.0368, <i>wR</i> ₂ = 0.0902
<i>R</i> indices (all data)	<i>R</i> ₁ = 0.0567, <i>wR</i> ₂ = 0.1008	<i>R</i> ₁ = 0.0452, <i>wR</i> ₂ = 0.1020
Largest diff. peak and hole (e.Å ⁻³)	0.406 and -0.387	0.314 and -0.248

Table 5-10 Crystal data and refinement parameters for compounds **11** & **12**.

	11	12
Empirical formula	C ₁₄ H ₁₅ N ₅ S	C ₁₅ H ₁₃ N ₅ S ₂
Formula weight	285.37	327.42
Temperature (K)	296(2)	123(2)
Crystal system , Space group	Triclinic, <i>P</i> -1	Monoclinic, <i>P</i> 21/ <i>m</i>
Unit cell dimensions		
<i>a</i> (Å)	7.9772(2)	9.6262(2)
<i>b</i> (Å)	8.5375(2)	6.6986(2)
<i>c</i> (Å)	11.8081(2)	11.7895(3)
α (°)	80.0870(10)	
β (°)	83.1420(10)	105.051(2)
γ (°)	62.6410(10)	
Volume (Å ³)	702.83(3)	734.13(3)
Z, Density (calculated) (g cm ⁻³)	2, 1.348	2, 1.481
Absorption coefficient (mm ⁻¹)	0.228	0.366
<i>F</i> (000)	300	340
θ range for data collection (°)	1.75 to 25.00	1.79 to 27.49
Reflections collected / unique	5536 / 2474 (<i>R</i> _{int} = 0.0173)	6973 / 1833 (<i>R</i> _{int} = 0.031)
Completeness	To θ = 25.00 : 100.0 %	To θ = 27.49 : 99.9 %
Data / restraints / parameters	2474 / 0 / 195	1833 / 1 / 133
Goodness-of-fit on <i>F</i> ²	1.026	1.044
Final <i>R</i> indices [<i>I</i> > 2 σ (<i>I</i>)]	<i>R</i> ₁ = 0.0368, <i>wR</i> ₂ = 0.0958	<i>R</i> ₁ = 0.0396, <i>wR</i> ₂ = 0.1025
<i>R</i> indices (all data)	<i>R</i> ₁ = 0.0441, <i>wR</i> ₂ = 0.1018	<i>R</i> ₁ = 0.0532, <i>wR</i> ₂ = 0.1111
Largest diff. peak and hole (e.Å ⁻³)	0.200 and -0.270	0.412 and -0.288

CHAPTER VI

Indolenine-based dibenzotetraaza[14]annulenes

6.1 Introduction

Dibenzotetraaza[14]annulenes (Figure 6-1, a) are a class of synthetic macrocyclic compounds which have attracted a great deal of continued interest since their introduction in 1969 [140, 141]. The attention on these compounds has been aroused mainly due to their resemblance to the naturally occurring porphyrins, thus their relevance in bioinorganic chemistry.

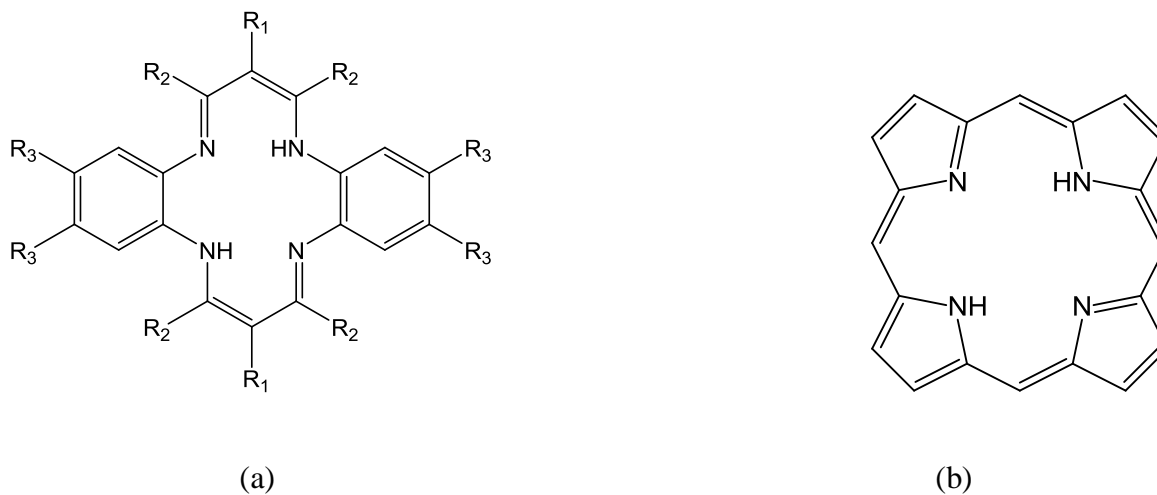


Figure 6-1 (a) Dibenzotetraaza[14]annulenes and (b) porphyrin.

Similar to porphyrins, dibenzotetraaza[14]annulenes possess a number of double bonds in their framework and have four nitrogen atoms in a plane which can easily be deprotonated to generate dianionic ligands towards metal ions. However, despite the fully delocalized aromatic ($4n+2$) system of porphyrins, dibenzotetraaza[14]annulenes are Hückel anti-aromatic ($4n$). Consequently, as structural and theoretical studies have revealed [142-145], there is a negligible delocalization between the two *o*-phenylene and the 1,3-

diiminato fragments and π -delocalization is mainly confined within the two types of fragments. As a result, compared to the essentially rigid planar porphyrins, dibenzotetraaza[14]annulenes are more flexible and can easily adopt different conformations, varying between planar and so-called “saddle-shaped” conformations. For the free ligands, as shown by crystallography, the planarity can persist when $R_2 = H$ (in Figure 6-1, a) whereas the molecules with $R_2 \neq H$ adopt a saddle-shaped conformation because of the steric interactions between the R_2 groups and the hydrogen atoms of *o*-phenylene rings (Figure 6-2).

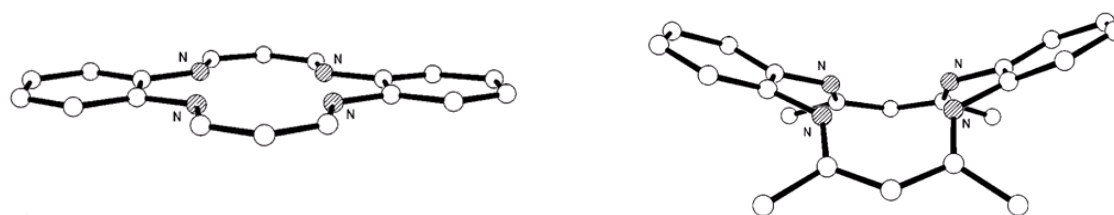
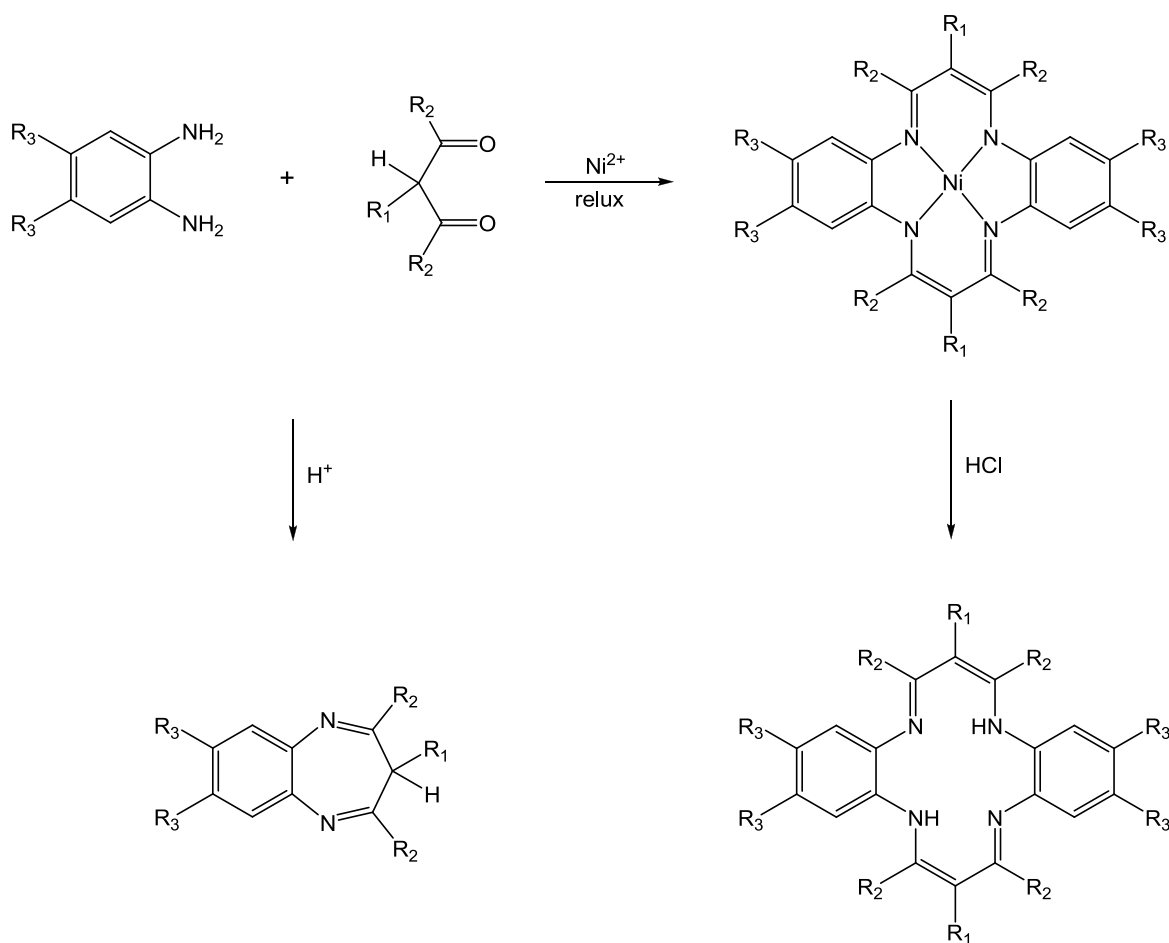


Figure 6-2 The planar and saddle-shaped conformations of dibenzotetraaza[14]annulenes.

Another difference between dibenzotetraaza[14]annulenes and porphyrins concerns the core size of the macrocycle, defined as the average distance from N to the mid-point of the four nitrogen atoms. Compared to the 16-membered inner ring of porphyrin, the central ring of dibenzotetraaza[14]annulenes are composed of fourteen atoms. This gives rise to a coordination hole size of 1.90-1.93 Å for the latter which is about 0.1 Å smaller than that of the porphyrins. The steric constraints imposed by the R_2 groups and the relatively small size of the central core, are the main reasons which lead the metal atom in many complexes

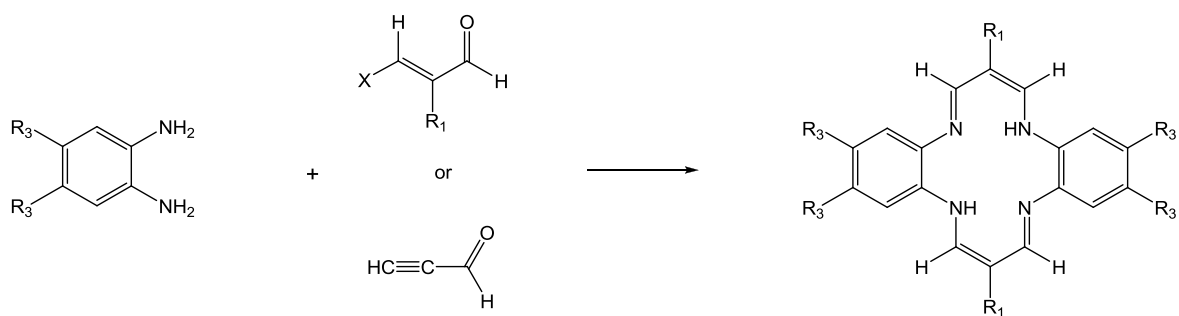
of dibenzotetraaza[14]annulenes to lie out of the N4 plane, although their porphyrin analogous have the metal in the coordination plane.

Dibenzotetraaza[14]annulenes are usually prepared by the so-called “ template synthesis” ,namely, 2:2 condensation of an *o*-phenylene diamine and a 1,3-dicarbonyl in the presence of Ni²⁺ [141, 146]. The metal ion can then be removed from the macrocycle using hydrochloric acid to give the corresponding free ligand. Without coordinating help of the divalent metal ion, in most of the cases, a 1:1 condensation reaction occurs to form the 1,5-benzodiazepine (Scheme 6-1).



Scheme 6-1.

The other methods for the synthesis of dibenzotetraaza[14]annulenes are the reactions of *o*-phenylene diamines with propynal or substituted acroleins [147] (Scheme 6-2).

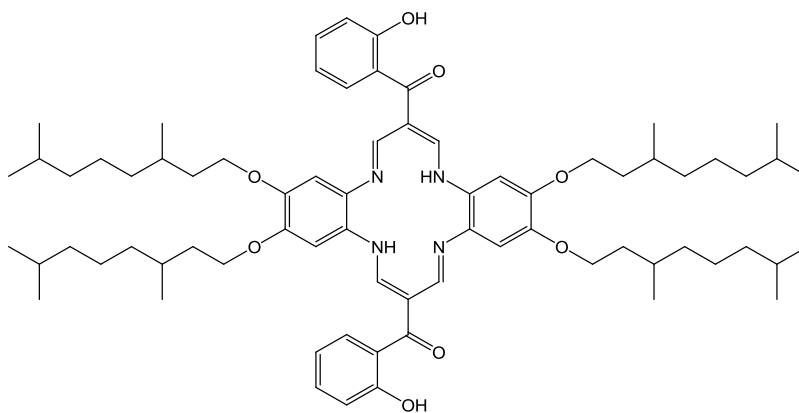


Scheme 6-2.

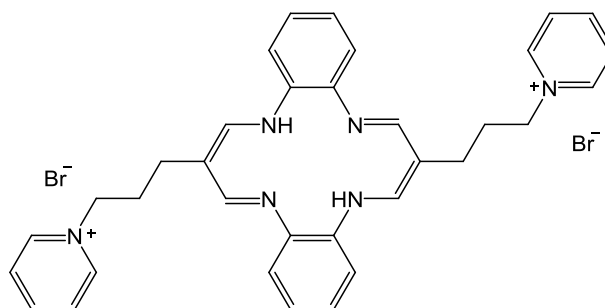
Up to now, a large number of dibenzotetraaza[14]annulene macrocycles with different peripheral substituents has been reported, some of which showing interesting properties from biological and material science points of view. As examples, γ,γ -bis(2-hydroxybenzoyl) derivative a (Figure 6-3) reported to exhibit liquid-crystalline behavior [148], while the dicationic macrocycles b and c in Figure 6-3 showed to be capable of strong interactions with *ct*-DNA [149].

On the basis of the existed synthetic protocols, we expected that 2-(diformylmethylidene)-3,3-dimethylindole, as a 1,3-dicarbonyl compound, can undergo 2:2 cyclocondensation with *o*-phenylene diamine to form a dibenzotetraaza[14]annulene core conjugated with the indolic fragment. In this work, we report the result of our studies on the synthesis, crystallographic analysis and metal complexation of such macrocycle.

(a)



(b)



(c)

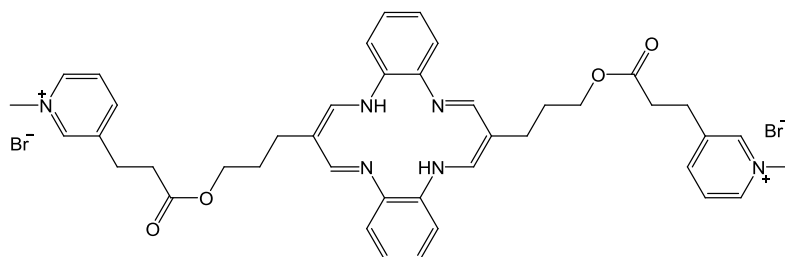
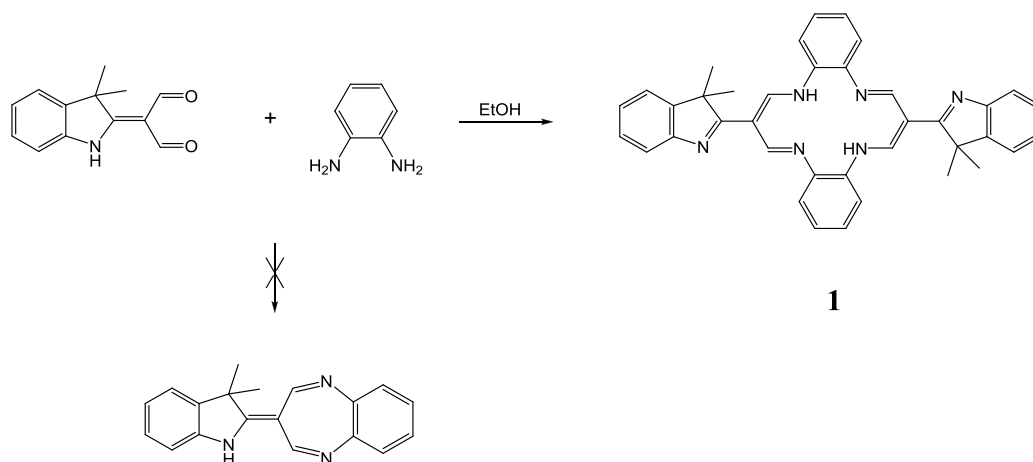


Figure 6-3 (a) liquid crystal and (b,c) DNA binding agents with dibenzotetraaza[14]annulene structures.

6.2 Results and discussion

According to the known synthetic routes, the reaction of 2-(diformylmethylidene)-3,3-dimethylindole with *o*-phenylene diamine was expected to generate the 1,5-benzodiazepine. On the other hand, synthesis of the related dibenzotetraaza[14]annulene would need the coordination help of Ni^{2+} ion, following by treatment with HCl to remove the metal ion. However, we were surprised to find out that the reaction of the dicarbonyl with phenylene diamine in ethanol and in the presence of acetic acid led to the straightforward formation of the desired 14-membered macrocycle, **1**, in 81% yield (Scheme 6-3).



Scheme 6-3.

The ^1H NMR spectrum of **1** shows the six protons of the 14-membered ring as a triplet at $\delta = 14.58$ ppm ($J = 6.1$ Hz) for the two internal *NH* and a doublet with the same coupling constant at 8.95 ppm for the four *CHN* protons. This is characteristic for such a ring system and has been explained in term of rapid imine-enamine tautomerism [150]. Figure 6-4 shows the crystal structure of molecule **1**. The asymmetric unit of the crystal consists of two-half molecules whose geometrical parameters differ only slightly, therefore

only one molecule is depicted. The center of the molecule lies at a crystallographic center of inversion. As expected for a dibenzotetraaza[14] annulene derived from a 1,3-dialdehyde, the tetraaza ring adopts a planar conformation. This ring is coplanar with the two attached indolic rings [maximum deviation = 0.043(4) Å] and the methyl groups lie on either side of the plane. The hole size of the macrocycle ring is 1.93 Å which falls within the expected range.

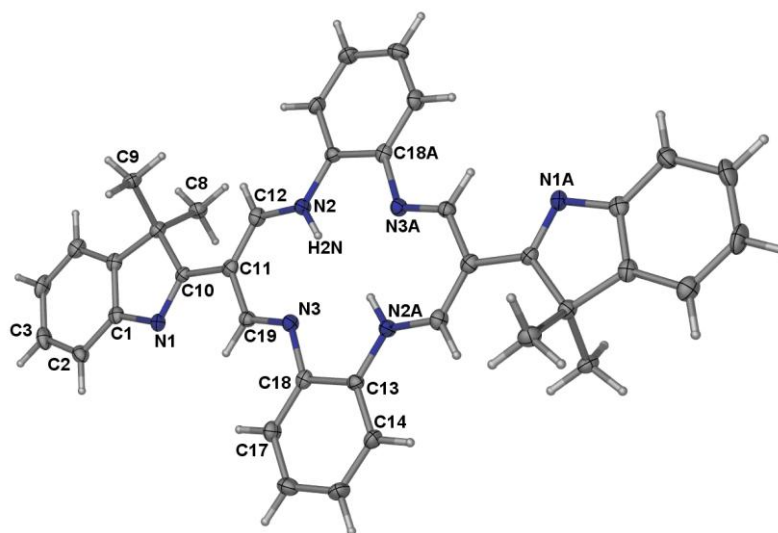


Figure 6-4 The molecular structure of molecule **1** (50% probability ellipsoids).

Table 6-1 Selected bond lengths (Å) and bond angles (°) for compound **1**.

<i>Bond lengths</i>			
N(1)-C(10)	1.305(5)	N(3)-C(18)	1.423(5)
N(2)-C(12)	1.341(5)	C(10)-C(11)	1.467(6)
N(2)-C(13)#1	1.392(5)	C(11)-C(12)	1.366(6)
N(3)-C(19)	1.290(5)	C(11)-C(19)	1.441(6)
<i>Bond angles</i>			
N(2)#1-C(13)-C(18)	117.5(4)	C(12)-C(11)-C(19)	122.5(4)
C(13)-C(18)-N(3)	116.4(3)	C(12)-C(11)-C(10)	121.9(4)

Symmetry transformations used to generate equivalent atoms: #1 -x+1, -y+1, -z+1

Figure 6-5 displays the packing view of the crystal structure in the *b* direction. The planar molecules are arranged in an anti-parallel manner above each other along the *a* axis with the centroid-centroid separation of 3.43 Å.

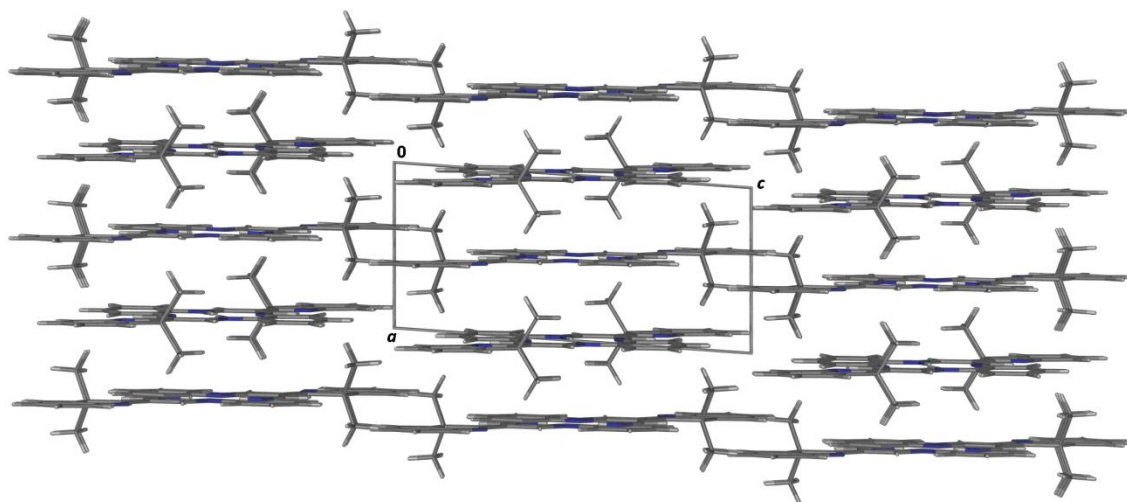


Figure 6-5 Packing view of compound **1**, looking down the *b* axis.

Upon recrystallization of the macrocyclic compound in CDCl_3 , the crystals of a chloroform solvate molecule (compound **2**) were obtained. As shown in Figure 6-6, two chloroform molecules are cocrystallized with each macrocycle and bonded to the 6-membered rings of the indolenine moieties *via* a C-H... π interaction [$\text{C}\dots\text{Cg} = 3.287(2)$ Å]. As a result, the planarity of the macrocycle is disrupted to a large extent, the r.m.s. deviation from the best plane passing through the 14 atoms of the tetraaza ring being 0.105 Å. The macrocycle molecule is centrosymmetric with the center of the molecule situated at a crystallographic inversion center.

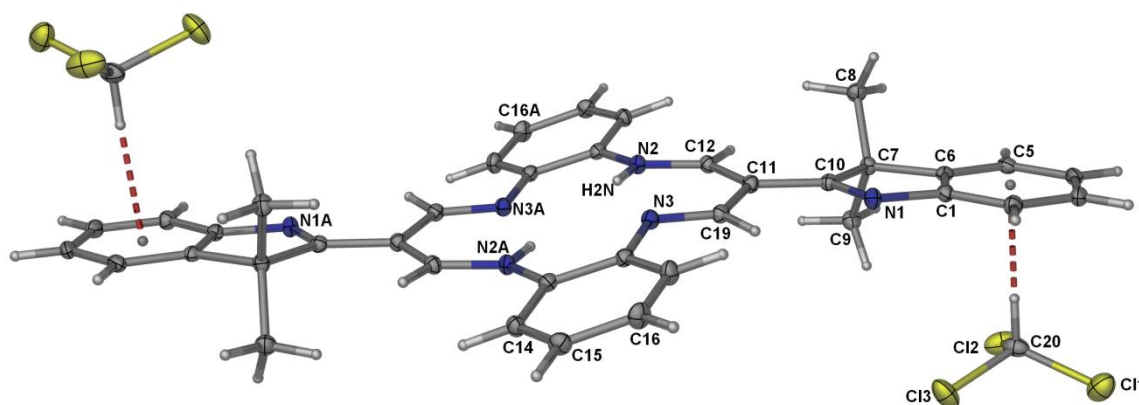


Figure 6-6 The molecular structure and atom labeling schemes of compound **2** (50% probability ellipsoids).

Table 6-2 Selected bond lengths (Å) and bond angles (°) for compound **2**.

<i>Bond lengths</i>			
N(1)-C(10)	1.3056(18)	N(3)-C(18)	1.4213(18)
N(2)-C(12)	1.3368(18)	C(10)-C(11)	1.4606(19)
N(2)-C(13)#1	1.4059(17)	C(11)-C(12)	1.3834(19)
N(3)-C(19)	1.2943(18)	C(11)-C(19)	1.4496(19)
<i>Bond angles</i>			
N(2)#1-C(13)-C(18)	117.96(12)	C(12)-C(11)-C(19)	122.08(12)
C(13)-C(18)-N(3)	116.88(12)	C(12)-C(11)-C(10)	120.87(12)

Symmetry transformations used to generate equivalent atoms: #1 -x, -y, -z+2

Table 6-2 lists the selected bond lengths and angles for the structure **2**. In the crystal, the macrocycles are connected into zigzag layers (Figure 6-7) *via* a C-H... π interaction (Table 6-4).

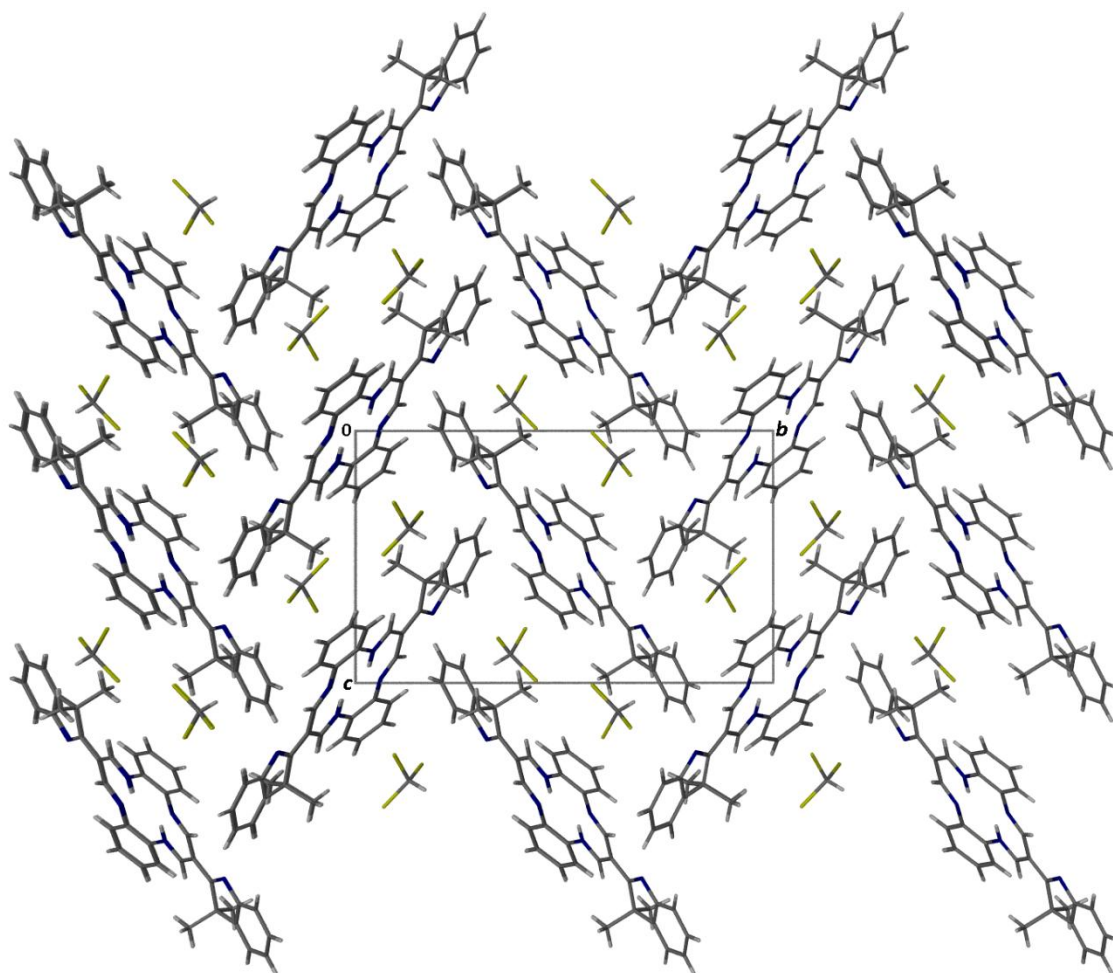


Figure 6-7 Packing view of compound **2**, looking down the *a* axis.

Recrystallization of macrocycle **1** in a mixture of trichloroethylene and ethyl acetate afforded the dichloride salt of the doubly protonated macrocycle (compound **3**). The crystal structure of the salt is presented in Figure 6-8 and the selected bond lengths and angles are given in Table 6-3. Comparing the bond lengths of the free macrocycle, **1**, and those of the chloride salt, **3**, revealed that the protonation of the indolenine nitrogen atoms resulted in shortening of C10-C11 which joins the indolic ring to the diiminato fragment, and

lengthening of N1-C10. Moreover, the molecule loses its planarity to some extent, the maximum deviation from the best plane running through the non-hydrogen atoms of the cation component (except for the methyl carbon atoms) being 0.334(2) Å for C7 atom.

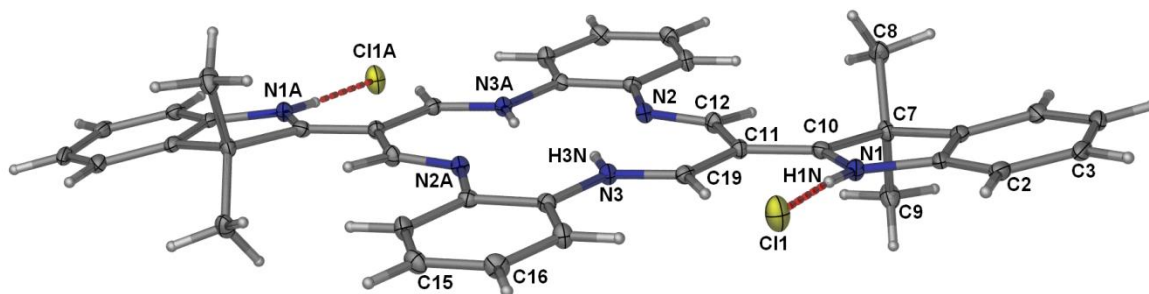


Figure 6-8 The molecular structure and atom labeling schemes of compound **3** (50% probability ellipsoids).

Table 6-3 Selected bond lengths (Å) and bond angles (°) for compound **3**.

<i>Bond lengths</i>			
N(1)-C(10)	1.328(2)	N(3)-C(18)	1.414(2)
N(2)-C(12)	1.289(2)	C(10)-C(11)	1.424(2)
N(2)-C(13)#1	1.423(2)	C(11)-C(19)	1.408(2)
N(3)-C(19)	1.313(2)	C(11)-C(12)	1.440(2)
<i>Bond angles</i>			
N(2)#1-C(13)-C(18)	117.52(14)	C(19)-C(11)-C(12)	121.51(15)
C(13)-C(18)-N(3)	117.44(15)	C(10)-C(11)-C(12)	119.07(15)

Symmetry transformations used to generate equivalent atoms: #1 -x, -y+1, -z+1

The center of the molecule lies on a crystallographic center of inversion and the chloride anions are hydrogen bonded to indoleninium nitrogen atoms. Figure 6-9 shows a packing view of the crystal structure, looking down the crystallographic c axis. In the crystal, the molecules are linked into infinite chains along the c axis through $\pi \dots \pi$ interactions [centroid-centroid distance = 3.4631(10) Å] formed by the indolic six-membered rings of the molecules related by symmetry operation $-x, -y+1, -z$. The chains are further connected into a three-dimensional polymeric structure *via* C-H... π interactions (Table 6-4).

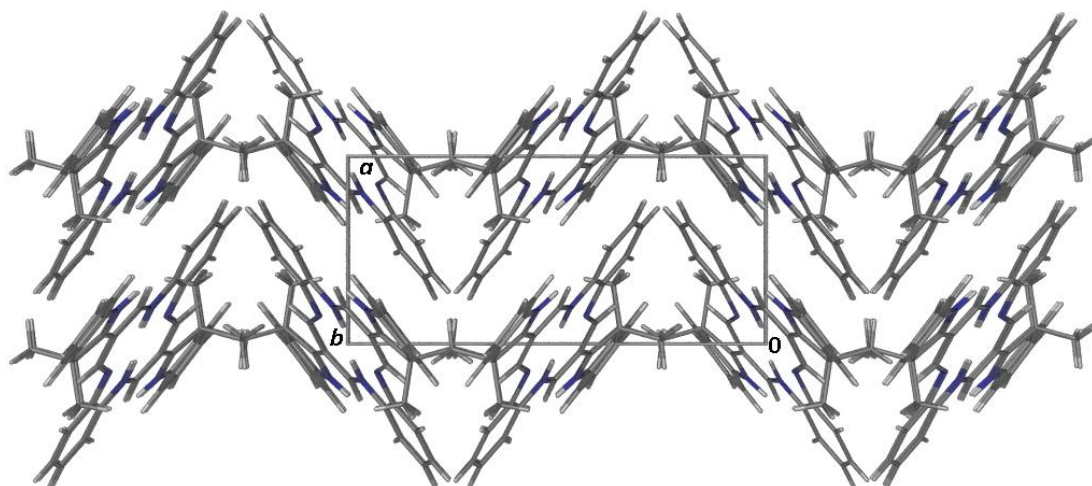


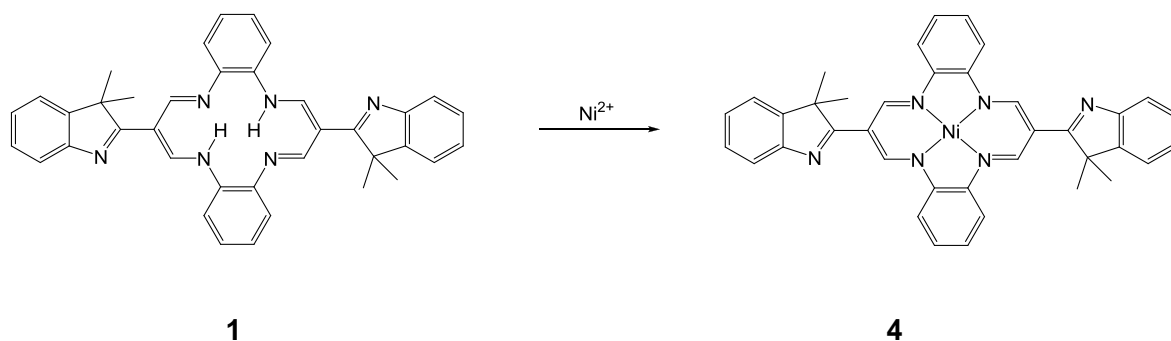
Figure 6-9 Packing view of compound **3**, looking down the c axis.

Table 6-4 Hydrogen-bond geometry for **2** and **3**. *Cg*(1) and *Cg*(2) are the centroids of the C1-C6 and C13-C18 rings, respectively.

	D-H...A	H...A (Å)	D...A (Å)	D-H...A (°)
Compound 2				
	N(2)-H(2N)...N(3)	2.047(16)	2.7213(16)	135.8(16)
	C(20)-H(20)... <i>Cg</i> (1)	2.32(2)	3.2867(17)	175.0(17)
	C(17)-H(17)... <i>Cg</i> (1)#1	2.82	3.6178(17)	143
Compound 3				
	N(3)-H(3N)...N(2)	1.996(17)	2.709(2)	138.9(17)
	N(1)-H(1N)...Cl(1)	2.189(15)	3.0653(15)	172.3(18)
	C(16)-H(16)... <i>Cg</i> (1)#2	2.84	3.545(2)	131
	C(5)-H(5)... <i>Cg</i> (2)#3	2.73	3.666(2)	169

Symmetry transformations used to generate equivalent atoms: #1 $x+1/2, -y+1/2, z+1/2$; #2 $-x+1, y+1/2, -z+1/2$ #3 $-x, y-1/2, -z+1/2$

The coordination behavior of the synthesized dibenzotetraaza[14]annulene, **1**, towards metal ions was then studied. The macrocycle structure offers two types of coordination site, namely the central cavity and the indolenine nitrogen atoms. The ligand was first reacted with nickel(II) acetate in the presence of triethylamine (Scheme 6-4). Good quality crystals of the product were obtained from a chloroform solution. The X-ray crystallographic analysis shows that the crystal structure of the nickel(II) complex, **4**, is isomorphous with that of the neutral free ligand. The asymmetric unit consists of two half-molecules with very similar geometrical parameters. The structure of one molecule is exhibited in Figure 6-10.



Scheme 6-4

Upon the reaction with Ni^{II} ion, the macrocycle amino groups underwent deprotonation to accommodate the metal ion within the central cavity. The resulting nickel(II) complex, **4**, is essentially planar (except for the methyl group) with the maximum deviation from the plane $0.046(7)$ Å. Table 6-5 compiles the selected bond lengths and angles for the nickel(II) complex. The average Ni-N distance of 1.862 Å is shorter than nitrogen-to-center distance, N-Ct, of the neutral free ligand (1.93 Å) because increased delocalization and contraction is associated with the loss of the two amino hydrogens as discussed by Goedken *et al.* [151]. The contraction is mainly reflected in the smaller N2A-C13-C18 and C13-C18-N3 angles in the nickel complex [$113.4(3)^\circ$ and $113.3(3)^\circ$] than those in the neutral free ligand [$117.5(4)^\circ$ and $116.4(3)^\circ$].

Figure 6-11 depicts two packing projection of the nickel complex, looking down the *a* and *b* axes. The molecules are stacked on top of each other with their Ni^{II} atoms aligned along the *a* direction, separated by a distance of 3.448 Å. Similar arrangements have been observed in partially oxidized forms of some related Ni(II), Pd(II) [152] and Pt(II) [153] complexes with metal-metal distances of 3.18 - 3.25 Å.

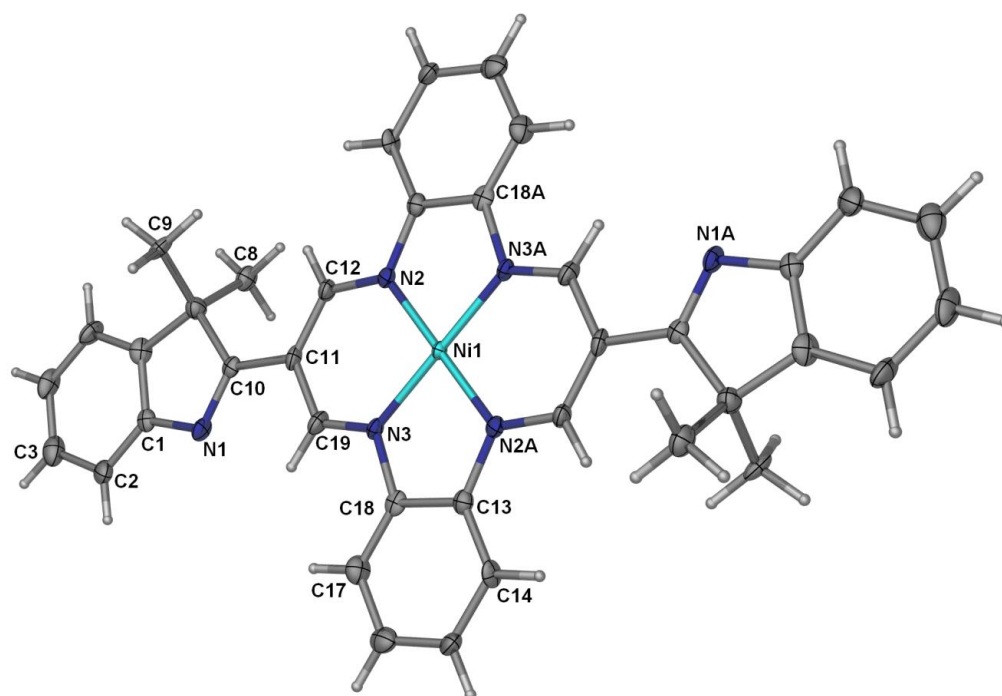


Figure 6-10 The molecular structure and atom labeling schemes of nickel(II) complex **4** (50% probability ellipsoids).

Table 6-5 Selected bond lengths (Å) and bond angles (°) for nickel(II) complex **4**.

<i>Bond lengths</i>			
Ni(1)-N(3)	1.858(3)	N(3)-C(19)	1.314(4)
Ni(1)-N(2)	1.867(3)	N(3)-C(18)	1.423(4)
N(1)-C(10)	1.297(4)	C(10)-C(11)	1.471(4)
N(2)-C(12)	1.325(4)	C(11)-C(12)	1.387(4)
N(2)-C(13)#1	1.417(4)	C(11)-C(19)	1.411(4)
<i>Bond angles</i>			
N(3)-Ni(1)-N(2)#1	85.73(11)	C(12)-C(11)-C(19)	121.6(3)
N(3)-Ni(1)-N(2)	94.27(11)	N(2)#1-C(13)-C(18)	113.4(3)
C(12)-C(11)-C(10)	123.2(3)	C(13)-C(18)-N(3)	113.3(3)

Symmetry transformations used to generate equivalent atoms: #1 $-x+1, -y+1, -z+1$

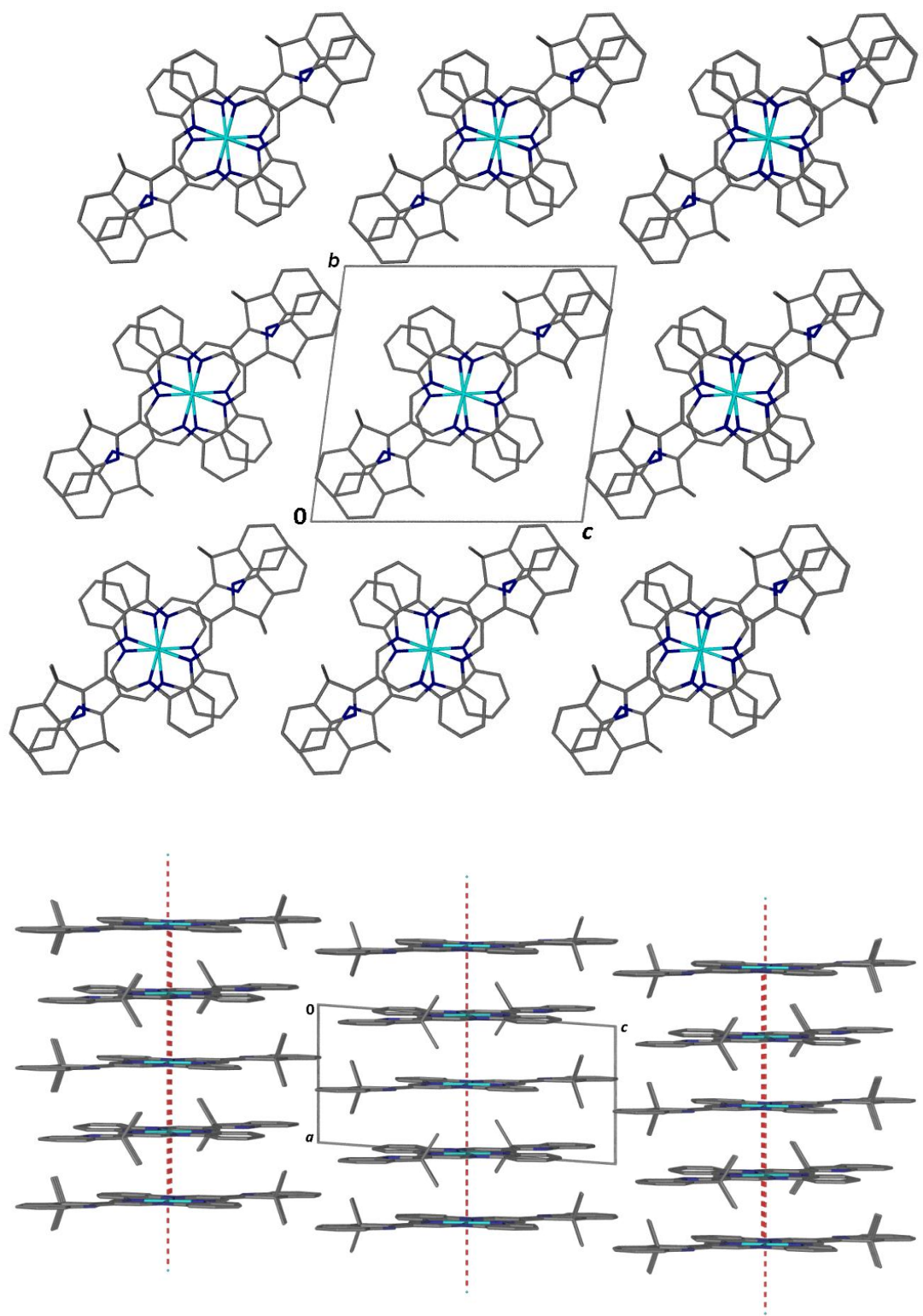
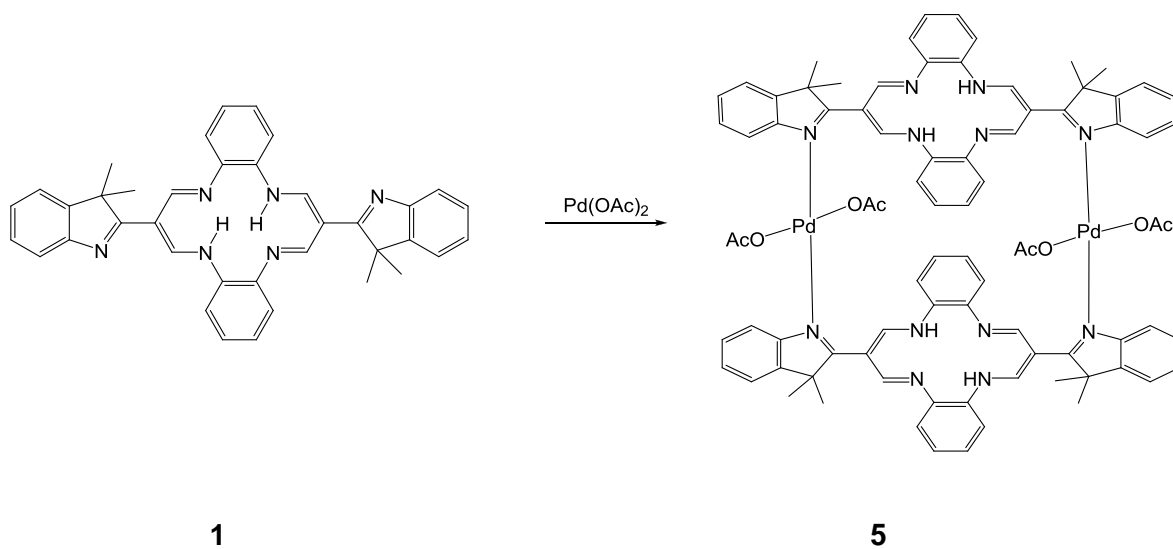


Figure 6-11 Packing views of structure 4.

The macrocyclic molecule was then reacted with a larger metal ion, *i.e.*, Pd²⁺ (Scheme 6-5). The X-ray crystallographic analysis of the product, compound **5**, shows that the neutral macrocyclic ligand applied its indolenine nitrogen atoms in coordination to the Pd(II) ions while its central core remains free. Pairs of the metal atoms are doubly bridged by two macrocyclic ligands into centrosymmetric dinuclear Pd^{II} complexes. Two *trans* located monodentate acetate ligands complete a square planar coordination environment around each palladium(II) ion. Within the dimeric molecule, the metal centers are separated by 10.83 Å and the planes passing through the 14-membered tetraaza rings (r.m.s. deviation = 0.108 Å) are separated by a distance of 3.32 Å. As shown in Figure 6-12, upon the complexation, the indolenine moieties of the ligands are rotated about the indolenine-diiminato C-C linkages to meet the requirement for the formation of the dimer. Thus, the 14-membered tetraaza ring and the two indolenine eight-membered rings are not coplanar anymore, the dihedral angles between them being 40.07(13) and 41.23(13) °.



Scheme 6-5.

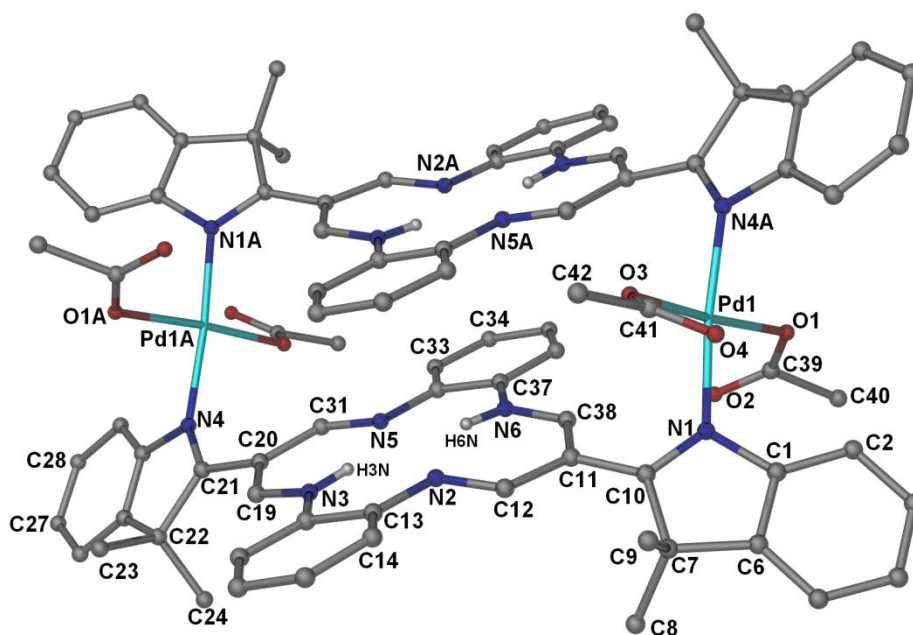


Figure 6-12 The molecular structure and atom labeling schemes of palladium(II) complex **5**.

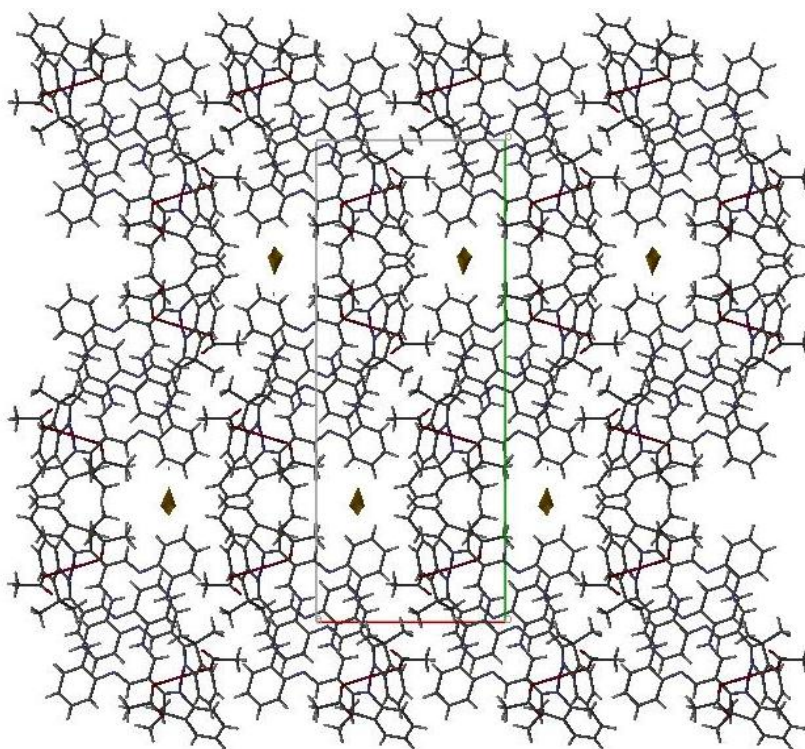


Figure 6-13 Packing view of structure **5**, showing void spaces in the lattice.

An interesting feature of the crystal structure of **5** is the presence of void spaces in the lattice with the size of 765 Å³ within which there is no evidence for included solvent (Figure 6-13).

Table 6-6 Selected bond lengths (Å) and bond angles (°) for palladium(II) complex **5**.

<i>Bond lengths</i>			
Pd(1)-N(4)#1	2.020(5)	N(5)-C(31)	1.300(8)
Pd(1)-N(1)	2.021(5)	N(5)-C(32)	1.423(8)
Pd(1)-O(3)	2.030(5)	N(6)-C(38)	1.333(8)
Pd(1)-O(1)	2.053(5)	N(6)-C(37)	1.407(8)
N(1)-C(10)	1.310(8)	C(10)-C(11)	1.439(9)
N(2)-C(12)	1.295(8)	C(11)-C(38)	1.392(9)
N(2)-C(13)	1.419(8)	C(11)-C(12)	1.426(9)
N(3)-C(19)	1.328(8)	C(19)-C(20)	1.367(9)
N(3)-C(18)	1.403(8)	C(20)-C(31)	1.444(9)
N(4)-C(21)	1.301(8)	C(20)-C(21)	1.464(9)
N(4)-Pd(1)#1	2.021(5)		
<i>Bond angles</i>			
N(4)#1-Pd(1)-N(1)	172.1(2)	C(19)-C(20)-C(31)	122.7(6)
N(4)#1-Pd(1)-O(3)	90.0(2)	N(2)-C(12)-C(11)	124.8(6)
N(1)-Pd(1)-O(3)	90.2(2)	C(18)-C(13)-N(2)	116.4(6)
N(4)#1-Pd(1)-O(1)	86.2(2)	C(13)-C(18)-N(3)	116.8(6)
N(1)-Pd(1)-O(1)	93.25(19)	C(32)-C(37)-N(6)	118.4(5)
O(3)-Pd(1)-O(1)	175.6(2)	C(37)-C(32)-N(5)	117.0(5)
C(38)-C(11)-C(12)	122.4(6)		

Symmetry transformations used to generate equivalent atoms: #1 -x+2, -y, -z+2

6.3 Conclusions

The study shows that indoleninyldibenzotetraaza[14]annule (1), the 2:2 condensation product of 2-(diformylmethylidene)-3,3-dimethylindole and *o*-phenylene diamine, has an essentially planar solid state structure. However, the planarity can be disrupted by different factors, *i.e.*, the presence of chloroform solvent molecules in the lattice, hydrochlorination of the indolenine moieties or coordination to a metal center *via* the indolenine nitrogen donor. Upon the reaction with a metal salt, the metal ion can be inserted in the central cavity of the macrocycle (as was observed in the nickel(II) complex), or be coordinated by the indolenine nitrogen atoms (as was observed in the palladium(II) complex). Due to the relatively small core size of the macrocyclic ligand, it would appear that the coordination mode of the ligand depends greatly on the size of the metal ion.

6.4 Experimental

2-(diformylmethylidene)-3,3-dimethylindole was synthesized as described in chapter IV. Microanalyses were carried out on a Perkin-Elmer 2400 elemental analyzer. The NMR spectra were recorded on a JEOL Lambda 400 MHz FT-NMR spectrometer. Chemical shifts are given in δ values (ppm) using TMS as the internal standard. The IR spectra were taken on a Perkin Elmer Spectrum 400 ATR-FT-IR spectrometer.

6.4.1 Synthesis of dibenzotetraaza[14]annulenes 1, 2 and 3

A solution of 2-(diformylmethylidene)-3,3-dimethylindole (0.43 g, 2 mmol) and *o*-phenylene diamine (0.216 g, 2 mmol) in ethanol (40 mL) in the presence of acetic acid (0.5

mL) was refluxed for 30 minutes whereupon the orange-red solid of the product precipitated. The solid was filtered off, washed with ethanol and dried over silica-gel, yield 0.465 g, 81%. *Anal. Calc.* for C₃₈H₃₄N₆: C, 79.41; H, 5.96; N, 14.62. Found: C, 79.00; H, 6.10; N, 14.68%. IR (ATR): ν (cm⁻¹) 3068w, 2957w, 2863w, 1631s, 1591m, 1569m, 1489m, 1454m, 1304s, 1260m, 773m, 725s, 530m. ¹H NMR (CDCl₃): δ 14.58 (t, 2H, *J* = 6.1, *NH*); 8.95 (d, 4H, *J* = 6.1, *CHN*); 7.54 (d, 2H, *Ar-H*); 7.38-7.40 (m, 4H, *Ar-H*); 7.29-7.34 (m, 4H, *Ar-H*); 7.16-7.19 (m, 4H, *Ar-H*); 1.60 (s, 12H, *CH₃*). ¹³C NMR (CDCl₃): δ 182.44 (*CHN*); 153.64, 150.09, 146.71, 137.56, 127.88, 126.10, 124.26, 120.77, 119.11, 115.40, 104.63; 52.56 (*CH₃CCH₃*); 26.39 (*CH₃CCH₃*).

The crystals of **1**, suitable for X-ray analysis, were grown from a CH₂Cl₂ solution at 5° C. Recrystallization of the macrocyclic molecule from CDCl₃ gave the crystals of the chloroform solvated molecule, **2**. The crystal of the hydrochloride salt of the macrocycle, **3**, was obtained unexpectedly from a solution of **1** in a mixture of trichloroethylene and ethylacetate, at room temperature.

6.4.2 Synthesis of nickel(II) complex **4**

A solution of nickel(II) acetate tetrahydrate (0.25 g, 1mmol) in a minimum amount of water was added to a solution of the ligand **1** (0.575 g, 1 mmol) in dioxane (80 ml). 1 ml triethylamine was added and the mixture was refluxed for 20 hr. The mixture was then cooled to room temperature and the dark red precipitate was filtered off, washed with ethanol and recrystallized from chloroform at room temperature to give the X-ray quality crystals of **4**.

6.4.3 Synthesis of palladium(II) complex **5**

The macrocyclic ligand, **1**, (0.575 g, 1 mmol) was dissolved in THF by heating. A few drops of triethylamine was added followed by the addition of a solution of palladium(II) acetate (0.224 g, 1 mmol) in THF. The mixture was heated at reflux for 2 hr and then evaporated to half volume under reduced pressure. The palladium complex, precipitated on addition of n-hexane to the solution, was collected and dried over silica-gel, yield 0.42 g, 53%. *Anal. Calc.* for C₈₄H₈₀N₁₂O₈Pd₂: C, 63.12; H, 5.04; N, 10.52. Found: C, 63.99; H, 5.56; N, 11.33%. IR (ATR): ν (cm⁻¹) 1731m, 1625s, 1593m, 1558m, 1456m, 1301s, 1261m, 769m, 752s, 726s, 528m.

The crystals of **5** were grown by slow diffusion of ethyl acetate into a chloroform solution of the compound.

6.4.4 Crystallography

Diffraction data for compounds **1**, **2** and **3** were measured using a Bruker SMART Apex II CCD area-detector diffractometer. For the nickel complex, **4**, a red plate crystal was mounted in the nitrogen cold stream provided by an Oxford Cryostream low temperature apparatus on the goniometer head of a Bruker D8 diffractometer equipped with an ApexII CCD detector at the Advanced Light Source, Berkeley, CA, beamline 11.3.1. Data were collected with the use of silicon (111) monochromated synchrotron radiation ($\lambda = 0.77490 \text{ \AA}$). The Advanced Light Source is supported by the Director, Office of Science, Office of Basic Energy Sciences, of the U.S. Department of Energy under Contract No. DE-AC02-05CH1123. For the palladium complex, **5**, a crystal was mounted in the nitrogen cold stream provided by a CRYO Industries CryoCool low temperature apparatus on the

goniometer head of a Bruker SMART Apex DUO equipped with an Incoatec I μ S Cu detector at the UC Davis, CA, U.S.A. The orientation matrix, unit cell refinement and data reduction were all handled by the Apex2 software (SAINT integration, SADABS absorption correction) [49]. The structures were solved using direct or Patterson methods in the program SHELXS-97 [50] and were refined by the full matrix least-squares method on F^2 with SHELXL-97. All the non-hydrogen atoms were refined anisotropically and all the C-bound hydrogen atoms were placed at calculated positions and refined isotropically. N-bound hydrogen atoms were located in difference Fourier maps and refined with distance restraints. Drawings of the molecules were produced with XSEED [51]. Crystal data and refinement parameters are summarized in Tables 6-7 and 6-8.

Table 6-7 Crystal data and refinement parameters for compounds **1**, **2** & **3**.

	C ₃₈ H ₃₄ N ₆ (1)	C ₃₈ H ₃₄ N ₆ .2CHCl ₃ (2)	C ₃₈ H ₃₆ N ₆ ⁺ .2Cl ⁻ (3)
Empirical formula	C ₃₈ H ₃₄ N ₆	C ₄₀ H ₃₆ Cl ₆ N ₆	C ₃₈ H ₃₆ Cl ₂ N ₆
Formula weight	574.71	813.45	647.63
Temperature (K)	100(2)	100(2)	90(2) K
Wavelength	0.71073 Å	0.71073 Å	0.71073 Å
Crystal system , Space group	Triclinic, <i>P</i> -1	Monoclinic, <i>P</i> 21/ <i>n</i>	Monoclinic, <i>P</i> 21/ <i>c</i>
Unit cell dimensions			
<i>a</i> (Å)	6.8570(5)	7.9871(2)	6.6659(3)
<i>b</i> (Å)	14.2898(8)	19.6913(2)	14.5944(7)
<i>c</i> (Å)	14.9747(9)	12.3598(2)	16.4058(8)
α (°)	82.332(3)		
β (°)	85.697(4)	105.868(2)	100.6060(10)
γ (°)	87.857(4)		
Volume (Å ³)	1449.52(16)	1869.83(6)	1568.77(13)
Z, Density (calculated) (g cm ⁻³)	2, 1.317	2, 1.445	2, 1.371
Absorption coefficient (mm ⁻¹)	0.079	0.499	0.246
<i>F</i> (000)	608	840	680
θ range for data collection (°)	1.38 to 25.05	2 to 27.00	2.79 to 27.97
Reflections collected / unique	7648 / 4927 [<i>R</i> _{int} = 0.0217]	17098 / 4076 [<i>R</i> _{int} = 0.0196]	12542 / 3758 [<i>R</i> _{int} = 0.0420]
Completeness	To $\theta = 25.00^\circ$: 96.2 %	To $\theta = 27.00^\circ$: 100.0 %	To $\theta = 27.00^\circ$: 99.4 %
Data / restraints / parameters	4927 / 2 / 407	4076 / 1 / 241	3758 / 2 / 216
Goodness-of-fit on <i>F</i> ²	1.096	1.035	1.013
Final <i>R</i> indices [<i>I</i> > 2 σ (<i>I</i>)]	<i>R</i> _{<i>I</i>} = 0.0778, <i>wR</i> ₂ = 0.2142	<i>R</i> _{<i>I</i>} = 0.0336, <i>wR</i> ₂ = 0.0859	<i>R</i> _{<i>I</i>} = 0.0406, <i>wR</i> ₂ = 0.0955
<i>R</i> indices (all data)	<i>R</i> _{<i>I</i>} = 0.937, <i>wR</i> ₂ = 0.2221	<i>R</i> _{<i>I</i>} = 0.0366, <i>wR</i> ₂ = 0.0882	<i>R</i> _{<i>I</i>} = 0.0627, <i>wR</i> ₂ = 0.1052
Largest diff. peak and hole (e.Å ⁻³)	0.382 and -0.331	0.517 and -0.440	0.448 and -0.398

Table 6-8 Crystal data and refinement parameters for compounds **4** & **5**.

	[Ni(C ₃₈ H ₃₂ N ₆)] (4)	[Pd ₂ (C ₃₈ H ₃₄ N ₆) ₂ (C ₂ H ₅ O ₂) ₂] (5)
Empirical formula	C ₃₈ H ₃₂ N ₆ Ni	C ₈₄ H ₈₀ N ₁₂ O ₈ Pd ₂
Formula weight	631.41	1598.40
Temperature (K)	150(2)	87(2)
Wavelength	0.77490 Å	1.54178 Å
Crystal system , Space group	Triclinic, <i>P</i> -1	Monoclinic, <i>P</i> 21/ <i>c</i>
Unit cell dimensions		
<i>a</i> (Å)	6.896(5)	12.9154(3)
<i>b</i> (Å)	14.223(10)	32.9705(6)
<i>c</i> (Å)	14.999(12)	9.9792(2)
<i>α</i> (°)	82.360(11)	
<i>β</i> (°)	85.388(7)	105.367(2)
<i>γ</i> (°)	87.456(7)	
Volume (Å ³)	1452.5(19)	4097.49(15)
Z, Density (calculated) (g cm ⁻³)	2, 1.444	2, 1.296
Absorption coefficient (mm ⁻¹)	0.708	4.027
<i>F</i> (000)	660	1648
<i>θ</i> range for data collection (°)	3.15 to 27.74	3.79 to 56.92
Reflections collected / unique	14648 / 4897 [<i>R</i> _{int} = 0.0366]	37260 / 5491 [<i>R</i> _{int} = 0.0469]
Completeness	To <i>θ</i> = 27.74° : 99.0 %	To <i>θ</i> = 27.00° : 99.8 %
Max. and min. transmission	0.9944 and 0.9587	0.9238 and 0.5651
Data / restraints / parameters	5229 / 0 / 414	5491 / 2 / 490
Goodness-of-fit on <i>F</i> ²	1.028	1.272
Final <i>R</i> indices [<i>I</i> > 2σ (<i>I</i>)]	<i>R</i> ₁ = 0.0433, <i>wR</i> ₂ = 0.1177	<i>R</i> ₁ = 0.0609, <i>wR</i> ₂ = 0.1397
<i>R</i> indices (all data)	<i>R</i> ₁ = 0.532, <i>wR</i> ₂ = 0.1239	<i>R</i> ₁ = 0.0651, <i>wR</i> ₂ = 0.1415
Largest diff. peak and hole (e.Å ⁻³)	0.649 and -0.372	1.680 and -1.208